Universidade Estadual de Londrina

JULIO CESAR TOLEDO PINTO

GENERALIZED SYMMETRIES, ANOMALIES, AND LONG-RANGE ENTANGLED SYSTEMS

Londrina
2025

Julio Cesar Toledo Pinto

Generalized Symmetries, Anomalies, and Long-Range Entangled Systems

Trabalho apresentado ao Departamento de Física da Universidade Estadual de Londrina, como requisito parcial à obtenção do título de Doutor.

Orientador: Dr. Pedro Rogerio Sergi Gomes

Londrina
2025

Ficha de identificação da obra elaborada pelo autor, através do Programa de Geração Automática do Sistema de Bibliotecas da UEL

J94g Pinto, Julio Cesar Toledo
Generalized Symmetries, Anomalies, and Long-Range Entangled Systems / Julio Cesar Toledo Pinto. – Londrina, 2025.
87f. : il.

Tese (Doutorado em Física) – Universidade Estadual de Londrina, Centro de Ciências Exatas, Programa de Pós-Graduação em Física, 2025.
Inclui bibliografia.

1. Strong correlated electrons – Tese. 2. Generalized Symmetries – Tese. 3. Long-range entangled states – Tese. I. Gomes, Pedro Rogerio Sergi. II. Universidade Estadual de Londrina. Centro de Ciências Exatas. Programa de Pós-Graduação em Física. III. Título.

CDU 53

JULIO CESAR TOLEDO PINTO

Generalized Symmetries, Anomalies, and Long-Range Entangled Systems

Trabalho de Conclusão de Curso apresentado à Universidade Estadual de Londrina - UEL, como requisito parcial para a obtenção do título de Doutor em Física.

BANCA EXAMINADORA

Orientador: Prof. Dr. Pedro Rogério Sérgi Gomes
Universidade Estadual de Londrina - UEL

Prof. Dr. Carlos André Hernaski
Universidade Estadual de Londrina

Prof. Dr. Rodrigo Corso B. Santos
Universidade Estadual de Londrina

Prof. Dr. Renann Lipinski Jusinskas
Institute of Physics of the Czech Academy of Sciences

Dr. Weslei Bernadino Fontana
National Tsing Hua University

Londrina, 14 de maio de 2025

To my family and friends, whose constant support and encouragement made this work possible.

Agradecimentos

Primeiramente, gostaria de registrar meus sinceros agradecimentos ao meu orientador, Dr. Pedro Rogerio Sergi Gomes, por seu apoio, paciência e orientação ao longo de todo este trabalho e dos anos que antecederam meu doutorado.

Em segundo lugar, expresso minha profunda gratidão à minha família, que sempre esteve ao meu lado em todos os momentos, oferecendo carinho e motivação. Sem o suporte familiar, este caminho teria sido muito mais desafiador.

Também gostaria de agradecer ao meu melhor amigo e físico, Guilherme Delfino, por sua ajuda incessante com assuntos de física, conselhos de vida e tantos outros aspectos. Sua generosidade e amizade inestimáveis foram fundamentais, tornando cada etapa muito mais leve e produtiva. Também gostaria de agradecer à minha amiga Samy por todo o carinho e apoio dados.

Por fim, reconheço e agradeço ao Conselho Nacional de Desenvolvimento Científico e Tecnológico (CNPq) pelo apoio financeiro e incentivo à pesquisa científica no Brasil.

"Science is generated by and devoted to free inquiry: the idea that any hypothesis, no matter how strange, deserves to be considered on its merits."

Carl Sagan

Resumo

PINTO, Julio Cesar Toledo. **Simetrias Generalizadas, Anomalias e Sistemas Com Emaranhamento de Longo Alcance**. 2025. 73fls. Tese de Doutorado em Física – Universidade Estadual de Londrina, Londrina, 2025.

Esta tese investiga a emergência de ordens topológicas a partir do empilhamento de fases de matéria protegidas por simetria (SPTs), explorando a relação entre simetrias, anomalias e emaranhamento de longo alcance. Introduzimos a construção por empilhamento anômalo (ASC), uma estrutura na qual a ordem topológica emerge de acoplamentos apropriados entre camadas SPT, guiados pela imposição de anomalias mistas de 't Hooft. Esta abordagem permite gerar fases topologicamente ordenadas em dimensões superiores a partir de blocos elementares de baixa dimensionalidade. Como resultado central, construímos e analisamos o código Levin-Gu-Fracton (LGF), obtido aplicando o ASC ao modelo de Levin-Gu. O código LGF apresenta excitações do tipo fracton e degenerescência do estado fundamental subextensiva, com restrições associadas a simetrias de subsistema e anomalias mistas. Tais características indicam seu potencial como plataforma para o estudo de ordens topológicas do tipo fracton. Estudamos também a abordagem de fios quânticos aplicada às fases de Hall quântico fracionário, recuperando descrições de teoria de campo efetiva e conectando os resultados à teoria de Chern-Simons e às dualidades. Esta construção reproduz os estados de Laughlin e sugere caminhos para a realização de fases topológicas não abelianas mais exóticas. Em conjunto, estas construções contribuem para o entendimento de como simetrias e anomalias podem ser usadas como ferramentas na construção de novas fases da matéria.

Palavras-chave: Simetrias generalizadas; Anomalias; Emaranhamento de longo alcance; Fases topológicas protegidas por simetria; Construção por camadas; Fios quânticos; Dualidades.

Abstract

PINTO, Julio Cesar Toledo. **Generalized Symmetries, Anomalies, and Long-Range Entangled Systems**. 2025. 73p. Doctoral Thesis – Universidade Estadual de Londrina, Londrina, 2025.

This thesis investigates the emergence of topological orders from stacks of symmetry-protected topological (SPT) phases, exploring the interplay between symmetries, anomalies, and long-range entanglement. We introduce the anomalous stacking construction (ASC), a framework where topological order arises from suitably coupled SPT layers guided by the enforcement of mixed 't Hooft anomalies. This approach enables the construction of higher-dimensional topologically ordered phases from lower-dimensional building blocks. A central result is the construction and analysis of the Levin-Gu-Fracton (LGF) code, obtained by applying the ASC to the Levin-Gu SPT. The LGF code exhibits fracton-like excitations and a subextensive ground state degeneracy, with constraints rooted in subsystem symmetries and mixed anomalies. These features highlight the model's potential as a platform to explore fracton topological order. Additionally, we study the quantum wire construction of fractional quantum Hall phases, recovering known effective field theory descriptions and establishing connections with Chern-Simons theory and dualities. This framework not only reproduces Laughlin states, but also suggests paths toward the realization of more exotic non-Abelian topological phases. Taken together, these constructions contribute to the understanding of how anomalies and symmetry principles can serve as guiding tools for building new phases of matter.

Keywords: Generalized symmetries; Anomalies; Topological phases; Symmetry-protected phases; Layer construction; Quantum wires; Dualities.

List of Figures

Contents

1 Introduction

Symmetries have long played a foundational role in physics, serving as guiding and organizing principles for constructing and understanding physical theories [1]. At the most basic level, symmetries are transformations that leave a physical system invariant, and their presence leads to powerful constraints on the dynamics of the system. Noether's theorem provides a connection between continuous symmetries and conservation laws, linking symmetry transformations to conserved quantities, such as energy, momentum, or charge [2].

In quantum field theory (QFT) and condensed matter physics, symmetries do more than merely conserve quantities, they organize the structure of physical theories. Ward identities, for instance, encode the implications of symmetry at the level of correlation functions, ensuring consistency between symmetry transformations and quantum dynamics. Symmetries also lead to selection rules, constraining the possible transitions or allowed operators in a theory. Beyond these direct consequences, symmetry often provides a unifying language across seemingly different phenomena, serving as a key organizing principle in classifying phases of matter, formulating effective field theories, and understanding the emergence of dualities [3, 4], where distinct theories describe the same underlying physics. In this sense, symmetry offers a deep form of universality.

Another central aspect of symmetries is spontaneous symmetry breaking, a mechanism with far-reaching consequences, from the emergence of Goldstone bosons in low-energy quantum field theories to the realization of ordered phases in condensed matter systems, such as ferromagnets and superfluids [5]. The nature of the symmetry-breaking pattern and the associated low-energy degrees of freedom play an important role in determining the system's physical properties. Even more subtle is the role of anomalies, which arise when classical symmetries fail to survive quantization. Far from being pathologies, anomalies often carry essential physical information. They can protect gapless edge modes, constrain renormalization group flows, and diagnose obstructions to gauging global symmetries. Anomalies can also be matched across different energy scales, providing nonperturbative constraints on the infrared behavior of quantum field theories, even in strongly coupled regimes [6, 7, 8].

The traditional classification of usual phases of matter is rooted in the Landau paradigm, which characterizes different phases by the spontaneous breaking of usual global symmetries and the associated local order parameters. Within this framework, phase transitions are understood through changes in symmetry-breaking patterns, and continuous transitions are described using renormalization group flows and critical exponents. This approach has been remarkably successful in describing a wide range of classical and

quantum systems, including ferromagnets, superconductors, and superfluids.

However, the discovery of quantum phases of matter that do not fit into this symmetry-breaking scheme has revealed fundamental limitations of the Landau paradigm [9]. Notably, topologically ordered phases, such as those appearing in the fractional quantum Hall effect [10, 11, 12, 13] and certain quantum spin liquids [14, 15], exhibit long-range entanglement and topologically dependent ground state degeneracy, without any local order parameter or symmetry breaking of usual symmetries. Similarly, symmetry-protected topological (SPT) phases are distinct from trivial phases only in the presence of a global symmetry, yet they do not exhibit spontaneous symmetry breaking [8, 16]. These examples illustrate that quantum phases of matter can exhibit structure beyond the reach of traditional classification schemes, necessitating new theoretical frameworks that incorporate entanglement, topology, and generalized notions of symmetry.

Recently, significant advancements in theoretical physics have expanded the notion of symmetry beyond conventional groups, leading to more sophisticated frameworks known as generalized symmetries [17, 18, 19, 20, 21]. These include higher-form, non-invertible, and subsystem symmetries, which offer powerful tools for classifying and understanding complex quantum phases that evade traditional symmetry-based approaches.

Higher-form symmetries generalize ordinary (0-form) global symmetries by acting on extended operators rather than point-like operators [22]. In QFT, p-form symmetries act on operators supported on p-dimensional manifolds, and the conserved charges for continuous symmetries are associated with integrals over codimension-$(p+1)$ surfaces. These symmetries have proven instrumental in diagnosing confinement and deconfinement phenomena, as well as in characterizing topologically ordered phases in gauge theories. In condensed matter systems, higher-form symmetries appear naturally in models with emergent gauge structures, such as the toric code and related lattice gauge theories.

Non-invertible symmetries do not admit an inverse operation in the usual group-theoretic sense. Instead, their fusions define algebraic structures often described by fusion categories [20]. In QFT, non-invertible symmetries arise in rational conformal field theories, topological quantum field theories, and more recently, in strongly coupled gauge theories. In condensed matter physics, they are tied to emergent anyonic excitations and dualities in low-energy effective theories.

Subsystem symmetries act on lower-dimensional submanifolds of space, such as lines or planes in a higher-dimensional system, rather than on the full spatial volume. These symmetries are central to the study of fracton phases of matter, which exhibit excitations with restricted mobility and an abundance of conserved quantities [23, 24]. Subsystem symmetries challenge conventional paradigms of symmetry breaking and classification, leading to novel types of order that are neither conventional symmetry-breaking nor topological in the usual sense.

Like their conventional counterparts, generalized symmetries serve as organizing

principles in both quantum field theory and condensed matter physics. They also constrain the dynamics of a system, lead to generalized selection rules, and govern the allowed operator content and possible phase transitions. These symmetries can also be spontaneously broken, giving rise to generalized versions of Goldstone modes or defect excitations associated with the broken symmetry. Moreover, generalized symmetries can possess anomalies, indicating an obstruction to gauging them or signaling the presence of nontrivial boundary degrees of freedom. These mechanisms, well-known in the study of ordinary global symmetries, extend meaningfully to these generalizations. A generalized Landau paradigm exists, fitting some of the unusual quantum phases of matter not captured by the usual paradigm [25].

Despite significant progress, several questions remain open regarding the interplay between symmetries, anomalies, and topological phases. This thesis aims to explore connections between these concepts, where the central themes are layer construction approaches. We study the emergence of higher-dimensional topological phases of matter from the stacking of lower-dimensional systems. In the following paragraphs, we discuss the main contributions of this thesis.

In our proposed construction, we consider a stack of SPT systems, each one defined on a lattice with periodic boundary conditions. We also impose periodic boundary conditions in the stacking direction. The SPTs stack have a symmetry structure inherited from the symmetry that protects each layer. We proceed by "coupling" the SPT layers, and the guide principle to the coupling is to enforce a mixed 't Hooft anomaly involving the stack symmetry and a new, chosen symmetry, possibly implying in long-range entanglement and non-trivial ground state degeneracy. We refer to this layer construction as Anomalous Stacking Construction (ASC) [8, 16, 26]. We use ASC to demonstrate explicitly how well-known topological orders such as the $D = 3$ toric code [27] can be obtained from the $D = 2$ cluster SPT, and how the generalization of the toric code to $D = 4$ can be obtained from a $D = 3$ higher-form SPT model.

Subsequently, we engineer a novel Hamiltonian model in $D = 4$ dimensions, derived by aplying the ASC on the Levin-Gu SPT. We refer to the resultant model as Levin-Gu-Fracton (LGF) code. We analyze the LGF code by computing its ground state degeneracy from the existence of topological constraints, and its examine the symmetries. In matter of fact, the LGF code has subsystem symmetries, signaling the existence of fractonic excitations. The topological nature of the LGF code is indicated by its non-trivial, subextensive ground state degeneracy, as well by the presence of topological constraints and mixed 't Hooft anomalies between the subsystem symmetries.

In the second application of the layer method, we employ the quantum wires construction to present a unified and insightful approach to understanding Laughlin states of the fractional quantum Hall systems [28, 29, 30, 31]. Through detailed mappings between microscopic and macroscopic degrees of freedom, we reveal direct connections between

different effective field theories. Crucially, this approach unveils a network of dualities in three-dimensional systems, further highlighting the role that anomalies play in constraining and characterizing these exotic quantum states.

The thesis is structured as follows. Chapter 2 provides a comprehensive discussion of gapped phases of matter. We first focus usual phases of matter. Afterwards, we focus on SPT phases and present the examples of the cluster and Levin-Gu models. Subsequently, we turn to topological orders and fracton orders, illustrating the discussion with the $D = 3$ toric code topological order, and plaquette and X-cube fracton orders. Chapter 3 elaborates on layer construction methods used to derive topological orders and fracton orders from lower-dimensional systems. In the first part, we present the anomalous stacking construction, exemplifying the method by deriving the $D = 3$ and $D = 4$ toric codes from the $D = 2$ cluster model and a $D = 3$ higher-form SPT. We then construct the LGF code using the $D = 3$ Levin-Gu model and analyze its properties. In the second part of Chapter 3, the quantum wires framework is applied to construct quantum Hall systems, with emphasis on QFT dualities between the possible effective field theory descriptions. Finally, Chapter 4 summarizes the key results and discusses their broader implications, outlining potential directions for future research.

2 Gapped Phases of Matter

One of the main goals of this thesis is to understand how symmetries and their properties shape the structure of quantum phases of matter. In this chapter, we investigate gapped phases of matter, which include usual phases, described by the Landay symmetry-breaking theory, as well as SPT phases, intrinsic topological orders, and fracton orders. As we will discuss along the chapter, these phases differ fundamentally in their entanglement structure and symmetry response. The distinction and interplay between SPTs, intrinsic topological orders, and fracton orders is central to modern condensed matter theory.

2.1 General Notion of Gapped Phases of Matter

In this section, we briefly present a general notion of a gapped quantum phase of matter, whose properties depends on how the atoms of the associated material are arranged and ordered. These arrangements and orders can be understood in terms of symmetries associated with the model capturing the underlying physics. Let us start with a broad definition of a gapped quantum phase of matter. Consider a general family of lattice quantum Hamiltonians $H(g,\Lambda)$, which depend smoothly on a parameter $g \in [0,1]$ and on a given lattice Λ. We say that the ground state $|0\rangle_{g,\Lambda}$ of $H(g,\Lambda)$ realizes a gapped quantum phase if there is a finite energy gap between $|0\rangle_{g,\Lambda}$ and excited states, no matter the size L_Λ of the lattice Λ. A phase transition occurs when the expectation value $\lim_{L_\Lambda\to\infty} \langle\mathcal{O}\rangle_{g_c,\Lambda}$ of a local operator $\mathcal{O}$ has a singular behavior for a given critical parameter g_c.

The notion of phase transition allows one to declare if two states, e.g. $|0\rangle_{0,\Lambda}$ and $|0\rangle_{1,\Lambda}$, represent the same phase of matter: if the energy gap of $H(g,\Lambda)$ remains finite for all values of $g \in [0,1]$, then there is no phase transition along the path g, meaning that the ground states for $g = 0,1$ realize the same gapped quantum phase of matter. Phrasing differently, if two gapped states $|0\rangle_{0,\Lambda}$ and $|0\rangle_{1,\Lambda}$ represent the same gapped quantum phase of matter, then it is always possible to find a family of Hamiltonians $H(g,\Lambda)$ such that the energy gap for $H(g,\Lambda)$ remains finite along the parameter path g. This continuous notion of phase of matter can be associated with a local unitary adiabatic connection between the states, which is a local unitary evolution [32].

2.2 Global Symmetries and Usual Gapped Phases of Matter

This section briefly introduces concepts of symmetry in closed usual quantum systems. Special emphasis is placed on the structure and implications of 0-form global symmetries, which act uniformly on local degrees of freedom [22]. These will serve as a

reference point for the generalized notions of symmetry, such as higher-form and subsystem symmetries, discussed in the following sections.

In many-body systems, we extend the concept of symmetry to transformations that act uniformly across space. These are called global symmetries. The simplest and most fundamental type of global symmetry is a 0-form symmetry, which acts on local degrees of freedom at each site in space. In the lattice context, this symmetry acts independently of spatial structure, i.e., it is defined by the tensor product over local unitary actions:

$$U = \bigotimes_i U_i, \tag{2.1}$$

where each U_i is a local unitary acting on the Hilbert space at site i. Such symmetries are often called onsite, and they play a central role in both statistical and quantum systems.

The importance of 0-form symmetries stems from their ubiquity and their compatibility with gauging procedures. Because the symmetry acts locally it is possible to couple the system to a background gauge field and to define gauged versions of the theory: an essential property for studying anomalies and dualities. Not all symmetries can be written in an onsite form. A symmetry is called non-onsite if it involves long-range entangling gates or nonlocal operations.

Symmetries place strong constraints on the dynamics of quantum systems. At the level of the Hamiltonian, symmetry requires that

$$UHU^\dagger = H, \tag{2.2}$$

which forbids symmetry-breaking terms and restricts the allowed interactions. At the level of observables, symmetry imposes selection rules and Ward identities.

For continuous symmetries, Noether's theorem establishes a deep connection between symmetry and conservation laws. Given a continuous symmetry generated by Q, invariance under this transformation implies

$$[H, Q] = 0 \quad \Rightarrow \quad \frac{dQ}{dt} = 0. \tag{2.3}$$

In lattice systems with a discrete time evolution, this statement translates into the conservation of Q under the Heisenberg picture evolution.

Other consequences of symmetry include:

- Constraints on the allowed terms in H, such as forbidding certain mass or interaction terms;
- Selection rules: if an operator O does not preserve symmetry sectors, its matrix elements vanish between states of different charge;
- Correlation constraints: for example, in a Z_2 symmetric theory, odd operators like ϕ must have vanishing expectation value in a symmetric phase: $\langle\phi\rangle = 0$.

Symmetries can also be broken spontaneously in the ground state of a system, even when the Hamiltonian is symmetric. This phenomenon is central to phase transitions and ordering phenomena. In the Landau paradigm, symmetry breaking is diagnosed by a local order parameter ϕ such that

$$\langle \phi \rangle \neq 0, \tag{2.4}$$

which transforms nontrivially under the symmetry. A classic example is the Ising model: in the broken phase, the Z_2 spin-flip symmetry is broken by nonzero magnetization.

For continuous symmetries, spontaneous breaking leads to Goldstone modes. Goldstone's theorem states that for every broken generator of a continuous symmetry, there exists a gapless excitation. In field-theoretic language, this appears as a pole in the two-point correlation function at zero energy. It is important to stress that the dynamics of such system is local, being a direct reflection of the locality of the order parameter, encoding the Goldstone bosons. This locality property is also associated with the short-range entanglement patterns of usual phases of matter.

In some cases, symmetries cannot be consistently realized at the quantum level. These are known as anomalies. More precisely, a quantum anomaly is an obstruction to gauging a classical symmetry, or to realizing a symmetry in a strictly local fashion. A familiar example is the chiral anomaly in 1+1D systems, where conservation of chiral current is violated at the quantum level despite being classically conserved. Another class of anomalies, called 't Hooft anomalies, appear when a symmetry cannot be realized as an onsite action on a local Hilbert space. These anomalies are important diagnostics of boundary theories and topological phases.

Anomalies have profound implications for the structure of physical systems. First, they imply that a system cannot be simultaneously gapped and symmetric unless it develops intrinsic topological order. Moreover, the boundary of a topological phase must either spontaneously break the symmetry or remain gapless, reflecting the obstruction to realizing the symmetry locally in a gapped way. Finally, anomalies indicate that certain symmetry patterns cannot be consistently realized in strictly D-dimensional systems, and must instead emerge at the boundary of higher-dimensional bulk phases.

These insights have profound implications for the classification of quantum phases. In particular, anomalies help identify boundaries of SPT phases and constrain renormalization group flows. In the next sections, we will generalize these notions of symmetry beyond the 0-form case. Higher-form symmetries, subsystem symmetries, and non-invertible symmetries provide a much broader and richer framework, capturing emergent conservation laws, fractonic behavior, and categorical symmetry structures.

2.3 Symmetry Protected Topological Phases

We now focus on SPT phases, which are gapped quantum phases of matter that cannot be distinguished by local order parameters. Instead, SPTs are characterized by their response to symmetry operations [16, 8, 33]. Generalized symmetries discussed earlier, including higher-form, non-invertible, and subsystem symmetries, play a crucial role in identifying and classifying these phases. This chapter provides a detailed exploration of SPT phases by presenting illustrative examples, highlighting their underlying physics, symmetry structures, and boundary phenomena. The first example is the cluster SPT. We indicate how the cluster state can be seen either as a $\mathbb{Z}_2 \times \mathbb{Z}_2$ SPT and a $\mathrm{Rep}(D_8)$ SPT. The second one is the Levin-Gu SPT, where we present its Hamiltonian description, the symmetry group $\mathbb{Z}_2$ that protects the phase, and some aspects of its boundary theory.

2.3.1 Defining SPT

A SPT phase can generally be defined as a phase of matter possessing a unique, gapped ground state on a closed manifold, with nontrivial boundary states on open manifolds that are protected by the symmetry of the system. These phases become trivial if the protecting symmetry is explicitly or spontaneously broken [16, 8]. Therefore, studying SPT phases naturally follows from understanding generalized symmetries, as they serve as essential tools for distinguishing between topologically trivial and nontrivial quantum phases.

When a Hamiltonian model H realizing an SPT is defined on a closed manifold, its ground state remains gapped from the excited states, with the energy gap tending to a constant as the volume of the system increases. Moreover, the Hamiltonian H possesses a global symmetry generated by an operator U, such that $[H, U] = 0$.

If the same model is defined on an open manifold or in the presence of an interface between distinct phases, it may exhibit protected boundary phenomena. These edge or interface features depend on the dimension of the system. In one-dimensional systems, there is often a ground state degeneracy; in two dimensions, either degeneracy or gapless edge modes can arise; and in three dimensions, one may encounter degeneracy, gapless modes, or even emergent topological order at the boundary.

These boundary features are protected by the global symmetry generated by U. That is, if the Hamiltonian is deformed to $H' = H + \delta H$, where δH is a symmetric perturbation that also commutes with U, the qualitative features of the boundary remain unchanged. This robustness under symmetric deformations is a defining aspect of SPT phases.

SPT phases are distinct from intrinsically topologically ordered phases in several important ways. They do not support topological ground state degeneracy on closed manifolds, nor do they host anyonic or fractonic excitations in the bulk. Furthermore, SPTs

lack intrinsic chirality and do not exhibit spontaneous symmetry breaking or symmetry anomalies in the bulk.

Several well-known models are not considered SPTs. Examples include the Majorana chain, the integer quantum Hall effect, the $p+ip$ superconductor, and the $\mathbb{E}_8$ model. These systems either break time-reversal symmetry, exhibit chirality, or support intrinsic topological order.

An intriguing aspect of SPT phases is that upon gauging the protecting global symmetry, the resulting theory may display spontaneous symmetry breaking of the dual symmetry. This can lead to new phases of matter with nontrivial dynamical or topological features that emerge from the gauged construction.

2.3.2 Cluster Model

The cluster model [34, 35] is a paradigmatic example of a SPT phase, illustrating how generalized symmetries can protect nontrivial quantum states. In this section and the next, we will discuss two SPT phases that exist in $D = 2$ and $D = 3$ dimensions. The SPT aspects of the ground state of each model will be explored using the interface definition of a SPT and the features that appears in the interfaces.

Product Model and Cluster Model

We introduce the cluster Hamiltonian and contrast it explicitly with trivial product state Hamiltonians, highlighting the essential role symmetries play in distinguishing nontrivial topological phases from trivial ones. The models associated with each of these SPTs are given by

$$H^{prod} = -\sum_{i=1}^{L} X_i \quad \text{and} \quad H^{cluster} = -\sum_{i=1}^{L} Z_{i-1}X_iZ_{i+1}, \tag{2.5}$$

where L is an even number. The model on the left realizes a ground state which is a product state given by $|prod\rangle = |++\cdots+\rangle$, while the model on the right realizes a ground state which is called cluster state. These cluster and product Hamiltonians and ground states are related as

$$H^{cluster} = VH^{prod}V^{-1} \quad \text{and} \quad |cluster\rangle = V|prod\rangle, \tag{2.6}$$

where the unitary operator V is given by

$$V = \frac{1}{2}\prod_{i=1}^{L}(1 + Z_i + Z_{i+1} - Z_iZ_{i+1}). \tag{2.7}$$

Both models have the global symmetries generated by

$$\begin{aligned} \eta^o &= X_1X_3\cdots X_{L-1}, \\ \eta^e &= X_2X_4\cdots X_L. \end{aligned} \tag{2.8}$$

Notice that V does not commute with η^o and η^e, meaning that the ground states of these models are equivalent if one disregard their symmetries. In the next section, we will check that these ground states are not equivalent when we consider the symmetries.

Difference between the phases

We explore in depth the distinction between trivial and cluster phases, focusing on how generalized symmetries provide diagnostic tools to identify and classify such distinctions. The procedure that we will use to check that the ground state of these models realize different $\mathbb{Z}_2 \times \mathbb{Z}_2$ SPTs goes as follows. Consider a periodic one-dimensional lattice of even length L, with a partition at position L' also even, and a interface Hamiltonian given by

$$H^{interface} = -\sum_{i=2}^{L'} Z_{i-1}X_iZ_{i+1} - \sum_{i=L'+1}^{L} X_i. \tag{2.9}$$

Notice that above we made a choice for the boundary conditions of this interface model. However as we will see, all the arguments we will gave are based on anomalies, which are properties that are independent of dynamics.

We will denote by $\mathcal{G}$ the ground state space of the Hamiltonian $H^{interface}$. It is possible to check that all the Hamiltonian operators commute with each other. Among them, there are $L'-2$ operators of the ZXZ type and $L-L'$ of the X type. Since the system has L $\mathbb{Z}_2$ degrees of freedom, and number of operators ixs $L-2$, the ground state degeneracy of such a model is

$$\dim \mathcal{G} = 2^{L-(L-2)} = 4. \tag{2.10}$$

The origin of this ground state degeneracy can be seen as follows. In the ground state space, any state $|\psi\rangle \in \mathcal{G}$ must satisfy

$$\begin{aligned} Z_{i-1}X_iZ_{i+1}|\psi\rangle &= +|\psi\rangle, \quad i \in \{2,3,\cdots,L'-1\}, \\ X_i|\psi\rangle &= +|\psi\rangle, \quad i \in \{L'+1, L'+2, \cdots, L\}. \end{aligned} \tag{2.11}$$

From these identities, one can show that

$$\begin{aligned} \eta^e|\psi\rangle &= \overbrace{X_2}^{Z_1Z_3}\overbrace{X_4}^{Z_3Z_5}\cdots\overbrace{X_{L'-2}}^{Z_{L'-3}Z_{L'-1}} X_{L'}\overbrace{X_{L'+2}}^{1}\overbrace{X_{L'+4}}^{1}\cdots\overbrace{X_L}^{1}|\psi\rangle \\ &= Z_1Z_{L'-1}X_{L'}|\psi\rangle \\ &= \eta^e_L\eta^e_R|\psi\rangle, \end{aligned} \tag{2.12}$$

where we have defined $\eta^e_L \equiv Z_1$ and $\eta^e_R \equiv Z_{L'-1}X_{L'}$. Analogously

$$\eta^o|\psi\rangle = \eta^o_L\eta^o_R|\psi\rangle, \tag{2.13}$$

where $\eta_L^o \equiv X_1 Z_2$ and $\eta_R^o \equiv Z_{L'}$. Notice that these operators commute with the Hamiltonian and that they satisfy the algebra

$$\eta_L^e \eta_L^o = -\eta_L^o \eta_L^e \quad \text{and} \quad \eta_R^e \eta_R^o = -\eta_R^o \eta_R^e, \tag{2.14}$$

indicating that the symmetries are anomalous (due to the projective representation). The anomaly leads to the observed ground state degeneracy. The existence of such edge modes indicates that the ground states are different $\mathbb{Z}_2 \times \mathbb{Z}_2$ SPTs. In what follows, we will discuss the non-invertible symmetry of the cluster model and explain how its ground state realizes a non-invertible SPT.

Non-invertible symmetry in the $D = 2$ cluster model

The cluster model serves as a rich example of non-invertible symmetries [36]. We discuss how these symmetries form a fusion category and how they impact the classification of the SPT phase realized by the cluster state.

Consider the cluster model, a system of qubits defined on the links of an one-dimensional periodic lattice, described by the Hamiltonian $H^{cluster}$,

$$H^{cluster} = -\sum_{i=1}^{L} Z_{i-1} X_i Z_{i+1}. \tag{2.15}$$

For L even, a symmetry of this model is generated by the operators

$$\eta^o = X_1 X_3 \cdots X_{L-1}, \quad \eta^e = X_2 X_4 \cdots X_L. \tag{2.16}$$

As shown in Ref. [36], there is an additional operator of interest in this model, defined by

$$D = T^{-1} D^e D^o, \tag{2.17}$$

where T is the lattice translation operator, and the operators D^e and D^o are given by

$$\begin{aligned} D^e &= \sqrt{2} e^{-\frac{2\pi i}{16} L} \frac{1+iX_2}{\sqrt{2}} \frac{1+iZ_2Z_4}{\sqrt{2}} \frac{1+iZ_4Z_6}{\sqrt{2}} \cdots \frac{1+iZ_{L-2}Z_L}{\sqrt{2}} \frac{1+iX_L}{\sqrt{2}} \frac{1+\eta^e}{2}, \\ D^o &= \sqrt{2} e^{-\frac{2\pi i}{16} L} \frac{1+iX_1}{\sqrt{2}} \frac{1+iZ_1Z_3}{\sqrt{2}} \frac{1+iZ_3Z_5}{\sqrt{2}} \cdots \frac{1+iZ_{L-3}Z_{L-1}}{\sqrt{2}} \frac{1+iX_{L-1}}{\sqrt{2}} \frac{1+\eta^o}{2}. \end{aligned} \tag{2.18}$$

Notice that the D operators involve factors like $(1+\eta)/2$, which are projectors into even sectors of η, indicating that the operator D is a non-invertible operator. From its definition, one can check that the D satisfies

$$\begin{aligned} DX_i &= Z_{i-1} Z_{i+1} D, \\ DZ_{i-1}Z_{i+1} &= X_i D, \end{aligned} \tag{2.19}$$

as well as $D = D^\dagger$. Using (2.19), one can show that D is a symmetry of the cluster state for a periodic lattice of even size L, since $DH^{cluster} = H^{cluster}D$. The symmetry operators η^o, η^e and D and their algebra (to be discussed later) form a structure called fusion category, specifically Rep(D_8), which is the full symmetry of the cluster model. In Chapter 2, we will briefly discuss how to extract physical consequences from the existence of the non-invertible symmetry.

A significant result we discuss is recognizing the cluster model as an SPT phase protected by a non-invertible symmetry. This discussion is based on Ref. [37]. We explicitly outline the connection between the cluster state and the non-invertible categorical symmetries, emphasizing the physical significance of these symmetries.

As we have discussed previously, the cluster model has a non-invertible symmetry generated by the operator D. It is possible to verify that the symmetry operators D, η^o and η^e satisfy the algebra

$$\begin{aligned} D\eta^e &= \eta^e D = \eta^o D = D\eta^o = D, \\ D^2 &= (1+\eta^e)(1+\eta^o), \\ D^\dagger &= D. \end{aligned} \tag{2.20}$$

The symmetry of the cluster state and its algebra in the previous equation can be captured by a fusion category called Rep(D_8), where η^e and η^o are one-dimensional irreducible representations and D is a two-dimensional irreducible representation. Using the identities

$$\eta^e \left|cluster\right\rangle = \eta^o \left|cluster\right\rangle = + \left|cluster\right\rangle, \tag{2.21}$$

and

$$D\eta^e = \eta^e D = \eta^o D = D\eta^o = D, \quad D^2 = (1+\eta^e)(1+\eta^o), \tag{2.22}$$

it is possible to conclude that

$$D \left|cluster\right\rangle = +2 \left|cluster\right\rangle, \tag{2.23}$$

indicating in fact that D is a symmetry of the cluster state. As we will argue in the following lines, the cluster state is a Rep(D_8) SPT, but it is not the only state realizing such SPT. Contrasting with the $\mathbb{Z}_2 \times \mathbb{Z}_2$ symmetry case, the product state is not a SPT of $Rep(D_8)$. However, mathematical results guarantee that there are three distinct Rep(D_8) SPT states, which we indicate below.

The Hamiltonian models that describe the three Rep(D_8) SPTs are given by

$$\begin{aligned} H^{cluster} &= -\sum_{i=1}^{L} Z_{i-1}X_iZ_{i+1}, \\ H^{even} &= +\sum_{i=1}^{L/2} Z_{2i}X_{2i+1}Z_{2i+2} - \sum_{i=1}^{L/2} Y_{2i+1}X_{2i+2}Y_{2i+3} + \sum_{i=1}^{L/2} Z_{2i}Z_{2i+1}X_{2i+2}Z_{2i+3}Z_{2i+4}, \\ H^{odd} &= +\sum_{i=1}^{L/2} Z_{2i-1}X_{2i}Z_{2i+1} - \sum_{i=1}^{L/2} Y_{2i}X_{2i+1}Y_{2i+2} + \sum_{i=1}^{L/2} Z_{2i-1}Z_{2i}X_{2i+1}Z_{2i+2}Z_{2i+3}, \end{aligned} \tag{2.24}$$

and these are defined on periodic lattices with even length L. We will now show that the ground states $|cluster\rangle$, $|even\rangle$ and $|odd\rangle$ of the cluster, even and odd models, respectively, realize the same $\mathbb{Z}_2\times\mathbb{Z}_2$ SPT, but different $\mathrm{Rep}(D_8)$ SPTs. To do so, consider the cluster and odd models in a periodic lattice of even length L and a even partition L', as previously discussed. The Hamiltonian of such an interface model is given by

$$\begin{aligned} H^{interface} = & - \sum_{i=1}^{L'} Z_{i-1}X_iZ_{i+1} \\ & + \sum_{i=L'/2+1}^{L/2} Z_{2i-1}X_{2i}Z_{2i+1} - \sum_{i=L'/2+1}^{L/2-2} Y_{2i}X_{2i+1}Y_{2i+2} + \sum_{i=L'/2+1}^{L/2-2} Z_{2i-1}Z_{2i}X_{2i+1}Z_{2i+2}Z_{2i+3}. \end{aligned} \tag{2.25}$$

As one can verify, the identities

$$\begin{aligned} Z_{i-1}X_iZ_{i+1} &= 1, \quad i\in\{1,2,\cdots,L'\}, \\ Z_{2i-1}X_{2i}Z_{2i+1} &= -1, \quad i\in\left\{\frac{L'}{2}+1,\frac{L'}{2}+2,\cdots\frac{L}{2}\right\}, \\ Y_{2i}X_{2i+1}Y_{2i+2} &= 1, \quad i\in\left\{\frac{L'}{2}+1,\frac{L'}{2}+2,\cdots\frac{L}{2}-2\right\}. \end{aligned} \tag{2.26}$$

hold when acting on any state $|\psi\rangle$ in the ground state space of $H^{interface}$. Using the above relations, we have

$$\begin{aligned} \eta^e|\psi\rangle &= \overbrace{X_2}^{Z_1Z_3}\overbrace{X_4}^{Z_3Z_5}\cdots\overbrace{X_{L'}}^{Z_{L'-1}Z_{L'+1}}\overbrace{X_{L'+2}}^{-Z_{L'+1}Z_{L'+3}}\cdots\overbrace{X_L}^{-Z_{L-1}Z_1}|\psi\rangle \\ &= |\psi\rangle, \end{aligned} \tag{2.27}$$

and

$$\begin{aligned} \eta^o|\psi\rangle &= \overbrace{X_1}^{Z_LZ_2}\overbrace{X_3}^{Z_2Z_4}\cdots\overbrace{X_{L'-1}}^{Z_{L'-2}Z_{L'}}X_{L'+1}\overbrace{X_{L'+3}}^{Y_{L'+2}Y_{L'+4}}\cdots\overbrace{X_{L-3}}^{Y_{L-4}Y_{L-2}}X_{L-1}|\psi\rangle \\ &= Z_LZ_{L'}X_{L'+1}Y_{L'+2}Y_{L-2}X_{L-1}|\psi\rangle \\ &= \eta^o_L\eta^o_R|\psi\rangle, \end{aligned} \tag{2.28}$$

where we have defined $\eta^o_L \equiv Y_{L-2}X_{L-1}Z_L$ and $\eta^o_R = Z_{L'}X_{L'+1}Y_{L'+2}$. This time, the local symmetry factors do not realize a projective algebra. The absence of an anomaly indicates that the ground states of the cluster and odd models realize the same $\mathbb{Z}_2\times\mathbb{Z}_2$ SPT.

However, we can consider also the non-invertible symmetry generated by D. The action of D in the ground state of this interface model can be obtained again by using the equations (2.26) [36],

$$\begin{aligned} D|\psi\rangle &= T^{-1}D^eD^o|\psi\rangle \\ &= (-1)^{\frac{L-L'}{4}}\left(D^{(1)}_LD^{(1)}_R + D^{(2)}_LD^{(2)}_R\right)|\psi\rangle, \end{aligned} \tag{2.29}$$

where

$$D_L^{(1)} \equiv Y_{L-2}Y_{L-1}Z_L, \quad D_R^{(1)} \equiv Z_{L'+1}, \quad D_L^{(2)} \equiv Z_{L-1}, \quad D_R^{(2)} \equiv Z_{L'}Y_{L'+1}Y_{L'+2}. \tag{2.30}$$

The local symmetry factors satisfy the algebra

$$\eta_L^o D_L^{(I)} = -D_L^{(I)}\eta_L^o, \quad \eta_R^o D_R^{(I)} = -D_R^{(I)}\eta_R^o, \quad I \in \{1,2\}\,. \tag{2.31}$$

The realization of this symmetry projective algebra indicates a 4-fold degenerate ground state space, and that when considering the full fusion category $\mathrm{Rep}(D_8)$ symmetry, the ground states of the cluster and odd model realize different SPTs. Analogous discussions could be done for the cluster-even and odd-even interfaces. These models in fact realize distinct $\mathrm{Rep}(D_8)$ SPT phases.

Selection rules and non-invertible symmetry in the cluster model

We explain how the existence of non-invertible symmetries in the cluster model results in selection rules for excitation and phase stability. This demonstrates the practical importance of categorical symmetries.

Every symmetry can be associated with selection rules, which constrain the expectation values of operators. We now analyze the consequences of non-invertible symmetries in the cluster model. Recall that the action of the symmetry operators on the cluster state is

$$\eta^e\,|cluster\rangle \;=\; \eta^o\,|cluster\rangle = +\,|cluster\rangle\,, \quad D\,|cluster\rangle = +2\,|cluster\rangle\,. \tag{2.32}$$

The algebra between the symmetry operators and the local operators reads

$$\begin{aligned} DX_i &= Z_{i-1}Z_{i+1}D, \quad DZ_{i-1}Z_{i+1} = X_iD, \\ Z_{2i+1}\eta^o &= -\eta^o Z_{2i+1}, \quad Z_{2i}\eta^e = -\eta^e Z_{2i}. \end{aligned} \tag{2.33}$$

From these identities, we can extract local constraints on the expectation values. For instance,

$$\begin{aligned} \langle cluster|\,Z_i\,|cluster\rangle &= \langle cluster|\,Z_i\eta^{o/e}\,|cluster\rangle \\ &= -\langle cluster|\,\eta^{o/e}Z_i\,|cluster\rangle \\ &= -\langle cluster|\,Z_i\,|cluster\rangle\,, \end{aligned} \tag{2.34}$$

where we use η^o (η^e) if i is odd (even), implying

$$\langle cluster|\,Z_i\,|cluster\rangle = 0, \tag{2.35}$$

indicating a zero magnetization in this ground state. Another constraint is obtained from

$$\begin{aligned}\langle cluster|\, X_i \,|cluster\rangle &= \frac{1}{2}\langle cluster|\, X_i D \,|cluster\rangle \\ &= \frac{1}{2}\langle cluster|\, D Z_{i-1} Z_{i+1} \,|cluster\rangle = \langle cluster|\, Z_{i-1} Z_{i+1} \,|cluster\rangle .\end{aligned} \tag{2.36}$$

This identity characterizes the ground-state space, as we have discussed before,

$$Z_{i-1} X_i Z_{i+1} = 1. \tag{2.37}$$

Now consider the symmetry operators which create domain walls,

$$U^o(k) = \prod_{i \le k\,:\,odd} X_i, \quad U^e(k) = \prod_{i \le k\,:\,even} X_i. \tag{2.38}$$

Notice that they are truncated versions of η^o and η^e. One can show that

$$DU^o(k) = Z_L Z_{k+1} D, \quad DU^e(k) = Z_1 Z_{k+1} D, \tag{2.39}$$

leading to

$$\begin{aligned}\langle cluster|\, U^o(k) \,|cluster\rangle &= \frac{1}{2}\langle cluster|\, DU^o(k) \,|cluster\rangle = \langle cluster|\, Z_L Z_{k+1} \,|cluster\rangle , \\ \langle cluster|\, U^e(k) \,|cluster\rangle &= \frac{1}{2}\langle cluster|\, DU^e(k) \,|cluster\rangle = \langle cluster|\, Z_1 Z_{k+1} \,|cluster\rangle .\end{aligned} \tag{2.40}$$

At this point, we invoke a general result known as Hastings' Theorem [38], which states that for gapped, short-range entangled ground states in one-dimensional systems with local Hamiltonians, all two-point correlation functions of local observables decay exponentially with the distance between them. Applying this to the cluster model, we obtain

$$\begin{aligned}\langle Z_1 Z_{k+1} \rangle_c &= \langle cluster|\, Z_1 Z_{k+1} \,|cluster\rangle - \langle cluster|\, Z_1 \,|cluster\rangle \langle cluster|\, Z_{k+1} \,|cluster\rangle \\ &\sim e^{-k/\xi},\end{aligned} \tag{2.41}$$

for some finite correlation length ξ. Since $\langle cluster|\, Z_i \,|cluster\rangle = 0$, this simplifies to

$$\langle cluster|\, Z_1 Z_{k+1} \,|cluster\rangle \sim e^{-k/\xi}, \tag{2.42}$$

which further implies that

$$\langle cluster|\, U^{o/e}(k) \,|cluster\rangle \sim e^{-k/\xi}. \tag{2.43}$$

The identity above shows that even though the truncated symmetry operators $U^{o/e}(k)$ are nonlocal (strings), their expectation values in the cluster ground state decay exponentially

with length, behaving as if they were local in a gapped phase. This reflects the short-range entangled nature of the cluster phase and is consistent with the notion that the non-invertible symmetry encoded by D is unbroken in the ground state. As a consequence , the cluster state does not support domain wall excitations.

The domain-wall selection rule, implied by the categorical symmetry algebra, still constrains possible deformations and excitations. This result would be extremely difficult to derive without knowledge of the underlying non-invertible symmetry.

2.3.3 Levin-Gu Model

The Levin-Gu model is a quantum spin system defined on the sites of a two-dimensional triangular lattice and is a prototypical example of a SPT phase. The discussion below follows Ref. [33].

The Levin-Gu model is described by the Hamiltonian

$$H^{LG} = -\sum_i P_i, \tag{2.44}$$

where the sum runs over the local projectors P_i for each vertex i on the lattice. These projectors are constructed using the X and Z Pauli operators, and their explicit form is shown in Fig. 1.

Figure 1 – Definition of the Levin-Gu projector P_i, acting on site i of the triangular lattice. It involves the Pauli-X operator at site i and a product over exponential terms containing Pauli-Z operators on vertices of the surrounding triangles.

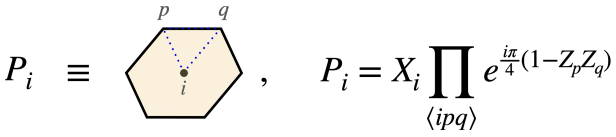

Fonte: o próprio autor.

The additional term involving Z_pZ_q introduces a nontrivial phase based on the Z-type measurements of the qubits at the vertices p and q, which are adjacent to vertex i. The factor $e^{i\frac{\pi}{4}(1-Z_pZ_q)}$ encodes the interaction between the qubits at those vertices in terms of a nontrivial entanglement structure. The key feature of the Levin-Gu model is that the projectors P_i commute with each other, making the Hamiltonian a commuting projector model. This commutativity is a hallmark of the model's structure, ensuring that the ground state is a product state of local singlets or a similar structure, and it allows for a nontrivial topological phase that is protected by symmetry.

The symmetry group $\mathcal{S}^{Levin-Gu}$ that protects the edge modes in the Levin-Gu SPT phase is a global $\mathbb{Z}_2$ symmetry. This symmetry acts nontrivially on the system and is represented by the operator W, which is defined as the product of X_i operators over

all the vertices i of the lattice:

$$\mathcal{S}^{Levin-Gu} = \{W_j\}, \quad W = \prod_i X_i. \tag{2.45}$$

This operator W can be interpreted as a symmetry that flips the state of the qubits in a way that preserves the overall topological order of the system. Crucially, this symmetry protects the topological edge modes of the system, ensuring that they are robust against perturbations as long as the symmetry is not broken.

The symmetry group $\mathcal{S}^{Levin-Gu}$ represents a global $\mathbb{Z}_2$ symmetry, meaning that it has two elements: the identity and the operator W. When the Levin-Gu model is placed on an open lattice (i.e., with boundary), this symmetry group becomes important because it protects the boundary or edge states of the system, which are typically associated with nontrivial quantum states, such as zero-energy modes or other robust topological phenomena.

Edge Modes in the Levin-Gu SPT Phase

A brief analysis of edge states in the Levin-Gu model clearly illustrates how symmetry protection manifests physically at boundaries, providing a tangible link between generalized symmetry concepts and measurable observables.

The edge modes in the Levin-Gu SPT phase are protected by the $\mathbb{Z}_2$ symmetry and the topological nature of the model. When the model is placed on a finite lattice with boundary, these edge modes manifest as low-energy states that are localized at the boundary of the system. These boundary states are typically protected by the symmetry and the topological order of the bulk. In the context of the Levin-Gu model, the edge states arise from the fact that the system is in a topologically nontrivial phase, and the boundary effectively breaks the translational symmetry, allowing the edge modes to become distinct.

The edge modes are described by operators that correspond to the actions of the global symmetry W at the boundary. The operators W_j act on the boundary qubits and protect the degeneracy of the edge modes. These modes remain at zero energy (gapless) as long as the symmetry is preserved. The structure of these modes is determined by the topological properties of the bulk. The Levin-Gu model is part of the broader class of $D = 3$ SPT phases protected by a global symmetry, and it serves as a concrete realization of such phases. These phases can be classified by the symmetry group protecting the topological order, and the Levin-Gu model specifically realizes an SPT phase protected by a $\mathbb{Z}_2$ symmetry.

In the language of the group cohomology, the Levin-Gu model corresponds to a phase described by the second cohomology class $H^2(\mathbb{Z}_2, U(1))$. The edge modes correspond to the nontrivial cohomology classes that protect the edge states from perturbations.

In this way, the Levin-Gu model serves as a key example of how SPT phases can be understood both in terms of local Hamiltonians (commuting projector models) and global symmetries.

The effect of boundary conditions on edge-state stability is explored, highlighting the role of symmetries and anomalies in preserving gapless boundary modes against local perturbations.

When the Levin-Gu model is placed on a finite lattice with open boundary conditions, the topological boundary modes become more apparent. These edge states are gapless and localized at the boundaries of the system. Importantly, they are insensitive to local bulk perturbations, such as changes to the Hamiltonian within the bulk, but are sensitive to perturbations that break the global $\mathbb{Z}_2$ symmetry. As long as the global symmetry is preserved, the edge states remain gapless and protected. This robustness is a hallmark of SPT phases. The stability of these edge states is related to the fact that the Levin-Gu model is described by a commuting projector Hamiltonian, and the edge states can be understood in terms of a nontrivial topological order that is protected by the global symmetry.

The edge modes arise from the fact that the bulk of the system is in a topologically nontrivial phase, and the presence of open boundaries effectively breaks the translational symmetry of the system. This symmetry breaking allows distinct edge states to appear at the boundaries, and these edge states are characterized by zero-energy modes that are protected by the global $\mathbb{Z}_2$ symmetry. To see this explicitly, we consider the action of the global symmetry operator W on the system, which is given by

$$W = \prod_i X_i. \tag{2.46}$$

The symmetry operator W acts nontrivially on the qubits of the system, flipping their states while preserving the overall topological order. At the boundary, the action of W leads to degenerate edge modes that remain gapless as long as the symmetry is not broken. The edge states themselves are typically localized at the boundary and form a protected subspace of the system.

The interaction between edge modes and the boundary geometry plays a key role in determining their structure. For instance, consider a boundary with multiple vertices. Each vertex introduces a degree of freedom at the edge, and the interaction between these edge modes can result in a number of distinct degenerate states. These degenerate states are linked to the topological order of the bulk and the geometry of the boundary. If we label the qubits at the boundary by an index j, the edge Hamiltonian can be expressed as

$$H_{\text{edge}} = \sum_j P_j. \tag{2.47}$$

The projector operators e P_j are defined similarly to the bulk projectors P_i, but their action is restricted to the boundary, leading to a protected ground state that is degenerate and gapless.

The degeneracy of the edge states is a manifestation of the nontrivial topological order. This degeneracy arises from the global symmetry $\mathcal{S}^{Levin-Gu}$, which protects the edge modes by maintaining the topological structure at the boundary. In the absence of symmetry-breaking perturbations, this degeneracy remains robust, and the edge modes will persist even in the presence of small bulk perturbations. However, if the symmetry is violated (for example, by adding interactions that mix edge and bulk states), the degeneracy can be lifted, and the edge modes may acquire a gap. In topological field theory, these edge modes reflect the bulk topological order encoded in the system. The edge states can be viewed as a form of entanglement between the qubits at the boundary, with the nontrivial entanglement structure being a consequence of the topological nature of the phase [39]. This entanglement can be quantified using the entanglement entropy, which for a region of the system can be written as

$$S_{\text{ent}} = -\text{Tr}(\rho \log \rho), \tag{2.48}$$

where ρ is the reduced density matrix for the subsystem. The entanglement entropy will reveal contributions from the edge states, which are typically topological in nature and remain unaffected by local perturbations as long as the global symmetry is preserved.

The specific structure of the edge modes is influenced by the boundary geometry. For example, a boundary with multiple vertices can lead to a richer structure of edge states, and the interactions between these states can give rise to different patterns of degeneracy. The action of the global symmetry operators W_j on the boundary qubits determines the structure of the edge state degeneracies. In some cases, these degeneracies can be related to topological invariants, such as the topological entanglement entropy, which provides a measure of the nontrivial topological order in the system. The open boundary conditions of the Levin-Gu model reveal the existence of robust edge states that are protected by the global $\mathbb{Z}_2$ symmetry. These edge modes provide a clear signature of the topological phase, and their behavior is intimately tied to the geometry of the boundary and the global symmetry of the system. The robustness of these edge states against local bulk perturbations makes them a crucial feature of the Levin-Gu model and other systems exhibiting SPT phases.

2.4 Topological Order

In this section, we transition from symmetry-protected phases to topologically ordered phases: gapped quantum phases of matter that exhibit long-range entanglement and are independent of any symmetry protection [40]. Topological orders represent a broader

class of gapped phases that go beyond the Landau paradigm for the usual symmetries, revealing a rich structure of quantum correlations and exotic excitations [41]. We aim to characterize these phases through physical, mathematical, and field-theoretic lenses, drawing connections to the symmetry-based principles discussed in earlier chapters.

2.4.1 Defining Topological Order

Topological order refers to a class of gapped quantum phases that fundamentally lie beyond the Landau symmetry-breaking paradigm for usual symmetries [42]. Unlike conventional phases of matter characterized by local order parameters and symmetry breaking, topologically ordered phases exhibit patterns of long-range quantum entanglement that cannot be captured by any local observable [40]. These phases are inherently nonlocal and cannot be described by spontaneous symmetry breaking or classified by local invariants.

A defining feature of topological order is the existence of ground-state degeneracy that depends on the topology of the underlying spatial manifold. For example, systems with topological order exhibit distinct degenerate ground states on the torus or higher-genus surfaces, even in the thermodynamic limit. This degeneracy is robust and cannot be lifted by any local perturbation, serving as a key signature of the nonlocal nature of the phase. Another essential characteristic is the presence of long-range entanglement. The ground state of a topologically ordered system cannot be adiabatically deformed into a trivial product state without closing the energy gap, even when no symmetry constraints are imposed [15]. This is in contrast to symmetry-protected topological (SPT) phases, which are also gapped and can appear nontrivial, but become trivial when the protecting symmetry is removed.

Topologically ordered phases also lack local order parameters. No single-site or finite-region observable can distinguish between the different ground states, and no local symmetry-breaking mechanism exists. Instead, the system is described by nonlocal order encoded in the pattern of entanglement and the behavior of extended operators such as Wilson loops or membrane operators.

Theoretical descriptions of topological order often involve emergent gauge structures. We discuss this aspect of TO in the Chap. 3, specifically in the construction of effective field theories for Laughlin states. In many models, the low-energy effective theory is a topological quantum field theory (TQFT), such as a Chern-Simons theory in $2+1$ dimensions or a BF theory in higher dimensions. These theories encode topological invariants that classify the braiding and fusion properties of quasiparticles or extended excitations.

Finally, topological order is intrinsically different from SPT phases. While both are gapped and may feature nontrivial boundary phenomena, SPT phases are short-range

entangled and require symmetry for their protection. Topological orders, in contrast, are long-range entangled and remain nontrivial regardless of symmetry considerations.

Non-local operators such as Wilson loops and membrane operators also play a central role in characterizing topological order. These operators create and move anyonic or higher-dimensional excitations along non-contractible loops or surfaces. Their algebra and braiding properties encode the fusion rules and statistical interactions of the excitations, further revealing the rich structure of the underlying topological phase.

2.4.2 Higher-Form Symmetries

Symmetries acting on extended objects, rather than on local fields or point-like operators, have emerged as a natural generalization of global symmetries in quantum field theory and many-body systems. These are known as higher-form symmetries, introduced to classify and constrain phases of matter where conventional symmetries are insufficient [22, 26]. A p-form symmetry acts on operators of spatial dimension p, and its associated conserved charges are supported on codimension-$(p+1)$ manifolds. Originally formulated in the context of gauge theories, higher-form symmetries now play a central role in the modern classification of gapped phases, particularly in topological orders and generalized anomaly inflow. In this section, we review their defining properties and structure the discussion around explicit models where such symmetries are manifest [17].

Consider a D-dimensional system with a higher-form symmetry $G^{(p)}$ of degree p. Associated to $G^{(p)}$ there are topological operators $D^{(g)}_{d-(p+1)}$ of dimension $D-(p+1)$ acting on the Hilbert space describing the states of such a system, where $g \in G^{(p)}$. For the case of higher-form symmetries, these operators are invertible, and their non-trivial linking rules with other operators define the operators that are charged under $G^{(p)}$. For continuous groups $G^{(p)}$, there is a Noether conservation law

$$d \star (J_{p+1}) = 0, \tag{2.49}$$

that allows the operators to be written as

$$D^{(g)}_{D-(p+1)} \sim e^{iQ(M_{D-(p+1)})}, \quad Q(M_{D-(p+1)}) = \int_{M_{D-p-1}} \star(J_{p+1}). \tag{2.50}$$

The topological operators fusion law follows the group composition law of $G^{(p)}$,

$$D^{(g)}_{D-(p+1)} \otimes D^{(h)}_{D-(p+1)} = D^{(gh)}_{D-(p+1)}, \quad g, h \in G^{(p)}. \tag{2.51}$$

The topological nature of $D^{(g)}_{D-(p+1)}$ is given by the fact that it depends only on the topology of the manifold $M_{D-(p+1)}$, as far as such manifold does not intersect any charged operators. In the next subsections, we will give two examples of models that exhibit higher-form symmetries.

2.4.3 $D = 3$ Toric Code

The $D = 3$ toric code [27] serves as a pivotal example of a system with higher-form symmetries on many-body quantum systems, exhibiting topological ground state degeneracies arising from a mixed 't Hooft anomaly. We explore explicitly how the anomaly governs the ground-state structure, clarifying the topological nature of its degenerate ground states. The system associated with the toric code is composed of qubits on the links of a square periodic lattice, and its Hamiltonian is given by

$$H^{TC} = -\sum_p B_p - \sum_s A_s, \quad B_p = \prod_{l \in p} Z_l, \quad A_s = \prod_{l \in s} X_l. \tag{2.52}$$

Above, p stands for plaquettes and $s \equiv star(i)$ for stars centered at the site i. One can show that this is a commuting projector Hamiltonian, since all the plaquette and star operators form a commuting set of operators. Therefore, on the ground state space $\mathcal{G}$, we have the identities

$$B_p = A_s = +1. \tag{2.53}$$

There are also topological constraints associated with these Hamiltonian operators, which are given by

$$\prod_p B_p = 1, \quad \prod_s A_s = 1. \tag{2.54}$$

Considering a 2-torus of size $L \times L$, there are $2L$ links, meaning that we have 2^{2L} distinct states in the Hilbert space. There are L operators of type B_p and L operators of type A_s, totaling $2L$ commuting operators. One could think that therefore the ground state space is non-degenerate, since the number of commuting operators is equal to the number of degrees of freedom. However, the existence of two topological constraints modifies this counting. In fact, the ground state degeneracy is given by

$$\dim \mathcal{G} = 2^{2L-(2L-2)} = 4. \tag{2.55}$$

We can understand the ground state degeneracy in terms of a mixed 't Hooft anomaly associated to the symmetry of the toric code. The global symmetries of H^{TC} are

$$W(\gamma) = \prod_{l \in \gamma} Z_l, \quad T(\gamma^*) = \prod_{l \in \gamma^*} X_l, \tag{2.56}$$

where γ are closed loops on the direct lattice and γ^* are closed loops on the dual lattice. Any contractible loop or dual loop operator can be shown to be equivalent to a product of plaquette or star operators, respectively, which clearly commute with the Hamiltonian. For this reason, we will consider only non-contractible loop operators, which we define as

$$W_a = \prod_{l \in \gamma_a} Z_l, \quad T_a = \prod_{l \in \gamma_a^*} X_l, \quad a \in \{1, 2\}. \tag{2.57}$$

In the above definitions, γ_a and $\gamma_a^\star$ stand for non-contractible loops along the a direction on the direct and dual lattice, respectively. These are $\mathbb{Z}_2$ symmetry operators since $W_a^2 = T_a^2 = 1$, and they are the generators of 1-form symmetries, since in $D = 3$ their co-dimension is equal to 2. In fact, these operators are topological, since any closed loop can be topologically deformed using plaquette and/or star operators, all of which commute with H^{TC}. For a deformation example, refer to Fig. 2.

Figure 2 – Topological deformation of the Wilson loop operator W_1 in the toric code. The initial non-contractible operator W_1 on the left (straight red line) is defined as a product of Z operators. Performing the product of W_1 with plaquette operators, also products of Zs, labeled B_1 to B_6 (dashed blue lines), results in W_1 on the right (dashed blue line). This process don't change the W_1 action on the ground state. This illustrates the topological nature of 1-form symmetry generators.

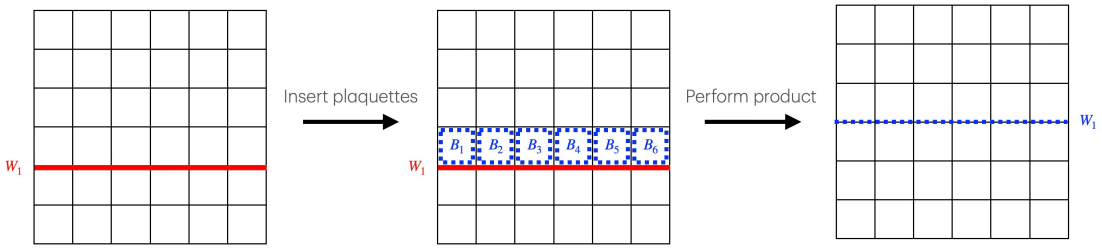

Fonte: o próprio autor.

The mixed 't Hooft anomaly between the symmetry operators,

$$W_1 T_2 = -T_2 W_1, \quad W_2 T_1 = -T_1 W_2, \tag{2.58}$$

indicates a mixed charging between Ws and Ts. This anomaly is also responsible for the 4-fold degeneracy in the ground state space, from the fact that diagonalizing with a 4-fold set of states $|{+}{+}\rangle, |{+}{-}\rangle, |{-}{+}\rangle, |{-}{-}\rangle$ satisfying

$$\begin{aligned} W_1|{+}{+}\rangle &= +|{+}{+}\rangle, \quad W_1|{+}{-}\rangle = +|{+}{-}\rangle, \\ W_1|{-}{+}\rangle &= -|{-}{+}\rangle, \quad W_1|{-}{-}\rangle = -|{-}{-}\rangle, \end{aligned} \tag{2.59}$$

and

$$\begin{aligned} W_2|{+}{+}\rangle &= +|{+}{+}\rangle, \quad W_2|{+}{-}\rangle = -|{+}{-}\rangle, \\ W_2|{-}{+}\rangle &= +|{-}{+}\rangle, \quad W_2|{-}{-}\rangle = -|{-}{-}\rangle, \end{aligned} \tag{2.60}$$

makes the T_a operators map one ground state to one of the other three. In fact, one can show that the four states $|{+}{+}\rangle, |{+}{-}\rangle, |{-}{+}\rangle, |{-}{-}\rangle$ are quantum superpositions of all possible dual loop configurations, where $|{+}{+}\rangle$ has no non-contractible loops, while the other ground states contain non-contractible ones, as shown in Fig.3.

Figure 3 – Four ground states of the toric code on the torus labeled by eigenvalues $(\pm,\pm)$ of loop operators (W_1, W_2). Red and blue lines indicate non-contractible loop operators T_1 (along x) and T_2 (along y), acting as products of X-Pauli matrices on the dual lattice.

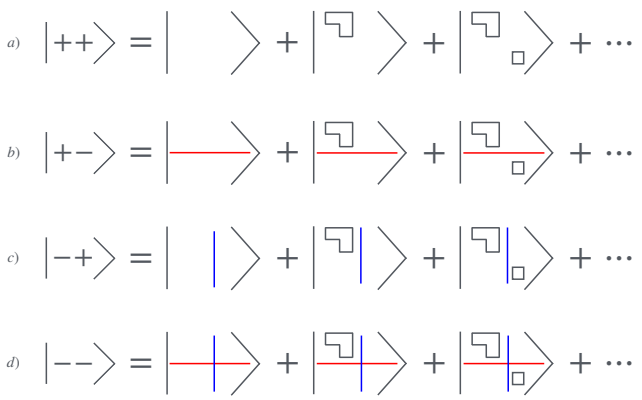

Fonte: o próprio autor.

The ground state $|{+}{+}\rangle$ of the toric code can be explicitly written as

$$|{+}{+}\rangle = \sum_{\{\theta_s\}} \prod_s A_s^{\theta_s} |\uparrow\uparrow\cdots\uparrow\rangle\,, \quad \theta_s \in \{0,1\}\,, \tag{2.61}$$

where $Z_i |\uparrow\rangle_i = +|\uparrow\rangle_i$ and $Z_i |\downarrow\rangle_i = -|\downarrow\rangle_i$, and the other ground states can be reached through the action of T_1, T_2 and T_1T_2.

Now, we turn our attention to the operators that create the toric code anyons and investigate the expectation values of local operators in the toric code ground state. In this fashion, we identify some topological order signatures of the underlying model. We begin by examining the excitations of the toric code. These excitations can be created by acting on the ground state with truncated symmetry operators. For example, open lines of Zs (Xs) on the original (dual) lattice, as illustrated in Fig. 4.

Figure 4 – Excitations in the toric code created by truncated symmetry operators. **Left:** A Z-string on the direct lattice creates a pair of bosonic vertex (electric) excitations e_1 and e_2. **Center:** An X-string on the dual lattice creates bosonic plaquette (magnetic) excitations m_1 and m_2. **Right:** Z and X strings generate fermionic f excitations, composed of an e and an m at the same site.

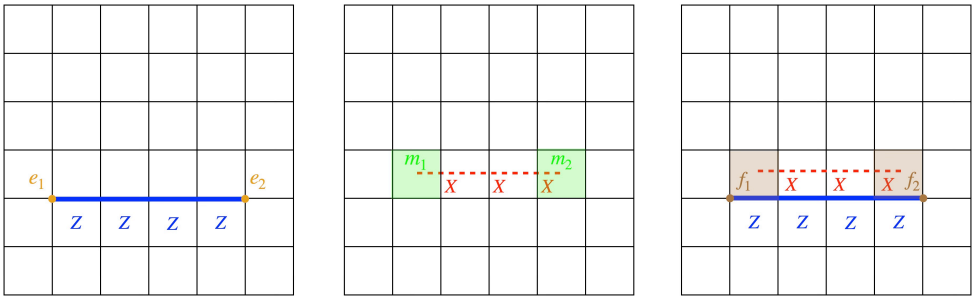

Fonte: o próprio autor.

The anti-commutation relation between these open strings and the Hamiltonian operators at their boundaries indicates that indeed create pairs of excitations. As illustrated in Fig. 4, open strings of Z operators on the direct lattice generate e particles at their endpoints, while open strings of X operators on the dual lattice produce m excitations. When both e and m are present at the same location, the resulting composite excitation f behaves as a fermion. Their creation is shown in the right panel of Fig. 4. All these excitation are anyons, and can be created, destroyed, and moved by acting with open strings of X and Z operators. The action of local operators cannot create, destroy, or move anyons. This anyonic structure of the toric code can be encoded by a non-trivial unitary modular tensor category, indicating the topological nature of the toric code phase.

To conclude the discussion of the toric code, we compute the matrix elements of local operators $\mathcal{O}$ in the ground state basis. The operator identity we want to prove is

$$\langle\xi|\,\mathcal{O}\,|\chi\rangle = C\delta_{\xi\chi}, \quad |\xi\rangle, |\chi\rangle \in \mathcal{G}, \tag{2.62}$$

where C is a constant. This condition implies that a local operator has the same expectation value in every topological ground state. It also ensures that distinct topological sectors are not connected by local operators.

For the $\xi = \chi$ case in (2.62), notice that

$$\langle\xi|\,\mathcal{O}\,|\xi\rangle = \langle\xi|\,U_\theta^\dagger U_\theta \mathcal{O} U_\theta^\dagger U_\theta\,|\xi\rangle = \langle\xi'|\,U_\theta \mathcal{O} U_\theta^\dagger\,|\xi'\rangle, \tag{2.63}$$

where we used the fact that for any $\theta = \{\theta_1, \theta_2\}$, we have $U_\theta \equiv T_1^{\theta_1} T_2^{\theta_2}$, $\theta_i \in \{0, 1\}$ as a symmetry operator that does not change the amplitude above, and the T_1 and T_2 operators map one ground state to another ground state. No matter if the local operator $\mathcal{O}$ intersects U_θ or not, it is always possible to deform the T_1 and T_2 topological operators inside it in order to remove such intersection. From this statement, we have

$$\langle\xi|\,\mathcal{O}\,|\xi\rangle = C, \quad \forall\,|\xi\rangle \in \mathcal{G}. \tag{2.64}$$

For $\xi \neq \chi$ we can use the fact that the symmetry of the toric code has a mixed 't Hooft anomaly, characterized by the equation

$$W_a T_b = -T_b W_a, \quad a \neq b. \tag{2.65}$$

This can be seen from example by defining $|\chi\rangle \equiv U_\theta\,|\xi\rangle$, where we have

$$\begin{aligned}
\langle\xi|\,\mathcal{O}\,|\chi\rangle &= \langle\xi|\,\mathcal{O} U_\theta\,|\xi\rangle \\
&= \langle\xi|\,\mathcal{O} T_1^{\theta_1} T_2^{\theta_2}\,|\xi\rangle \\
&= \langle\xi|\,W_a^2 \mathcal{O} W_a^2 T_1^{\theta_1} T_2^{\theta_2}\,|\xi\rangle \\
&= (-1)^{\theta_{\bar{a}}} (w_a^\xi)^2\,\langle\xi|\,\mathcal{O} T_1^{\theta_1} T_2^{\theta_2}\,|\xi\rangle \\
&= (-1)^{\theta_{\bar{a}}}\,\langle\xi|\,\mathcal{O}\,|\chi\rangle,
\end{aligned} \tag{2.66}$$

where $\bar{a} = 2\delta_{1a} + \delta_{2a}$, and we have used the identities

$$\begin{aligned} W_a^2 &= 1, \quad W_a \mathcal{O} W_a = \mathcal{O}, \\ W_a T_b^{\theta_b} &= (-1)^{\theta_b} T_b^{\theta_b} W_a, \quad a \neq b, \\ W_a |\xi\rangle &= w_a^\xi |\xi\rangle, \quad (w_a^\xi)^2 = 1. \end{aligned} \tag{2.67}$$

The above identity is $\langle\xi| \mathcal{O} |\chi\rangle = -\langle\xi| \mathcal{O} |\chi\rangle$ for the case $\theta_{\bar{a}} = 1$ that the operator U_θ would not be the identity. Therefore, no matter what the initial state $|\xi\rangle$ is, we proved that

$$\langle\xi| \mathcal{O} |\chi\rangle = 0, \quad \forall\, |\xi\rangle \neq |\chi\rangle \in \mathcal{G}. \tag{2.68}$$

Therefore,

$$\langle\xi| \mathcal{O} |\chi\rangle = C\delta_{\xi\chi}, \tag{2.69}$$

for any local operator $\mathcal{O}$. This indicates the absence of spontaneous symmetry breaking of 0-form symmetries, and that the toric code phase does not fit the usual Landau paradigm. The presence of the mixed 't Hooft anomaly discussed previously signals a SSB of 1-form symmetries, exemplifying the relation between SSB and intrinsic topological orders. For more details on this connection between higher-form anomalies and intrinsic topological orders, see Ref. [43].

2.5 Fracton Orders

Fracton phases of matter are a striking subclass of topological orders where the excitations have restricted mobility. These models challenge conventional notions of topological order and introduce new phenomena such as subsystem symmetries and foliation structures. This subsection outlines the key features of fracton orders and their connection to layered constructions.

2.5.1 Defining Fracton Order

Fracton phases exhibit an unique form of fractionalization, which manifests through the restricted mobility of excitations [44]. The excited state space contain sub-dimensional particles that can only move in coordination with others. These immobile point-like excitations are called fractons. In some cases, mobility is not entirely restricted—certain excitations can move along one-dimensional lines or two-dimensional planes. These are referred to as lineons and planons, respectively [45].

The sub-dimensional nature of these excitations can be naturally understood through a foliation structure. As a simple example, consider multiple uncoupled copies of the 3D toric code stacked along a fourth dimension, as illustrated in Fig. 5. In the thermodynamic limit, this construction forms a four-dimensional system with a clearly defined

foliated structure. Since the layers remain uncoupled, excitations (electric or magnetic) are restricted to their respective planes, naturally giving rise to planons. This simple construction provides key intuition: fracton systems can be understood as emerging from coupled lower-dimensional systems. This idea was formalized in Ref. [46] in terms of networks of topological defects embedded within stratified 3+1D TQFTs. The authors further conjecture that all gapped phases, including fracton phases, can be described through a topological defect network framework

Figure 5 – Copies of stacked uncoupled toric codes, with electric and magnetic anyons.

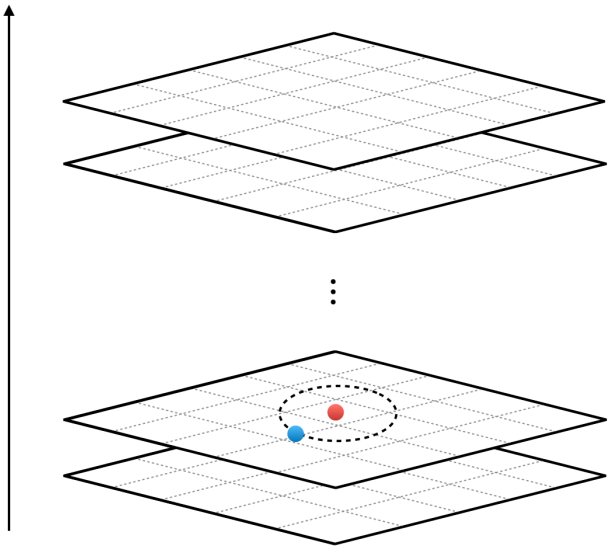

Fonte: o próprio autor.

Examples of fracton topological order include the X-cube model (see Sec. 2.5.3), Haah's code, and the Levin-Gu-Fracton code (see Sec. 3.2). The X-cube model features sub-dimensional particles such as fractons and lineons, arising from a stabilizer code with cubic symmetry and subsystem conservation laws. Haah's code, on the other hand, introduces an even more exotic type of immobility where fracton excitations are not only strictly immobile but also cannot be separated without creating a fractal pattern of excitations. The Levin-Gu-Fracton code, discussed in detail in Chapter 3.2, provides an alternative route to fracton physics by starting from stacked SPT phases and deforming the local symmetry algebra to induce a sub-extensive ground-state degeneracy and fractonic excitations.

A connection between SPT phases and intrinsic topological orders was explored in Ref. [33] through the process of gauging global symmetries. When a global symmetry of an SPT phase is gauged in $D = 3$ dimensions, the resulting system transitions into a topologically ordered phase. This transformation replaces the symmetry-protected boundary states with deconfined bulk excitations, leading to emergent gauge charges and fluxes that characterize intrinsic topological order.

Subsystem symmetries play an important role in the fracton physics. These symmetries act on lower-dimensional sections or subsystems within a system, fundamentally different from the usual higher-form symmetries due to their rigidity [47, 48, 49, 50]. Their presence often indicates fracton-like behavior in the system. Fractons appear in two types, where the type I have fracton topological excitations that have restricted mobility on lower-dimensional manifolds, while the type II have immobile fracton topological excitations. In this section, we will review subsystem symmetries and their relation with fractons. It is hard to discuss a general theory of subsystem symmetries, and for this reason we will explore them through examples. For review papers on the topic, we refer the reader to [45, 44].

In the next chapter, we propose a framework for constructing topological orders and fracton phases through the anomalous stacking of $D = 3$ SPTs. By stacking and suitably coupling layers of lower-dimensional SPT phases, one can engineer higher-dimensional systems that exhibit restricted mobility of excitations, as well as emergent higher-form and subsystem symmetries. This approach reveals a deep structural connection between SPT phases and intrinsic topological order: small deformations of the SPT layer Hamiltonians can lead to new gapped phases with long-range entanglement and fractonic properties. We illustrate this mechanism by stacking and coupling $D = 3$ layers of Levin-Gu layers, resulting in a system we refer to as the Levin-Gu-Fracton code. This model features immobile excitations and an enforced anomaly structure. We believe that anomalous stacking and gauging constructions are closely related, and that exploring this connection is a promising direction for future research.

2.5.2 Plaquette model

This subsection explores the subsystem symmetries within the plaquette model, demonstrating how these symmetries lead directly to restricted mobility excitations, highlighting the link between subsystem symmetry and fractonic phenomena. This model is also known as Xu-Moore code and was proposed in Ref. [51]. Consider a system of qubits on the sites of a periodic square lattice of size $L_x \times L_y$, described by the Hamiltonian

$$H^{plaquette} = -\sum_p B_p - h\sum_i X_i, \quad B_p = \prod_{i\in p} Z_i, \tag{2.70}$$

where p stand for unit plaquettes on the lattice. We can check that any non-contractible loop $\gamma_{j,a}$ along the a direction and that goes through site j defines a symmetry operator

$$W(\gamma_{j,a}) = \prod_{i\in\gamma_{j,a}} X_i. \tag{2.71}$$

As we have line operators in $D = 3$, one could think that they generate a 1-form symmetry. However, they are not topological, since they cannot be deformed. In fact, the symmetry generated by these operators is a subsystem symmetry.

As we will discuss now, subsystem symmetries are responsible for the emergent lineon-like excitations in this model. Applying a Pauli X at a site i creates four plaquette excitations, as expected since such operators do not commute with $H^{plaquette}$. A rigid line of X operators along the x or y-direction moves two of the four excitations. Notice that these operations that move lineon-like excitations can be thought as open versions of the symmetry operators. Analyzing $H^{plaquette}$ for general h values can be challenging. We will restrict our analysis to the $h \ll 1$ regime.

Even in this regime, the ground state degeneracy cannot be determined. However, the low-energy physics is dominated by the plaquette excitations. Therefore, we set $h = 0$ and interpret the $h \ll 1$ regime using perturbation theory to gain insights into the ground state space organization. In the $h = 0$ point we have

$$H^{plaquette}|_{h=0} = -\sum_p B_p. \tag{2.72}$$

All the B_p operators commute with each other, and therefore the Hamiltonian is manifestly gapped. We can count the ground state degeneracy by counting the number of degrees of freedom, Hamiltonian $\mathbb{Z}_2$ operators and topological constraints. The ground state space $\mathcal{G}$ is defined by the condition

$$B_p = +1. \tag{2.73}$$

On a 2-torus of size $L_x \times L_y$, we have $L_x \times L_y$ degrees of freedom and B_p. Furthermore, the number of constraints between the different plaquette operators is sub-extensive, since there is one for each non-contractible loop on the x or y direction. The constraints are given by

$$\prod_{j \in \gamma_{j,a}} B_{p_j} = 1, \tag{2.74}$$

where p_j stands for the plaquette of which the most down left corner is at site j. There are L_y distinct non-contractible loops in the x direction and L_x along the y direction, but the product of B_p along all these lines are not independent, since each line fixes the eigenvalue of one B_p. Therefore, there is a total of $L_x + L_y - 1$ constraints. Using this counting, the ground state degeneracy is also sub-extensive, and it is given by

$$\dim \mathcal{G} = 2^{L_x L_y - [L_x L_y - (L_x + L_y - 1)]} = 2^{L_x + L_y - 1}. \tag{2.75}$$

As we turn on the h parameter, we expect both the ground state degeneracy and the gap to continue to exist, since the subsystem symmetry is not broken.

2.5.3 X-Cube model

The X-Cube model [52] exemplifies the role of subsystem symmetries in producing fracton physics, including immobile excitations and constrained dynamics. The explicit construction and implications of these symmetries are discussed.

The $\mathbb{Z}_2$ X-cube model describes qubits on the links of a three-dimensional cubic periodic lattice, an its Hamiltonian is

$$H^{X-cube} = -\sum_{\vec{x}} C_{\vec{x}} - \sum_{\vec{x},a} A^{(a)}_{\vec{x}}, \tag{2.76}$$

where the cube and star operators are defined in the Fig.6.

Figure 6 – Illustration of the stabilizer operators in the X-Cube model. Panel (a) shows the cubic terms involving Pauli X operators, enforcing local constraints on spin degrees of freedom. Panel (b) displays the star terms involving Pauli Z operators.

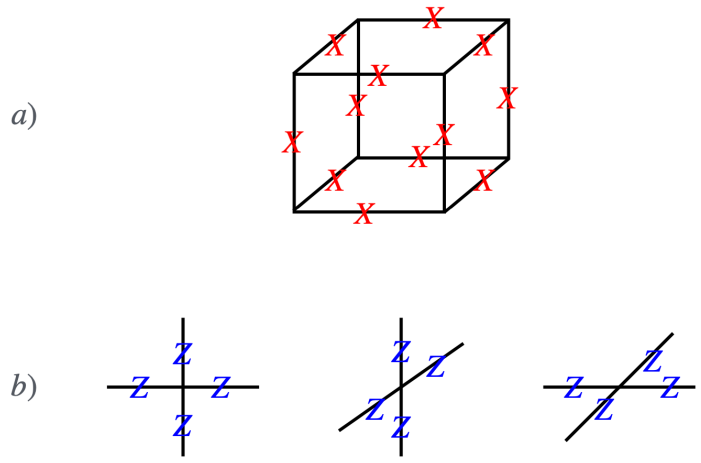

Fonte: o próprio autor.

This is a commuting projector Hamiltonian, so expect it to describe a gapped phase. The symmetries of this model are generated by

$$W_{a,\vec{x}} = \prod_{l \in \gamma_{a,\vec{x}}} Z_l, \quad T_{a,j^*} = \prod_{l \in \gamma^*_{a,l^*}} X_l, \tag{2.77}$$

where $\gamma_{a,\vec{x}}$ is the non-contractible loop going through the site $\vec{x}$ along the direction a, and γ^*_{a,l^*} is the non-contractible loop going through the link l^* along the direction a. Each of these generate a $\mathbb{Z}_2$ subsystem symmetry.

An open line of $W_{a,\vec{x}}$ produces a dipole of star excitations that can move freely, but only along the direction of the dipole, due to the rigidity of the lines. Applying X operators on open membranes align with the coordinate planes creates four cube excitations at the corners of the membrane. These membrane can be deformed into any shape, and the excitations can only move as bound states.

3 Layer Construction of Topological Orders

Building upon our discussions of generalized symmetries, anomalies, and SPT phases [8, 16], this chapter proposes a method to generate higher-dimensional topological orders by "stacking and coupling" lower-dimensional SPT phases. We refer to this method as Anomalous Stacking Construction (ASC) . General layer constructions provide systematic approaches to understanding how complex quantum phases arise from simpler, well-characterized systems by stacking and coupling them. We demonstrate the efficacy of this method through examples, including constructions $D = 3$ and $D = 4$ toric codes, as well as a new $D = 4$ topological model derived via ASC from the Levin-Gu SPT.

In the second part of this chapter, we discuss the quantum wire construction of topological orders, focusing on applications to quantum Hall systems [53, 54]. We highlight how distinct low-energy effective field theories can emerge and reveal novel dualities within the quantum Hall framework [3].

3.1 Anomalous Stacking Construction

This section explores the construction of topological orders, proposing that "stacking and coupling" SPT models can induce a mixed 't Hooft anomaly, which have several consequences and long-range entangled states and non-trivial ground state degeneracy.

3.1.1 General Picture

The general idea behind layer construction is explicitly outlined, where multiple lower-dimensional SPT phases are stacked and coupled to form a higher-dimensional topologically ordered phase. Even though the overall philosophy resembles a foliated construction [23, 55], here symmetries and anomalies of the underlying lower-dimensional systems are a key ingredient.

Consider a system composed of N copies of a SPT phase, each described by a Hamiltonian H_j^{SPT} defined on d-dimensional lattice Λ_j indexed by j (see Fig. 7), and written as a sum of commuting operators P_{ij},

$$H = \sum_{j=1}^{N} H_j^{SPT}, \quad H_j^{SPT} = -\sum_{i\in\Lambda_j} P_{ij}, \quad [P_{ij}, P_{i'j'}] = 0. \tag{3.1}$$

Figure 7 – Stacking of SPTs with symmetries $\mathcal{S}_i$, generated by W_i.

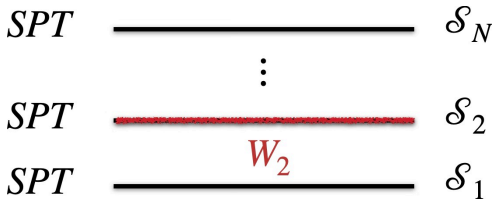

Fonte: o próprio autor.

In general, the spatial stack can be of any dimension greater than d. We also impose periodic boundary conditions along the stacking direction. The symmetry of the full stack is the Cartesian product of the individual layer symmetries $\mathcal{S}^{stack} = \mathcal{S}_1 \times \mathcal{S}_2 \times \cdots \times \mathcal{S}_N$. The full stack symmetry in this case is realized by the local symmetric algebra, given by

$$\mathcal{A}^{stack} = span\left\{P_{ij}\right\}. \tag{3.2}$$

In general, a local symmetric algebra associated with a symmetry $\mathcal{S}$ is the set of operators that commute with the symmetry operators,

$$\mathcal{A} \equiv \left\{\mathcal{O} \,|\, \mathcal{O}U = U\mathcal{O},\ \forall U \in \mathcal{S}\right\}. \tag{3.3}$$

These local symmetric operators can be used to construct general Hamiltonian models that realize a given symmetry [56]. Building on this framework, we construct a gapped, long-range entangled phase whose symmetry $\mathcal{S}^{\text{enforced}}$ contains the original stack symmetry $\mathcal{S}^{\text{stack}}$ and exhibits a prescribed 't Hooft anomaly. The choice of $\mathcal{S}^{\text{enforced}}$ is, in principle, arbitrary.

In general, H^{stack} does not realize $\mathcal{S}^{enforced}$. In order to realize $\mathcal{S}^{enforced}$, we consider a deformed local symmetric algebra $\mathcal{A}^{deformed}$ by imposing some requirements that changes the initial stack algebra $\mathcal{A}^{stack}$. The elements of $\mathcal{A}^{deformed}$ will be used as building blocks to compose the new Hamiltonian $H^{deformed}$ that realizes the gapped long-range entangled system with an anomalous symmetry.

The general deformation we make over $\mathcal{A}^{stack}$ follows some rules:

1. The new algebra must be obtained by using elements of $\mathcal{A}^{stack}$ in such way that $\mathcal{A}^{deformed} = span\left\{P'_{ij}\right\}$ realizes the symmetry $\mathcal{S}^{enforced}$. This means that the elements of the algebra commutes with the generators of the new enforced symmetry (see Fig. 8);

2. $\mathcal{A}^{deformed}$ must realize higher-dimensional lattice model, where the operators that compose the deformed Hamiltonian $H^{deformed}$ couple different layers;

3. The deformed Hamiltonian will have a gapped spectrum spectrum by demanding that $H^{deformed}$ is composed by commuting operators.

Figure 8 – Anomaly enforcement guide based on the original symmetries $\mathcal{S}_i$.

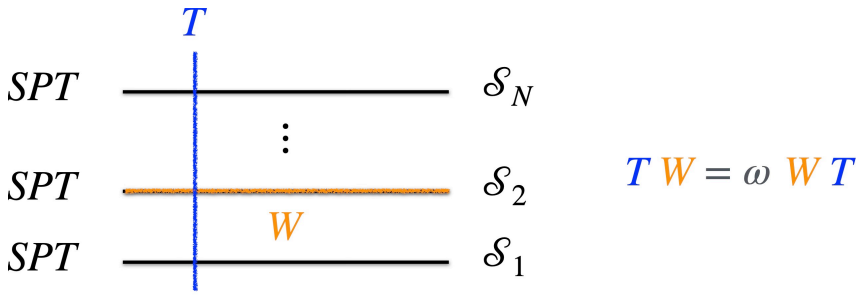

Fonte: o próprio autor.

After the steps described above, we will have a deformed Hamiltonian constructed from $P'_{ij} \in \mathcal{A}^{deformed}$,

$$H^{deformed} = -\sum_{ij} P'_{ij}. \tag{3.4}$$

Notice that under such construction of $\mathcal{A}^{deformed}$ might realize a deformed symmetry $\mathcal{S}^{accidental}$ which is bigger than the enforced symmetry $\mathcal{S}^{enforced}$, since we required that at least $H^{deformed}$ realizes $\mathcal{S}^{enforced}$. In other words, we expect some "accidental" symmetries to appear in the end of the process, meaning that the final symmetry might contain more symmetries than we wanted in the first place. A schematically representation of the construction is present in the Fig. 9.

Figure 9 – Schematic representation of constructing long-range entangled phases with enforced $\mathbb{Z}_2$ 't Hooft anomaly. Initially, a stack of N SPT layers with symmetry $\mathcal{S}^{\text{stack}}$ and algebra $\mathcal{A}^{\text{stack}}$ is considered. By deforming this algebra to $\mathcal{A}^{\text{deformed}}$, coupling layers, a new gapped Hamiltonian H^{deformed} realizes the anomalous symmetry $\mathcal{S}^{\text{accidental}}$ that contains $\mathcal{S}^{enforced}$ and $\mathcal{S}^{\text{stack}}$.

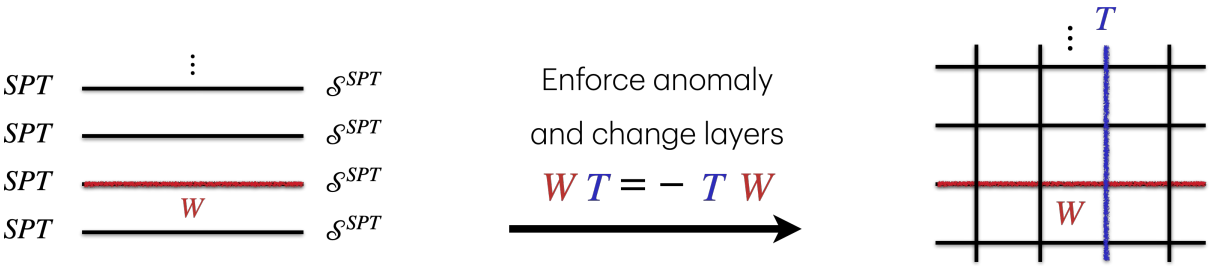

Fonte: o próprio autor.

There are some general, scale-independent statements that we can make about this construction. The Hamiltonian H^{deformed} realizes a gapped, nontrivial phase with a 't Hooft anomalous symmetry $\mathcal{S}^{\text{accidental}}$. This anomaly is nontrivial and does not depend on the specific realization determined by the operator content of H^{deformed}, even though a particular realization must still be chosen within this framework. Consequently, the

partition function obtained by gauging the emergent symmetry $\mathcal{S}^{\text{accidental}}$ is not well-defined. This implies that the anomaly cannot be removed by adding any counterterm that depends only on background gauge fields. However, the anomaly can be canceled in a higher-dimensional theory defined on an open manifold, where the boundary is governed by H^{deformed} and the bulk theory is an invertible TQFT.

3.1.2 From the $D = 2$ cluster model to the $D = 3$ toric code model

We explicitly present the construction of the $D = 3$ toric code [27] via anomalous stacking construction of $D = 2$ cluster SPT phases. This construction illustrates how the resulting model inherits nontrivial topological features, including ground state degeneracy and fractional excitations, from the underlying SPT phases.

Consider a stack of $\mathbb{Z}_2$ cluster models, each defined on a one-dimensional lattice with an even number of sites L_x and periodic boundary conditions, with qubits placed at the sites. The stacked cluster model is described by the Hamiltonian

$$H^{stack} = -\sum_{j=1}^{L_y}\sum_{i=1}^{L_x} Z_{i-1,j}X_{i,j}Z_{i+1,j}. \tag{3.5}$$

We also imposed periodic boundary conditions along the stacking direction. The anomaly-free symmetry group of the cluster model is $\mathbb{Z}_2^{(0)} \times \mathbb{Z}_2^{(0)}$, and it is generated by

$$W_j^o = \prod_{i=0}^{L_x/2-1} X_{2i+1,j}, \quad W_j^e = \prod_{i=1}^{L_x/2} X_{2i,j}. \tag{3.6}$$

We will use the stacked cluster model to construct a topologically ordered phase using the ASC.

The stack symmetry is given by the union over layers, $\mathcal{S}^{stack} = \bigcup_{j=1}^{L_y} \left\{W_j^o, W_j^e\right\}$, which is realized by the local symmetric algebra

$$\mathcal{A}^{stack} = span\left\{Z_{i-1,j}X_{i,j}Z_{i+1,j}\right\}. \tag{3.7}$$

We now consider a 't Hooft anomalous symmetry $\mathcal{S}^{enforced} \supset \mathcal{S}^{stack}$. In this construction, we choose the symmetry generated by

$$\mathcal{S}^{enforced} = \mathcal{S}^{stack} \cup \left\{T_i = \prod_{j=1}^{L_y} Z_{i,j}\right\}. \tag{3.8}$$

This choice is relatively simple, as the added generators consist of Pauli-Z operators along the stacking direction. Under this choice, the 't Hooft anomaly manifests in the symmetry algebra as

$$W_j^o T_{2i+1} = -T_{2i+1}W_j^o, \quad W_j^e T_{2i} = -T_{2i}W_j^e, \tag{3.9}$$

while all other operator pairs commute. We now proceed to the algebra deformation.

To motivate the deformation from the algebra $\mathcal{A}^{stack}$ to the algebra $\mathcal{A}^{deformed}$, we highlight the physical intuition and symmetry constraints guiding the construction. The original algebra $\mathcal{A}^{stack}$ respects only the local symmetry generated within each one-dimensional cluster model. However, the introduction of the anomalous symmetry $\mathcal{S}^{enforced}$ demands a redefinition of local operators so that the new symmetry generators T_i commute with the algebra elements. Physically, this corresponds to coupling adjacent layers along the stacking direction, transforming the initially trivial stacked system into one with genuine three-dimensional structure.

To realize this explicitly, we observe that operators in $\mathcal{A}^{stack}$ fail to commute with T_i due to the presence of isolated Pauli-X single-layer terms. To satisfy the symmetry conditions, the operators must couple pairs of neighboring layers, ensuring commutation with the global Z-string operators T_i. Thus, a possible deformation is to replace the intra-layer ZXZ operator with $ZXXZ$ operator, where the extra Pauli-X comes from an adjacent layer (see Fig. 10).

Figure 10 – Examples of the deformation of local symmetric algebra on the lattice.

Fonte: o próprio autor.

By alternating the position of Pauli-X insertions between even and odd lattice sites in adjacent layers, potential anti-commutation arising from overlapping Pauli operators is systematically eliminated. This guarantees the existence of a stabilizer algebra structure, essential for describing a well-defined, gapped Hamiltonian.

Therefore, an algebra deformation that satisfies the required conditions is

$$\mathcal{A}^{deformed} = span\left\{Z_{2i-1,j}X_{2i,j}X_{2i,j-1}Z_{2i+1,j},\ Z_{2i,j}X_{2i+1,j}X_{2i+1,j+1}Z_{2i+2,j}\right\}. \tag{3.10}$$

The most general Hamiltonian related to this deformed algebra is given by

$$H^{deformed} = -\sum_{j=1}^{L_y}\sum_{i=1}^{L_x/2}\left(Z_{2i-1,j}X_{2i,j}X_{2i,j-1}Z_{2i+1,j} + Z_{2i,j}X_{2i+1,j}X_{2i+1,j+1}Z_{2i+2,j}\right). \tag{3.11}$$

The full symmetry realized by $H^{deformed}$ is $\mathcal{S}^{accidental} = \mathbb{Z}_2^{(1)} \times \mathbb{Z}_2^{(1)}$, and this Hamiltonian can be mapped into the $D = 3$ toric code Hamiltonian when L_x and L_y are even.

3.1.3 From the $D = 3$ higher-form SPT model to the $D = 4$ toric code model

We detail the application of ASC to a higher-form SPT phase (see Ref. [57]), resulting the emergence of the $D = 4$ toric code model [58]. We start with a stack of $2d$ SPT models described by local Hilbert spaces of qubits on sites and links of a square lattice, with periodic boundary conditions on the layers and on the stacking direction. The stacked Hamiltonian, with layers labeled by k, is given by

$$\begin{aligned} H^{stack} &= -\sum_{k=1}^{L_z}\sum_{i=1}^{L_x}\sum_{j=1}^{L_y}(S_{ijk}+H_{ijk}+V_{ijk}), \\ S_{ijk} &= Z_{i-1/2,j,k}Z_{i,j-1/2,k}Z_{i,j,k}Z_{i,j+1/2,k}Z_{i+1/2,j,k}, \\ H_{ijk} &= X_{i-1,j,k}X_{i+1/2,j,k}X_{i+1,j,k}, \\ V_{ijk} &= X_{i,j-1,k}X_{i,j+1/2,k}X_{i,j+1,k}. \end{aligned} \tag{3.12}$$

The indices $i, j \in \mathbb{Z}$ label the coordinates of sites, $i + \frac{1}{2}, j + \frac{1}{2}$ label the links, and $k \in \mathbb{Z}$ labels the layers. We impose periodic boundary conditions along the stacking direction. This commuting projector Hamiltonian describes a stack of $D = 3$ SPTs protected by the higher-form symmetry generated by

$$\mathcal{S}^{stack} = \{W_k(\gamma), T_k\}, \quad W_k(\gamma) = \prod_{l\in L(\gamma)} X_{l,k}, \quad T_k = \prod_{ij} Z_{i,j,k}. \tag{3.13}$$

Here, γ is any closed loop in the xy plane and $L(\gamma)$ denotes the set of links along γ. The local symmetric algebra of H^{stack} that realizes $\mathcal{S}^{stack}$ is

$$\mathcal{A}^{stack} = span\{S_{ijk}, H_{ijk}, V_{ijk}\} \tag{3.14}$$

Following our procedure, we choose to enforce the symmetry

$$\mathcal{S}^{enforced} = \mathcal{S}^{stack} \cup \{W_{ij}\}, \quad W_{ij} = \prod_k X_{i,j,k}, \tag{3.15}$$

and its associated 't Hooft anomaly is captured by commutation relation

$$W_{ij}T_k = -T_kW_{ij}. \tag{3.16}$$

To motivate the deformation from the algebra $\mathcal{A}^{stack}$ to the algebra $\mathcal{A}^{deformed}$ in this higher-dimensional setting, we follow analogous symmetry and physical arguments to those used in the previous example. Initially, the algebra $\mathcal{A}^{stack}$ represents independent layers of $2d$ higher-form SPT phases, each symmetric under the generators $\mathcal{S}^{stack}$. However, by introducing the additional symmetry operators W_{ij}, which form part of the enforced symmetry $\mathcal{S}^{enforced}$, the original operators no longer satisfy commutation conditions with these new generators.

We require a redefinition of local operators to ensure commutation with W_{ij}. Physically, this implies coupling layers along the stacking direction, converting the initially

independent stack into a coherent, intrinsically four-dimensional structure. Concretely, the operators S_{ijk}, H_{ijk}, and V_{ijk} fail to commute with the global symmetry operators W_{ij} due to their strictly local nature in each layer.

To restore symmetry compatibility, we deform S_{ijk} by introducing Pauli-Z operators from adjacent layers, yielding:

$$S_{ijk} \to A_{ijk} = Z_{i,j,k+1} S_{ijk}. \tag{3.17}$$

This specific choice ensures commutation with W_{ij} operators, as it now incorporates operators from multiple layers, forming inter-layer connections.

Similarly, to guarantee commutation among all algebra elements, operators H_{ijk} and V_{ijk} are replaced by plaquette operators B_p, consisting of products of Pauli-X operators arranged symmetrically in the xy-plane and connecting multiple layers. These plaquette operators form closed loops, ensuring mutual commutation and thus achieving a stabilizer structure necessary for topological order:

$$H_{ijk}, V_{ijk} \to B_p = \prod_{e \in p} X_e. \tag{3.18}$$

The carefully constructed deformation thus not only resolves the symmetry anomaly but also naturally results in a gapped, long-range entangled state. Hence, the deformation from $\mathcal{A}^{stack}$ to $\mathcal{A}^{deformed}$ is physically motivated by symmetry enforcement and the necessity of creating topological order, characterized by robust ground-state degeneracies and fractionalized excitations.

Therefore, a possible deformation of $\mathcal{A}^{stack}$ that realizes $\mathcal{S}^{enforced}$ and fulfills our requirements is

$$\begin{aligned} \mathcal{A}^{deformed} &= \{A_{ijk},\, B_p\}\,, \\ A_{ijk} &= Z_{i,j,k+1} S_{ijk}, \\ B_p &= \prod_{e \in p} X_e. \end{aligned} \tag{3.19}$$

Using this deformed algebra, we can construct the most general Hamiltonian realizing $\mathcal{S}^{deformed}$,

$$H^{deformed} = -\sum_{ijk} A_{ijk} - \sum_{p} B_p. \tag{3.20}$$

The resulting model realizes the $D = 4$ toric code, and the emergent symmetry $\mathcal{S}^{\text{accidental}}$ corresponds to the symmetry of the $D = 4$ toric code, as one can check from the operator content of $H^{deformed}$.

3.2 $D = 4$ Levin-Gu-Fracton Code

We introduce a novel $D = 4$ topological model constructed via ASC of Levin-Gu SPT phases [33]. We refer to this model as the Levin-Gu-Fracton (LGF) code. We describe

the stacking procedure in detail. We explore several features of the LGF code, including its sub-extensive ground state degeneracy and subsystem symmetries.

3.2.1 ASC for the Levin-Gu SPT

Recall that the Levin-Gu SPT is defined by a system of qubits on the sites of a two-dimensional triangular lattice, and its Hamiltonian description is given by

$$H^{stack} = -\sum_{j=1}^{L_z}\sum_{i} P_{i,j}, \tag{3.21}$$

with the $P_{i,j}$ projectors defined in Fig. 1. The stacked system is protected by the global symmetry $\mathbb{Z}_2^{\otimes L_z}$ global symmetry, where the generator set is

$$\mathcal{S}^{stack} = \{W_j\}, \quad W_j = \prod_i X_{i,j}. \tag{3.22}$$

Figure 11 – Stacking of Levin-Gu SPTs.

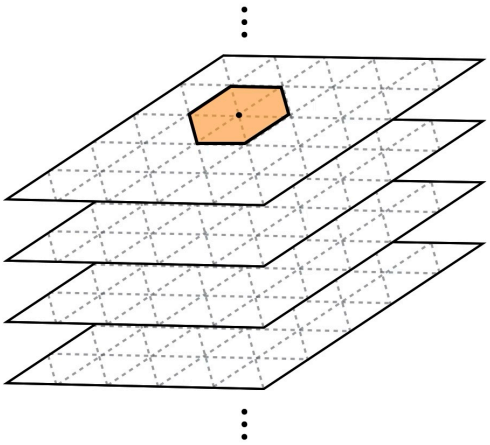

Fonte: o próprio autor.

The associated local symmetric algebra realizing $\mathcal{S}^{stack}$ is

$$\mathcal{A}^{stack} = span\{P_{ij}\}. \tag{3.23}$$

We choose to enforce the following anomalous symmetry:

$$\mathcal{S}^{enforced} = \mathcal{S}_1 \cup \{T_i\}, \quad T_i = \prod_j Z_{i,j}. \tag{3.24}$$

The mixed 't Hooft anomaly in $\mathcal{S}^{enforced}$ is reflected by the commutation relation

$$W_j T_i = -T_i W_j \quad \forall\, i, j. \tag{3.25}$$

Notice that $\mathcal{S}^{enforced}$ is not a symmetry of the stacked Hamiltonian H^{stack}. However, we can construct a modified model that realizes this symmetry.

To motivate the deformation from $\mathcal{A}^{stack}$ to $\mathcal{A}^{deformed}$ for the stacked Levin-Gu SPT model, we first consider the symmetry requirements imposed by the anomalous enforced symmetry $\mathcal{S}^{enforced}$. Initially, each layer independently realizes a Levin-Gu SPT, protected by the global symmetry generators W_j. However, when enforcing the additional symmetry generated by T_i, the original algebra elements $P_{i,j}$ no longer commute with this enlarged symmetry group, as one can check.

Figure 12 – Diagrammatic representation of the choice of deformed symmetry generators.

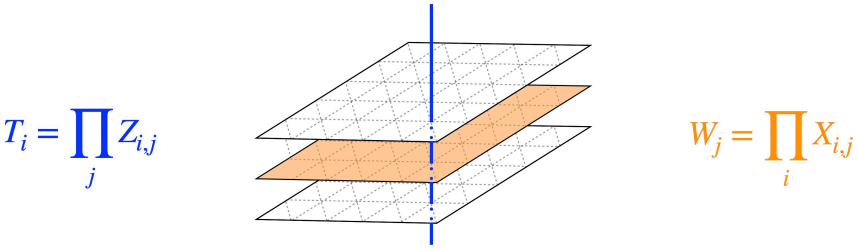

Fonte: o próprio autor.

Resolving this problem necessitates modifying the local projectors $P_{i,j}$ to ensure compatibility with the symmetry generated by T_i. Physically, this corresponds to creating interactions across adjacent layers, thereby transitioning from a simple stack of independent Levin-Gu SPTs to a genuinely three-dimensional structure on the lattice.

Explicitly, we deform the original projectors by introducing inter-layer coupling through the hexagonal operators $H_{i,j}$, composed of Pauli-Z operators around hexagons centered at site i in layer j. The resulting deformed algebra elements take the form shown in the figure below:

Figure 13 – Schematic representation of the local symmetric algebra deformation for the Levin-Gu SPT case.

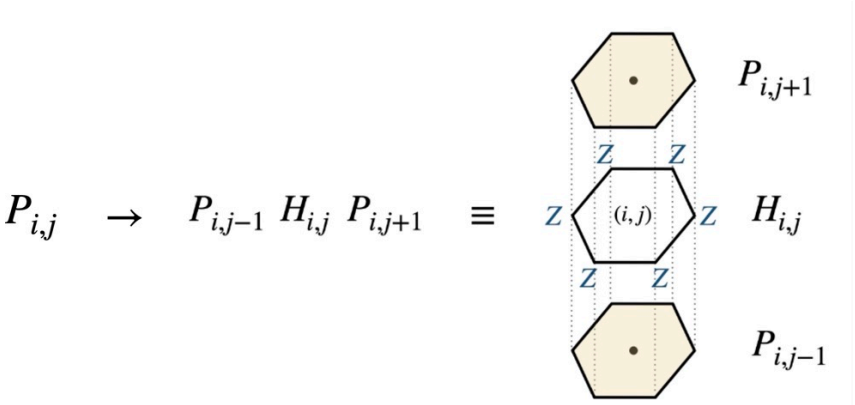

Fonte: o próprio autor.

This choice of deformation ensures commutation with the T_i operators, as it effectively incorporates the vertical interactions that were absent in the initial stack. Moreover,

the specific combination $P_{i,j-1}H_{i,j}P_{i,j+1}$ ensures mutual commutation among all deformed operators. The presence of the hexagonal operator $H_{i,j}$, flanked symmetrically by projectors from adjacent layers, provides precisely the necessary conditions to achieve stabilizer structure and thus a topologically ordered ground state. Hence, the deformation from $\mathcal{A}^{stack}$ to $\mathcal{A}^{deformed}$ is not only symmetry-driven but also crucial for the emergence of a stable, long-range entangled topologically ordered phase. Therefore, a possible deformed algebra fulfilling our conditions is given by

$$\mathcal{A}^{deformed} = span\left\{P_{i,j-1}H_{i,j}P_{i,j+1}\right\}. \tag{3.26}$$

In this fashion, we can use $\mathcal{A}^{deformed}$ to build a general Hamiltonian $H^{deformed}$ that realizes the deformed, anomalous symmetry $\mathcal{S}^{deformed}$. The Hamiltonian we consider is given by

$$H^{deformed} = -\sum_{i,j} P_{i,j-1}H_{i,j}P_{i,j+1}. \tag{3.27}$$

We expect this model to describe a gapped, degenerate, long-range entangled phase. In what follows, we explore the physical properties of $H^{deformed}$.

3.2.2 Ground state degeneracy

We calculate and analyze the ground state degeneracy of the LGF code, illustrating its direct relation to the topology and symmetry structure of the underlying system.

From our prescription, we expect

$$H^{LGF} \equiv -\sum_{i,j} P_{i,j-1}H_{i,j}P_{i,j+1} \tag{3.28}$$

to describe a gapped, degenerate, long-range entangled phase, properties which can be understood in terms of the mixed 't Hooft anomaly and topological constraints in the symmetry of this model. We now examine the topological constraints responsible for the ground state degeneracy [59]. The general form of a topological constraint for the LGF code is given by

$$\mathcal{O}_t \equiv \prod_{ij} \left(P_{i,j-1}H_{i,j}P_{i,j+1}\right)^{t_{ij}} = 1. \tag{3.29}$$

In this case, the topological constraints are encoded by a set of $\mathbb{Z}_2$ parameters $\{t_{ij}\}$, as the Hamiltonian operators square to the identity. The general constraint can be written as

$$\mathcal{O}_t = \prod_{ij} \mathcal{F}(Z_{i,j}) X_{i,j}^{t_{i,j-1}+t_{i,j+1}}, \tag{3.30}$$

where $\mathcal{F}(Z_{i,j})$ can involve products of Pauli-Z operators and Pauli-Z exponentials. Taking the specific form of $\mathcal{F}(Z_{i,j})$ into account, we can rewrite $\mathcal{O}_t$ as

$$\mathcal{O}_t = \prod_{ij} Z_{ij}^{f_{ij}} X_{i,j}^{g_{ij}}, \tag{3.31}$$

where f_{ij} and g_{ij} above are integer functions defined mod 2. It is possible to determine the form of the functions g_{ij} and f_{ij} pictorially,

$$\begin{aligned} f_{ij} &= t_{(x_1+1,x_2),j} + t_{(x_1,x_2+1),j} + t_{(x_1-1,x_2+1),j} + t_{(x_1-1,x_2),j} + t_{(x_1,x_2-1),j} + t_{(x_1+1,x_2-1),j}, \\ g_{ij} &= t_{(x_1,x_2),j-1} + t_{(x_1,x_2),j+1}, \end{aligned} \tag{3.32}$$

where (x_1, x_2) labels the plane sites using two basis vectors $\vec{e}_1$ (along the L_x direction) and $\vec{e}_2$ (along the L_y direction) that spans the triangular lattice.

The constraint $\mathcal{O}_t = 1$ holds only when the functions f_{ij} and g_{ij} vanish modulo 2 for all i, j. For a visual clarification of the local constraints $f_{ij} = 0$ and $g_{i,j} = 0$, refer to Fig. 14 and 15.

Figure 14 – Visual representation of the constraint defined in Eq. (3.32). The triangular lattice is labeled using the basis vectors $\hat{e}_1$ and $\hat{e}_2$, and the highlighted sites correspond to the positions involved in the topological relation $f_{ij} = 0 \mod 2$. Specifically, the variables a, b, c, d, e, and f take values in $\{0, 1\}$, and their sum must vanish modulo 2 to satisfy the local constraint.

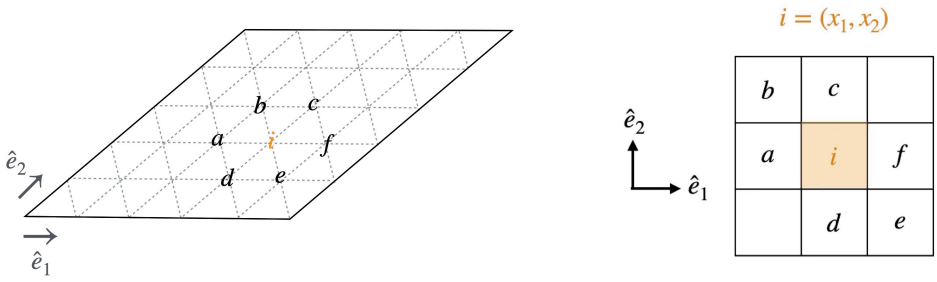

Fonte: o próprio autor.

Any valid solution for $\mathcal{O}_t = 1$ must satisfy $t_{i,j-1} + t_{i,j+1} = 0 \mod 2 \ \forall \ i, j$, meaning that the product along the j-direction must follow a two-step pattern, as shown in Fig. 15. When L_z is even, there are two classes of solutions for topological constraints, each starting on odd or even layers, while when L_z is odd, there is only one product that winds twice along the j-direction. We have obtained the ground-state degeneracy of H^{LGF} from the topological constraints above via two different methods.

The first method was by trial-and-error, where we have examined which types of products could result in identities. For all L_x, L_y and L_z sizes, we have found four types of general constraints.

The first type of support pattern is a staircase-like product of the hexagons. The second type is of products of hexagon operators along lines in the triangular directions $\hat{e}_1$ or $\hat{e}_2$. For example, all product lines along the $\vec{e}_2$ direction are independent and result in L_x different constraints. An analogous pattern happens for $\vec{e}_1$, except that using the previous L_x vertical constraints and all-but-one of these $\vec{e}_1$ constraints results in the one,

Figure 15 – Illustration of the topological constraint along the stacking (j) direction. The product of LGF operators in the j-direction must follow a two-step pattern to satisfy $t_{i,j} + t_{i,j+2} = 0 \mod 2$. This leads to a nontrivial winding structure: for even L_z, two distinct classes of solutions exist depending on whether the sequence starts on odd or even layers; for odd L_z, there is a unique winding product.

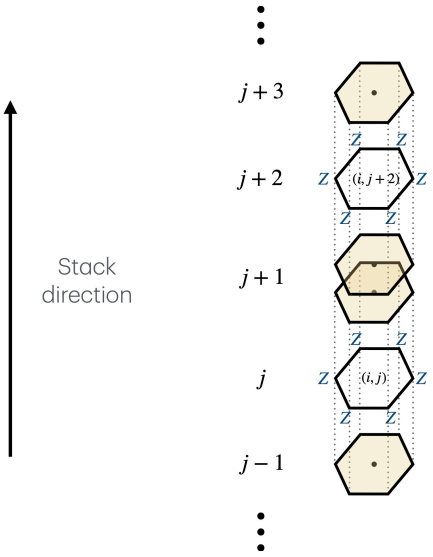

Fonte: o próprio autor.

resulting in $L_y - 1$ independent constraints. Along the third, diagonal direction $\hat{e}_1 - \hat{e}_2$, the number of independent constraints is $\gcd(L_x, L_y) - 2$, where the subtraction accounts for the staircase-like and a diagonal constraint (both already counted). Examples of the constraint can be seen in Fig. 16.

Figure 16 – Examples of patterns for the support of products of $P_{i,j}$ operators along the plane labeled by i, for the case $L_x = L_y = 6$. Cells marked with 1 indicate an operator insertion at the corresponding site $i = (x_1, x_2)$. **Left:** special constraint. **Center:** line constraint along $\hat{e}_2$. **Right:** diagonal constraint along $\hat{e}_1 - \hat{e}_2$.

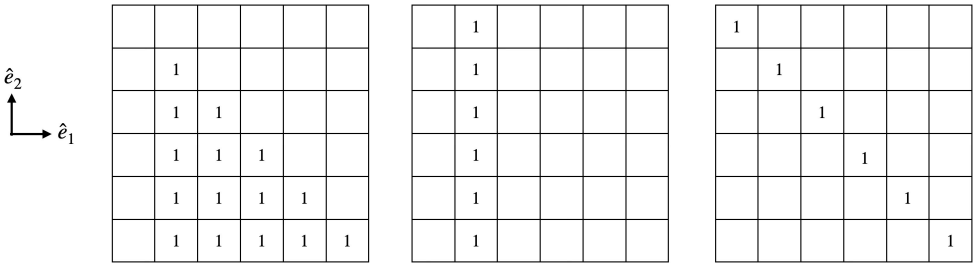

Fonte: o próprio autor.

Defining, $\mathcal{N} \equiv L_x + L_y + \gcd(L_x, L_y) - 2$, the number of independent topological

constraints $\mathcal{N}_{independent}$ is given by

$$\mathcal{N}_{independent} = \begin{cases} 2\mathcal{N} \text{ for } L_z \text{ even}, \\ \mathcal{N} \text{ for } L_z \text{ odd}, \end{cases} \tag{3.33}$$

where the L_z-dependency of the factor of 2 in the above expression comes from the winding structure of stacking along j.

Now that we have the number of independent topological constraints, we determine the GSD by counting the number of physical states and independent quantum numbers. Given that we have $L_x \times L_y \times L_z$ qubits degrees of freedom, the dimension of the LGF Hilbert space is

$$\dim \mathcal{H}^{LGF} = 2^{L_x \times L_y \times L_z}. \tag{3.34}$$

Each state can be labeled by a set $(\lambda_1, \lambda_2 \cdots, \lambda_{L_x \times L_y \times L_z})$ of eigenvalues of the $P_{i,j-1}H_{i,j}P_{i,j+1}$ operators, which take values ± 1. However, there are topological constraints between these labeling operators. For each constraint $\mathcal{O}_t = 1$, an eigenvalue λ_i is fixed in terms of the others, resulting in $2^{L_x \times L_y \times L_z - \mathcal{N}_{independent}}$ independent labels. Therefore the GSD is given by the ratio between the number of states and the number of labels,

$$\text{GSD} = 2^{\mathcal{N}_{independent}}. \tag{3.35}$$

The second method we used to count the ground state degeneracy was a brute-force one, in which we recast the problem as follows. All topological constraints must include stacking along the whole j-direction in such a way that the original Levin-Gu operators square to the identity. Therefore, the constraint analysis can be projected into each individual layer, and the only operators that will contribute are products of Zs along hexagons. We represent each layer as a matrix of size (L_x, L_y), and its components correspond to the lattice sites. Now, the insertion of a hexagonal operator in a given site $i = (x_1, x_2)$ can be thought of as $t_{(x_1,x_2)} = 1$ in the component of the correspondent site, while the absence of the operator corresponds to a $t_{(x_1,x_2)} = 0$. Each layer site is shared by 6 different hexagons, and a constraint corresponds to a matrix that components satisfy the condition $f_{i,j} = 0 \mod 2$ as in Eq. (3.32), or Fig. 14. In this language, the problem is translated to a computational problem:

1. Given a size (L_x, L_y), construct all matrices formed by 0s and 1s.
2. For each matrix, check if each component satisfies the local constraint $f_{ij} = 0 \mod 2$.
3. Count the number of matrices $\mathcal{N}_{total}$ that satisfy the local constraints everywhere.

Below we present a flowchart associated with the algorithm used.

Figure 17 – Flowchart representation of the algorithm used to count the number of valid configurations $\mathcal{N}_{\text{total}}$ that satisfy the local constraint $f_{ij} = 0 \mod 2$ on a triangular lattice of size $L_x \times L_y$. The procedure recursively generates all binary matrices, checks each configuration for compliance with the constraint, and counts only those that satisfy it at every site.

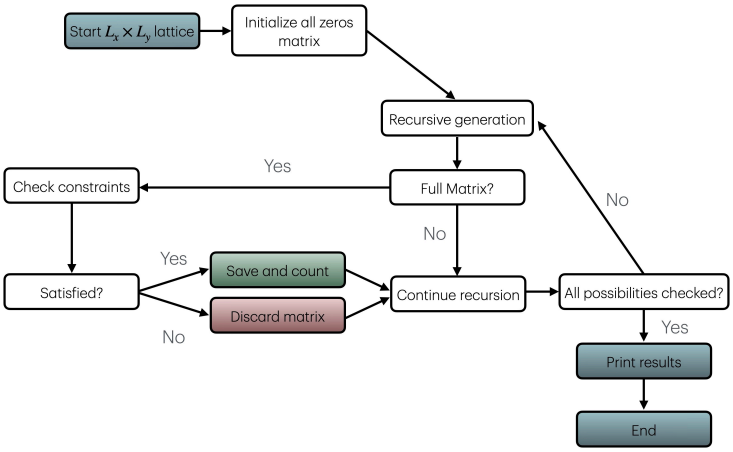

Fonte: o próprio autor.

Using the above algorithm, we got the number

$$\mathcal{N}_{total} = 2^{\mathcal{N}}. \tag{3.36}$$

Each valid matrix corresponds to a layer constraint, and the count obtained computationally matches the previously derived number of linearly independent constraints $\mathcal{N}$.

3.2.3 Symmetries of the LGF Code

The LGF code displays hallmark features of fractonic topological phases, most notably the emergence of excitations with restricted mobility and a rich symmetry structure that includes both global and subsystem symmetries. In this subsection, we characterize the symmetry content of the LGF model.

The LGF Hamiltonian is defined by a deformation of stacked Levin-Gu layers as follows:

$$H^{LGF} = -\sum_{i,j} P_{i,j-1} H_{i,j} P_{i,j+1}, \tag{3.37}$$

where $P_{i,j}$ denotes the Levin-Gu operator acting at site i in layer j, and $H_{i,j}$ is the corresponding hexagon operator.

This Hamiltonian is invariant under a set of global symmetry operations:

$$\mathcal{S}^{\text{enforced}} = \left\{ W_j = \prod_i X_{i,j}, \quad T_i = \prod_j Z_{i,j} \right\}, \tag{3.38}$$

where W_j acts within a single layer (as a layer-wise X flip), and T_i acts vertically across layers (as a column-wise Z operator). These two operators do not commute, and instead

satisfy a mixed 't Hooft anomaly:

$$W_j T_i = -T_i W_j, \tag{3.39}$$

indicating that $\mathcal{S}^{\text{enforced}}$ cannot be realized in an onsite, tensor-product fashion. This anomaly originate from topological invariants of the underlying Levin-Gu layers and give rise to symmetry operators supported on rigid lines or staircase-like subsets of the lattice.

Beyond the global symmetry group $\mathcal{S}^{\text{enforced}}$, the LGF model exhibits a set of emergent, rigid subsystem symmetries. These arise from the local constraint structure:

$$f_{ij} = 0 \mod 2, \quad g_{ij} = 0 \mod 2, \tag{3.40}$$

which impose parity constraints on configurations of neighboring sites in each layer. These constraints are derived from topological invariants of the original Levin-Gu layers and lead to the emergence of symmetry generators supported along rigid lines or fractal-like subsets of the lattice.

To understand how these symmetries arise, let us examine the building blocks of the LGF model. The Levin-Gu operator $P_{i,j}$ is defined as

$$P_{i,j} = X_{i,j} \prod_{\langle ipq \rangle} e^{i\frac{\pi}{4}(1-Z_{p,j}Z_{q,j})}, \tag{3.41}$$

where the product runs over the six triangles $\langle ipq \rangle$ adjacent to site i in layer j. Each $P_{i,j}$ acts nontrivially on its own site via a Pauli-X, and applies phase gates that depend on the Z-configurations of neighboring qubits. The hexagon operator $H_{k,j}$ acts as a product of Pauli-Z operators around a hexagon centered at site k:

$$H_{k,j} = \prod_{\ell \in \text{hex}(k)} Z_{\ell,j}. \tag{3.42}$$

Since all $P_{i,j}$ commute with each other, and all $H_{k,j}$ commute among themselves, we need only consider the commutation between $P_{i,j}$ and $H_{k,j}$. Importantly, the exponential phase terms in $P_{i,j}$ commute with $H_{k,j}$, so the nontrivial commutator arises solely from the Pauli-X operator. One finds:

$$[P_{i,j}, H_{k,j}] = 0 \quad \text{if } i \notin \text{hex}(k), \tag{3.43}$$

$$\{P_{i,j}, H_{k,j}\} = 0 \quad \text{if } i \in \text{hex}(k). \tag{3.44}$$

Now consider products of Levin-Gu operators over rigid submanifolds within a single layer. For instance, along the lattice direction $\hat{e}_2$, we define:

$$\mathcal{O}_{\hat{e}_2,j} = \prod_{i \in \mathcal{L}_{\hat{e}_2}} P_{i,j}, \tag{3.45}$$

where $\mathcal{L}_{\hat{e}_2}$ is a straight line of lattice sites oriented in the $\hat{e}_2$ direction. Due to the cancellation of phase terms and the commutation of the involved $P_{i,j}$ with all relevant $H_{k,j}$, this composite operator commutes with the full Hamiltonian:

$$[\mathcal{O}_{\hat{e}_2,j}, H^{LGF}] = 0. \tag{3.46}$$

Similar operators can be defined along the $\hat{e}_1$ and $\hat{e}_3 = \hat{e}_1 - \hat{e}_2$ directions, each forming a rigid, 1D symmetry of the model.

Additionally, the product of $P_{i,j}$ over the staircase-like pattern also commutes with the Hamiltonian and define further subsystem symmetries. These are not manifest in the microscopic Hamiltonian, but emerge from the topological deformation of the stacked Levin-Gu layers.

The full symmetry structure of the LGF model can be organized into two distinct classes:

1. Subsystem symmetries, generated by the operators T_i, which act on lower-dimensional submanifolds of the system. However, these generators are not all independent, as we will show below.

2. Accidental rigid subsystem symmetries, arising from topological constraints within each layer. These are generated by extended products of plaquette terms $P_{i,j}$ arranged along line and staircase-like patterns. Such operators take the form:

$$\mathcal{O}_\sigma = \prod_{i \in \sigma} P_{i,j}, \tag{3.47}$$

where σ denotes a subset of sites whose structure is determined by the topological features of the model. The total number of linearly independent such operators is given by

$$L_x + L_y + \gcd(L_x, L_y) - 2,$$

reflecting the interplay between the subsystem symmetry structure and the global geometry of the lattice.

These independent subsystem symmetries and their mixed 't Hooft anomalies are central to the fractonic nature of the model, leading to constrained mobility of excitations, sub-extensive ground state degeneracy, and robust long-range entanglement. We intend to explore the fracton properties of the LGF code in future research.

In this fashion, we conclude the discussion on the physical properties of the LGF code. In the second part of the current chapter, we focus on the quantum wire approach to constructing topological orders, with particular emphasis on models describing Laughlin states in the fractional quantum Hall effect.

3.3 Quantum Wires Approach for Laughlin States

Starting from the so-called quantum wires system, which is a semi-microscopic description in terms of $D = 2$ theories, we discuss the emergence of $D = 3$ low-energy effective field theories by using different maps connecting the microscopic degrees of freedom with the macroscopic ones. We show the origin of these maps by embedding the

bosonized version of the original quantum wires model in a gauge invariant theory and using particle vortex-duality. This whole section is based on Ref. [60].

3.3.1 Particle-Vortex Duality

In one of its simplest incarnations, the particle-vortex duality is the equivalence between the two 2+1 dimensional relativistic theories,

$$S_1 \equiv \int |D_B\phi|^2 - V(\phi) \quad \Leftrightarrow \quad S_2 \equiv \int |D_\alpha\tilde{\phi}|^2 - \tilde{V}(\tilde{\phi}) + \frac{1}{2\pi} B d\alpha, \tag{3.48}$$

where B is a background gauge field for the global $U(1)$ symmetry and α is a dynamical gauge field, with covariant derivatives $D_B \equiv \partial - iB$ and $D_\alpha \equiv \partial - i\alpha$, and the potentials $V(\phi)$ and $\tilde{V}(\tilde{\phi})$ admit spontaneous symmetry breaking, e.g.,

$$V(\phi) = M^2|\phi|^2 + \frac{\lambda}{4}|\phi|^4 \quad \text{and} \quad \tilde{V}(\tilde{\phi}) = \tilde{M}^2|\tilde{\phi}|^2 + \frac{\tilde{\lambda}}{4}|\tilde{\phi}|^4. \tag{3.49}$$

This has been recently found to be a central element in the so-called web of dualities, a remarkable series of connections between 2+1 dimensional quantum field theories [4, 61, 62]. In the context of QHE and building on the results of [29], Fuji and Furusaki were able to cast the quantum wires description of the Abelian fractional QHE in different forms by using certain maps between microscopic degrees of freedom [63].

Effective field theory descriptions of the Laughlin class of Abelian fractional QHE can be embedded into the bosonic particle-vortex duality [64, 65, 13, 66]. The basic idea is to gauge the global $U(1)$ symmetry of (3.48) to make the gapless excitations unphysical, along with the introduction of suitable Chern-Simons terms. More explicitly, we introduce in both sides of (3.48) the term $\frac{k}{4\pi} BdB + \frac{1}{2\pi} AdB$, and promote B to a dynamical gauge field a, with A denoting the external electromagnetic field used to measure Hall conductivity[1].

This sequence of operations leads to the relation

$$\begin{aligned} S_1 &= \int |D_a\phi|^2 - V(\phi) + \frac{k}{4\pi} ada + \frac{1}{2\pi} Ada \\ \Leftrightarrow \quad S_2 &= \int |D_\alpha\tilde{\phi}|^2 - \tilde{V}(\tilde{\phi}) + \frac{1}{2\pi} ad(\alpha + A) + \frac{k}{4\pi} ada. \end{aligned} \tag{3.50}$$

We can further reduce the theory S_2 by making the shift $\alpha \to \alpha - A$, and integrating out the field a that appears quadratically,

$$\begin{aligned} S_1 &= \int |D_a\phi|^2 - V(\phi) + \frac{k}{4\pi} ada + \frac{1}{2\pi} Ada \\ \Leftrightarrow \quad S_2 &= \int |D_{\alpha-A}\tilde{\phi}|^2 - \tilde{V}(\tilde{\phi}) - \frac{1}{4\pi k} \alpha d\alpha. \end{aligned} \tag{3.51}$$

[1] We use the notation that capital letters $A, B, \ldots$ denote external fields, whereas lowercase letters $a, b, \alpha, \ldots$ represent dynamical ones.

The action S_1 is the Wen-Zee effective description of the Laughlin class of the fractional QHE. The electromagnetic field is coupled to the topological current $J = \frac{1}{2\pi} da$, parametrized by the hydrodynamic field a. The action includes a Chern-Simons term for the field a with a properly quantized level. This emergent field couples to the quasi-particle current, written in terms of the scalar field ϕ. Electron excitations correspond to the vortices of ϕ. The action S_2 is the relativistic counterpart of the original ZHK description of QHE (the nonrelativistic setting will be discussed below). The external field couples to the particle current of the field $\tilde{\phi}$. The statistical field α, without a properly quantized Chern-Simons level, attaches an odd number m of flux units to the $\tilde{\phi}$-excitations, which effectively turns them into fermions. This is known as the composite boson picture. In this case, quasi-particles are described by the vortices of the field $\tilde{\phi}$.

It is useful for our purposes to consider the IR limit of the duality (3.51) in the phase describing the Laughlin state. It corresponds to the symmetric phase of S_1 ($M^2 > 0$) and to the Higgs phase of S_2 ($\tilde{M}^2 < 0$). Then, we have

$$\int -\frac{1}{96\pi M} f_a^2 + \frac{k}{4\pi} a da + \frac{1}{2\pi} A da \quad \Leftrightarrow \quad \int \frac{|\tilde{M}^2|}{2\tilde{\lambda}} (\alpha_\mu - A_\mu)(\alpha^\mu - A^\mu) - \frac{1}{4\pi k} \alpha d\alpha, \quad (3.52)$$

where the Maxwell term in theory S_1 comes from one-loop contributions. There are several interesting points in this relation. First, we observe in (3.51) that the scalar field $\tilde{\phi}$ is charged under both α and A. In the Higgs phase (3.52), we have absorbed the phase of the field into α_μ, which means that the redefined α_μ field is now charged under the $U(1)_A$. Second, in the deep IR limit (M and $|\tilde{M}^2| \to \infty$), integrating out the dynamical fields reduces both sides of (3.52) to $-\frac{1}{4\pi k} A dA$, yielding the Hall conductivity of the Laughlin state $\sigma_{xy} = \frac{1}{2\pi k}$. Finally, by turning off the external field A in (3.52), we obtain the known duality between Maxwell-Chern-Simons (MCS) and the Self-Dual (SD) Model [67], leading to the identification

$$|\tilde{M}^2| = \frac{6\tilde{\lambda}}{\pi} M. \quad (3.53)$$

Therefore, the MCS-SD duality by itself can also be framed as a particle-vortex type. This is supported simply by the fact that the electromagnetic field couples to the vortex current $\frac{1}{2\pi} da$ in MCS, whereas it couples to the ("Higgsed") particle current $-\frac{|\tilde{M}^2|}{\tilde{\lambda}}(\alpha - A)$ in the SD model in (3.52). The form of the duality in (3.52) will be important later when connecting the quantum wires description with field theories in the continuum limit.

3.3.2 Nonrelativistic Setting

Next, it will be enlightening to discuss the nonrelativistic counterpart of the duality (3.51) [64, 13]. We simply replace ϕ and $\tilde{\phi}$, that create both particle and anti-particles, by their nonrelativistic counterparts ψ and $\tilde{\psi}$, accompanied by the respective chemical potentials μ and $\tilde{\mu}$ to control the average number of particles. The nonrelativistic duality

then reads

$$S_1 = \int i\psi^*(\partial_t - ia_t - i\mu)\psi - \frac{1}{2M}|(\partial_i - ia_i)\psi|^2 - V(\psi) + \frac{k}{4\pi}ada + \frac{1}{2\pi}Ada \quad (3.54)$$

$$\Leftrightarrow \qquad S_2 = \int i\tilde{\psi}^*(\partial_t - i(\alpha_t - A_t) - i\tilde{\mu})\tilde{\psi} - \frac{1}{2\tilde{M}}|(\partial_i - i(\alpha_i - A_i))\tilde{\psi}|^2 - V(\tilde{\psi}) - \frac{1}{4\pi k}\alpha d\alpha.$$

As before, we consider the IR limit describing the Laughlin state in the nonrelativistic case. Relying only on gauge invariance, now without Lorentz covariance, the integration over the matter fields produces

$$\int c_1 f_{a,0i}^2 + c_2 f_{a,ij}^2 + \frac{k}{4\pi}ada + \frac{1}{2\pi}Ada \;\Leftrightarrow\; \int \tilde{c}_1(\alpha_0 - A_0)^2 + \tilde{c}_2(\vec{\alpha} - \vec{A})^2 - \frac{1}{4\pi k}\alpha d\alpha, \quad (3.55)$$

where $c_1 \neq c_2$ and $\tilde{c}_1 \neq \tilde{c}_2$ are constants depending on the parameters of the theories in (3.54). The above relation is the nonrelativistic version of the duality between Maxwell-Chern-Simons and the Self-Dual model, which can be established with the usual construction of the interpolating (master) Lagrangian. As a by-product of this analysis, we will be able to find the relation between the parameters c_1, c_2 and $\tilde{c}_1, \tilde{c}_2$. The master Lagrangian is

$$\mathcal{L}_{master}[a, \alpha; A] \;=\; q_1(\alpha_0 - A_0)^2 + q_2(\alpha_i - A_i)^2 + \frac{1}{2\pi}\alpha da + \frac{k}{4\pi}ada, \quad (3.56)$$

with q_1, q_2, q_3 denoting constant parameters. As we will see, integrating out the fields (α_0, α_i) or (a_0, a_i) leads to MCS or SD theory, respectively.

Let us start with the integration of (a_0, a_i). Their equations of motion can be cast as

$$d\alpha + kda = 0 \quad \Rightarrow \quad a = -\frac{1}{k}\alpha. \quad (3.57)$$

Plugging them back in the master Lagrangian leads to

$$\mathcal{L}_{master}[\alpha; A] = q_1(\alpha_0 - A_0)^2 + q_2(\alpha_i - A_i)^2 - \frac{1}{4\pi k}\alpha d\alpha. \quad (3.58)$$

Now, comparing this Lagrangian with the Self-Dual model in (3.55), we readily see that

$$q_1 = \tilde{c}_1 \quad \text{and} \quad q_2 = \tilde{c}_2. \quad (3.59)$$

On the other hand, the equations of motion of α can be expressed as

$$\alpha_0 = A_0 - \frac{1}{4\pi q_1}\epsilon_{ij}\partial_i a_j, \quad \alpha_i = A_i + \frac{1}{4\pi q_2}\epsilon_{ij} f_{a,0j}, \quad (3.60)$$

such that the master Lagrangian is rewritten as

$$\mathcal{L}_{master}[a; A] = -\frac{1}{16\pi^2 q_2} f_{a,0i}^2 - \frac{1}{32\pi^2 q_1} f_{a,ij}^2 + \frac{k}{4\pi}ada + \frac{1}{2\pi}Ada. \quad (3.61)$$

A direct comparisson with the Maxwell-Chern-Simons theory (3.55) yields

$$-\frac{1}{16\pi^2 q_2} = c_1 \quad \text{and} \quad -\frac{1}{32\pi^2 q_1} = c_2, \quad (3.62)$$

Finally, combining the identifications (3.59) and (3.62) leads to

$$c_1\tilde{c}_2 = -\frac{1}{16\pi^2} \quad \text{and} \quad c_2\tilde{c}_1 = -\frac{1}{32\pi^2}. \quad (3.63)$$

In the relativistic case ($c_1 = -2c_2$ and $\tilde{c}_1 = -\tilde{c}_2$) these two equations reduce to a single one.

3.3.3 Hamiltonian Analysis

Now we would like to express the dual theories of (3.52) in a form that can be directly compared with the quantum wires formulation. In this case, the Hamiltonian description is more transparent.

The canonical momenta in the MCS theory (3.52) are

$$\Pi_0 = 0 \quad \text{and} \quad \Pi_i = \frac{1}{24\pi M} f_{0i} + \frac{1}{2\pi}\epsilon_{ij}\left(A_j + \frac{k}{2}a_j\right). \tag{3.64}$$

The first relation defines a primary constraint. Then, the canonical Hamiltonian is given by

$$\begin{aligned} \mathcal{H}_{MCS} &= \Pi_i(\partial_0 a_i) - \mathcal{L} \\ &= \frac{1}{48\pi M}\left(\vec{e}^2 + b^2\right) - \frac{a_0}{2\pi}\left(B + k\,b + \frac{1}{12M}\nabla\cdot\vec{e}\right) - \frac{1}{2\pi}A_0 b. \end{aligned} \tag{3.65}$$

Here we have introduced the electric and magnetic fields $e_i \equiv f_{0i}$ and $b \equiv \epsilon_{ij}\partial_i a_j$, respectively. The component a_0 plays the role of a Lagrange multiplier enforcing the Gauss's law

$$B + k\,b + \frac{1}{12M}\nabla\cdot\vec{e} = 0, \tag{3.66}$$

which gives a secundary constraint and ensures the time independence of the primary constraint $\Pi_0 = 0$. On the constrained surface defined by the full set of constraints, the Hamiltonian reduces to

$$\mathcal{H}_{MCS} = \frac{1}{48\pi M}(\vec{e}^2 + b^2) - \frac{1}{2\pi}A_0 b. \tag{3.67}$$

The canonical commutation relations imply the gauge invariant algebra

$$[e_i(\vec{x}), e_j(\vec{x}')] = -i(24\pi M)^2\frac{k}{2\pi}\epsilon_{ij}\delta(\vec{x} - \vec{x}') \tag{3.68}$$

and

$$[b(\vec{x}), e_i(\vec{x}')] = -i(24\pi M)\epsilon_{ij}\partial_j\delta(\vec{x} - \vec{x}'). \tag{3.69}$$

As a consistency check, we can see that the constraint (3.66) commutes with e_i and b and consequently with the Hamiltonian. Together with the Hamiltonian (3.67), we will see that the above algebra enables a direct comparison with the canonical structure emerging in the continuum limit of the quantum wires system.

Next we consider the SD model in (3.52), with canonical momenta,

$$\tilde{\Pi}_0 = 0 \quad \text{and} \quad \tilde{\Pi}_i = -\frac{1}{4\pi k}\epsilon^{ij}\alpha_j, \tag{3.70}$$

which are primary constraints. The corresponding canonical Hamiltonian reads

$$\mathcal{H}_{SD} = \frac{1}{2\pi k}\alpha_0\left(\epsilon_{ij}\partial_i\alpha_j\right) - \frac{\tilde{M}}{2}\left(\alpha_0 - A_0\right)^2 + \frac{\tilde{M}}{2}\left(\vec{\alpha} - \vec{A}\right)^2, \tag{3.71}$$

where we have defined the mass parameter

$$\tilde{M}_{\tilde{\lambda}} \equiv \frac{|\tilde{M}^2|}{\tilde{\lambda}}. \tag{3.72}$$

It is convenient to shift the component α_0 as $\alpha_0 \to \alpha_0 + A_0$, leading to

$$\mathcal{H}_{SD} = \frac{1}{2\pi k}(\alpha_0 + A_0)(\epsilon_{ij}\partial_i\alpha_j) - \frac{\tilde{M}_{\tilde{\lambda}}}{2}(\alpha_0)^2 + \frac{\tilde{M}_{\tilde{\lambda}}}{2}\left(\vec{\alpha} - \vec{A}\right)^2. \tag{3.73}$$

After using the algebraic equation of motion $\frac{d}{dt}\tilde{\Pi}_0 = -\frac{\delta}{\delta\alpha_0}H_{SD} = 0$, the Hamiltonian $\mathcal{H}_{SD}$ is recast as

$$\mathcal{H}_{SD} = \frac{\tilde{M}_{\tilde{\lambda}}}{2}\left(\vec{\alpha} - \vec{A}\right)^2 + \frac{1}{2\tilde{M}_{\tilde{\lambda}}}\frac{1}{(2\pi k)^2}(\epsilon_{ij}\partial_i\alpha_j)^2 + \frac{1}{2\pi k}A_0(\epsilon_{ij}\partial_i\alpha_j). \tag{3.74}$$

Finally, the canonical commutation relations can be obtained using the Dirac formalism for second class constraints:

$$[\alpha_i(\vec{x}), \alpha_j(\vec{x}')] = -i(2\pi k)\epsilon_{ij}\delta(\vec{x} - \vec{x}'), \tag{3.75}$$

offering an alternative interpretation for the continuum limit of the quantum wires system.

The dual formulation of the Hamiltonians $\mathcal{H}_{MCS}$ and $\mathcal{H}_{SD}$ is the backbone of our analysis on the underlying dualities of the fractional quantum Hall effect.

3.3.4 Quantum Wires Formulation

The quantum wires setup starts with a collection of noninteracting one-dimensional wires supporting electrons in the presence of an external magnetic field. The linearized excitations around the Fermi points are gapless, described by the Hamiltonian

$$H_0 = v_F \sum_y \int dx\, (\psi^\dagger_{L,y} i\partial_x \psi_{L,y} - \psi^\dagger_{R,y} i\partial_x \psi_{R,y}), \tag{3.76}$$

where v_F is the Fermi velocity and y labels the different wires. There are two types of interactions in such a system, intrawire and interwire, and we would like to model the ones able to destabilize the critical theory (3.76) and drive the system to the Laughlin phase. As the different wires in (3.76) do not interact, charge is conserved inside each wire. Furthermore, (3.76) is invariant under chiral transformations $\psi_{R/L,y} \to e^{\pm i\alpha}\psi_{R/L,j}$. These symmetries imply conservation of the currents $J_{R/L,y} \equiv \psi^\dagger_{R/L,y}\psi_{R/L,y}$, which in turn can be used to introduce current-current (forward) intrawire interactions of type

$$H_{JJ} = \pi \int dx \sum_y \left\{\lambda_a[(J_{R,y})^2 + (J_{L,y})^2] + 2\lambda_b J_{R,y}J_{L,y}\right\}, \tag{3.77}$$

where λ_a and λ_b are coupling constants. Under bosonization, the role of H_{JJ} is to renormalize the kinetic parameters.

Interwire interactions describe more general processes in which electric charge is exchanged between different wires. Charge conservation applies to the system as a whole, not inside each wire, effectively realizing a higher dimensional phase. As shown in the pioneering works of [68, 69], the interactions responsible for driving the system to the Laughlin phase at the filling fraction $\nu = 1/m$ are given by

$$H_{inter}^{1/m} = -g \int dx \sum_{y=1}^{N} (\psi_{L,y+1}^{\dagger})^{\frac{m+1}{2}} (\psi_{R,y+1})^{\frac{m-1}{2}} (\psi_{L,y}^{\dagger})^{\frac{m-1}{2}} (\psi_{R,y})^{\frac{m+1}{2}} + H.c.. \tag{3.78}$$

If we further submit the system to a probe external field A to measure Hall responses, the minimally coupled action associated with H_0 is

$$S_0[A] = \int dtdx \sum_y \left\{ i\psi_{R,y}^{\dagger} \left(D_0 + v_F D_1\right) \psi_{R,y} + i\psi_{L,y}^{\dagger} \left(D_0 - v_F D_1\right) \psi_{L,y} \right\}, \tag{3.79}$$

where $D_0 \equiv \partial_t - iA_{0,y}$ and $D_1 \equiv \partial_x - iA_{1,y}$.

Fermionic operators at coincident points must be treated carefully, so that they are point-split regularized in a gauge invariant way. In the case of the currents $J_{R/L}$, this amounts to define the gauge-invariant operator through the insertion of a Wilson line along x-direction

$$J_{R/L,y} \equiv \lim_{\epsilon_\parallel \to 0} \psi_{R/L,y}^{\dagger}(x+\epsilon_\parallel)\, e^{i\int_x^{x+\epsilon_\parallel} dx A_{1,y}} \psi_{R/L,j}(x) - \langle \psi_{R/L,y}^{\dagger}(x) \psi_{R/L,y}(x) \rangle, \tag{3.80}$$

where $\epsilon_\parallel$ is a short-distance cutoff along the wires, and the divergent part of the current operator has been subtracted. A similar treatment can be applied to the $H_{inter}^{1/m}$ operator [70], introducing Wilson lines along the discretized y-direction between fermion operators that are raised to the same power. For example,

$$(\psi_{L,y+1}^{\dagger} \psi_{R,y})^{\frac{m+1}{2}} \;\rightarrow\; (\psi_{L,y+1}^{\dagger}\, e^{i\int_y^{y+1} dy A_{2,y}} \psi_{R,y})^{\frac{m+1}{2}}. \tag{3.81}$$

More generally, the interactions in $H_{inter}^{1/m}$ are implicitly built with point-splitting along the x-direction.

3.3.5 Bosonization

Having defined all the ingredients of the quantum wires system, we are ready to proceed with bosonization. This is done through the field redefinition

$$\psi_{R,y} = \frac{\kappa_y}{\sqrt{2\pi\epsilon_\parallel}} e^{i(\varphi_y + \theta_y)}, \qquad \psi_{L,y} = \frac{\kappa_y}{\sqrt{2\pi\epsilon_\parallel}} e^{i(\varphi_y - \theta_y)}, \tag{3.82}$$

where $\epsilon_\parallel$ is the short-distance cutoff previously introduced and κ_y denotes the Klein factors ensuring that fermions from different wires anticommute. The only nontrivial commutation rule between the bosonic fields is given by

$$[\theta_y(x), \varphi_{y'}(x')] = i\pi\delta_{yy'}\Theta(x - x'), \tag{3.83}$$

where $\Theta(x-x')$ is the Heaviside function.

Using (3.82), the bosonized action associated to the system H_0+H_{JJ} is written as

$$S[A]=\frac{1}{2\pi}\int dtdx\sum_y\left\{-2\partial_x\theta_y(\partial_t\varphi_y-A_{0,y})-v(\partial_x\varphi_y-A_{1,y})^2-u(\partial_x\theta_y)^2\right\}, \tag{3.84}$$

where u and v are given in terms of the parameters of the forward interactions (3.77),

$$u=v_F+\lambda_a+\lambda_b \quad \text{and} \quad v=v_F+\lambda_a-\lambda_b. \tag{3.85}$$

The corresponding Hamiltonian reads

$$H[A]=\frac{1}{2\pi}\int dx\sum_y\left\{-2\partial_x\theta_yA_{0,y}+v\left(\partial_x\varphi_y-A_{1,y}\right)^2+u\left(\partial_x\theta_y\right)^2\right\}, \tag{3.86}$$

while the interwire Hamiltonian (3.78) is recast as

$$\begin{aligned}H_{inter}^{1/m} &= -g\int dx\sum_y\kappa_{y+1}\kappa_y e^{i(-\Delta_y\varphi_y+\epsilon_\perp A_{2,y}+mS\theta_y)}+H.c.\\ &= -\int dx\sum_y g_{y,y+1}\sin\left(-\Delta_y\varphi_y+\epsilon_\perp A_{2,y}+mS\theta_y\right).\end{aligned} \tag{3.87}$$

Here $\Delta_y\varphi_y\equiv\varphi_{y+1}-\varphi_y$, $S\theta_y\equiv\theta_{y+1}+\theta_y$, and in the last line we have absorbed the Klein factors into the coupling constants $g_{y,y+1}$. The parameter $\epsilon_\perp$ denotes the interwire spacing.

In the absence of an external background, the field configurations that minimize the potential are the constant ones given by $\varphi_y\equiv\varphi_0$ and $\theta_y\equiv\theta_0=\frac{\pi}{4m}$. Note that the value of φ_0 remains unspecified since the Hamiltonian involves only derivatives and differences of φ's. It is then simpler to set the expectation value φ_0 to zero via a field shift. In this case, (3.87) becomes

$$H_{inter}^{1/m}=-\int dx\sum_y g_{y,y+1}\cos\left(-\Delta_y\varphi_y+\epsilon_\perp A_{2,y}+mS\theta_y\right), \tag{3.88}$$

where now $\varphi_0=\theta_0=0$.

It is more convenient to rewrite the parameters u and v as

$$u=\mathsf{v}/K \quad \text{and} \quad v=\mathsf{v}K, \tag{3.89}$$

with

$$\mathsf{v}\equiv\sqrt{(v_F+\lambda_a)^2-\lambda_b^2} \quad \text{and} \quad K\equiv\sqrt{\frac{v_F+\lambda_a-\lambda_b}{v_F+\lambda_a+\lambda_b}}. \tag{3.90}$$

We can then rescale the fields φ and θ,

$$\varphi_y\to\varphi_y/\sqrt{K} \quad \text{and} \quad \theta_y\to\sqrt{K}\theta_y, \tag{3.91}$$

bringing the Hamiltonian to the canonical normalization. Note that these rescalings do not change the commutator (3.83). Finally, the complete Hamiltonian becomes

$$\begin{aligned}H &= \frac{1}{2\pi}\int dx\sum_y\left\{-2\sqrt{K}\partial_x\theta_yA_{0,y}+\mathsf{v}(\partial_x\varphi_y-\sqrt{K}A_{1,y})^2+\mathsf{v}\left(\partial_x\theta_y\right)^2\right\}\\ &- \int dx\sum_y g_{y,y+1}\cos\left(\Delta_y\varphi_y/\sqrt{K}-\epsilon_\perp A_{2,y}-m\sqrt{K}S\theta_y\right).\end{aligned} \tag{3.92}$$

The strongly coupled limit of the quantum wires system is expected to realize the Laughlin state. A key feature of the bosonized theory is that both strongly coupled and continuum limits can be simultaneously taken, leading to a simple structure that may be readily compared with the continuum theories. In the next subsections we summarize the results of [31] and [71], which arrive at the description of Laughlin series in terms of the Maxwell-Chern-Simons theory starting from the quantum wires approach and introducing suitable prescriptions of microscopic degrees of freedom in terms of emergent gauge fields. The prescriptions in these two papers differ but ultimately connected through particle-vortex duality, as we will clarify soon.

3.3.6 Strongly Coupled Continuum Limit I: Maxwell-Chern-Simons Theory

We start with the discussion of [31], with the Hamiltonian in (3.92) and the following identifications[2]:

$$b_y \equiv \frac{2\sqrt{K}}{\epsilon_\perp}\partial_x\theta_y, \tag{3.93a}$$

$$e_{1,y} \equiv 2\pi g\left(\frac{1}{\sqrt{K}}\Delta_y\varphi_y - m\sqrt{K}S\theta_y - \epsilon_\perp A_{2,y}\right), \tag{3.93b}$$

$$e_{2,y} \equiv -\frac{2\nu\sqrt{K}}{\epsilon_\perp}\left(\partial_x\varphi_y - \sqrt{K}A_{1,y}\right). \tag{3.93c}$$

This identification can be tested via their canonical algebra and Hamiltonian. The Hamiltonian (3.92) written in terms of (e, b) becomes

$$H = \int dx \sum_j \epsilon_\perp \left\{-\frac{1}{2\pi}b_y A_{0,y} + \frac{1}{8\pi}\left(\frac{1}{\nu\Lambda_K}e_{2,y}^2 + \frac{\nu}{\Lambda_K}b_y^2 + \frac{1}{\Lambda_g}e_{1,y}^2\right) + \cdots\right\}, \tag{3.94}$$

where we have defined the energy scales

$$\Lambda_K \equiv K\epsilon_\perp^{-1} \quad \text{and} \quad \Lambda_g \equiv \pi\epsilon_\perp g_{y,y+1}. \tag{3.95}$$

The energy scale Λ_K can be interpreted as a gap for excitations propagating along the wires, because it involves the forward coupling constants. For similar reasoning, Λ_g can be interpreted as a gap for excitations propagating in the perpendicular direction. The ellipsis stand for terms that are either constant or higher-order in the cosine expansion.

The identifications in (3.93) imply the constraint

$$\frac{1}{2\Lambda_g}\partial_x e_{1,y} + \frac{1}{2\nu\Lambda_K}\frac{\Delta_y}{\epsilon_\perp}e_{2,y} + \frac{1}{2}mSb_y + B_y = 0. \tag{3.96}$$

[2] Note that the normalization constants used in [31] are slightly different from those used here.

The (e, b) algebra can be explicitly computed using (3.83), and is given by

$$[e_{1,y}(x), e_{2,y'}(x')] = -i4\pi m \mathsf{v} \Lambda_g \Lambda_K \frac{1}{\epsilon_\perp} (\delta_{y,y'} + \delta_{y,y'+1}) \delta(x - x'), \tag{3.97}$$

$$[b_y(x), e_{1,y'}(x')] = -i4\pi \Lambda_g \frac{\Delta_y}{\epsilon_\perp} \frac{1}{\epsilon_\perp} \delta_{y,y'} \delta(x - x'), \tag{3.98}$$

$$[b_y(x), e_{2,y'}(x')] = i4\pi \mathsf{v} \Lambda_K \frac{1}{\epsilon_\perp} \delta_{y,y'} \partial_x \delta(x - x'). \tag{3.99}$$

To consider the continuum limit we take neighboring wires to be infinitesimally close, i.e. $\epsilon_\perp \to 0$. This limit is only regular if we also take $K \to 0$ and $g_{y,y+1} \to \infty$, setting the respective scales to constant values. From equation (3.90), we see that the limit $K \to 0$ corresponds to $\lambda_a, \lambda_b \to \infty$. Therefore, the continuum limit $\epsilon_\perp \to 0$ is consistent with the strongly coupled regime. Besides, $\sum_y \epsilon_\perp$ is identified as an integral over the perpendicular direction y, such that $\frac{\delta_{yy'}}{\epsilon_\perp} \to \delta(y - y')$.

We can see from the Hamiltonian (3.94) that a spatially isotropic two-dimensional phase emerges when

$$\Lambda_g = \mathsf{v} \Lambda_K. \tag{3.100}$$

To compare with the relativistic theories in subsection 3.3.3 we further set $\mathsf{v} = 1$. Together with the continuum limit discussed above, the Hamiltonian (3.94) becomes

$$H = \int d^2x \left[-\frac{1}{2\pi} b A_0 + \frac{1}{8\pi\Lambda_K} \left(\vec{e}^2 + b^2 \right) - \frac{a_0}{2\pi} \left(\frac{1}{2\Lambda_K} \nabla \cdot \vec{e} + mb + B \right) \right], \tag{3.101}$$

where we have used an auxiliary field a_0 to impose the constraint (3.96) dinamically. The algebra reduces to

$$[e_i(\vec{r}), e_j(\vec{r}')] = -i (4\pi\Lambda_K)^2 \frac{m}{2\pi} \epsilon_{ij} \delta(\vec{r} - \vec{r}'), \tag{3.102}$$

$$[b(\vec{r}), e_i(\vec{r}')] = -i4\pi\Lambda_K \epsilon_{ij} \partial_j \delta(\vec{r} - \vec{r}'). \tag{3.103}$$

Therefore, a direct comparison with the respective objects in subsection 3.3.3 leads to

$$m = k \quad \text{and} \quad \Lambda_K = 6M. \tag{3.104}$$

Using all these identifications, the continuum bosonic quantum wires system explicitly realizes the MCS theory.

3.3.7 Strongly Coupled Continuum Limit II: Self-Dual Theory

The work of [71] starts with the Hamiltonian (3.92) and makes the following field identifications:

$$\alpha_{1,y} \equiv \frac{1}{\sqrt{K}} \partial_x \varphi_y \quad \text{and} \quad \alpha_{2,y} \equiv \frac{1}{\epsilon_\perp \sqrt{K}} (\Delta_y \varphi_y - mKS\theta_y). \tag{3.105}$$

Using (3.83), it is easy to show they satisfy the algebra

$$[\alpha_{1,y}(x), \alpha_{2,y'}(x')] = -\frac{i\pi m}{\epsilon_\perp}(\delta_{y,y'+1} + \delta_{y,y'})\delta(x - x'). \tag{3.106}$$

The associated magnetic field $b_\alpha \equiv \epsilon_{ij}\partial_i\alpha_j$ is cast as

$$b_{\alpha,y} = -2\pi m\rho_y, \tag{3.107}$$

where ρ_y is the two-dimensional electron density,

$$\rho_y = \frac{1}{2\pi\epsilon_\perp}\sqrt{K}\partial_x S\theta_y. \tag{3.108}$$

The expression for b_α in terms of ρ resembles the flux-attachment condition imposed by the Chern-Simons field, with magnetic field determined by the particle density.

Following the same strategy of the previous subsection, we rewrite the Hamiltonian (3.92) in terms of α,

$$H = \int dx \sum_y \epsilon_\perp \left\{ -A_{0,y}\rho_y + \frac{\mathsf{v}\Lambda_K}{2\pi}[(\alpha_{1,y} - A_{1,y})^2 + \frac{\Lambda_g}{\mathsf{v}\Lambda_K}(\alpha_{2,y} - A_{2,y})^2] + \frac{\mathsf{v}}{2\pi}\Lambda_K\pi^2 4\rho_y^2 \right\}, \tag{3.109}$$

and take its strongly coupled continuum limit,

$$H = \int d^2x \left\{ -A_0\rho + \frac{\mathsf{v}\Lambda_K}{2\pi}\left[(\alpha_1 - A_1)^2 + \frac{\Lambda_g}{\mathsf{v}\Lambda_K}(\alpha_2 - A_2)^2\right] + \frac{\mathsf{v}}{2\pi}\frac{\pi^2}{\Lambda_K}\frac{1}{(2\pi m)^2}(\epsilon_{ij}\partial_i\alpha_j)^2 \right\}. \tag{3.110}$$

The algebra becomes

$$[\alpha_i(\vec{x}), \alpha_j(\vec{x}')] = -2\pi i m\epsilon_{ij}\delta(\vec{x} - \vec{x}'). \tag{3.111}$$

We see that the spatially isotropic case is given precisely by (3.100), and we also set here $\mathsf{v} = 1$. Once more, comparing these results with their counterpart in the subsection 3.3.3 leads to

$$m = k \quad \text{and} \quad \Lambda_K = \pi\tilde{M}_{\tilde{\lambda}}. \tag{3.112}$$

Through (3.104) we again find the relation between the macroscopic parameters in (3.53). Therefore, the MCS/SD duality can be viewed as a macroscopic manifestation of the quantum wires description of the Laughlin states of the fractional quantum Hall effect. The duality is embodied by the underlying identification of the microscopic degrees of freedom in the bosonized description with the gauge field or its field-strength.

Finally, let us briefly comment on the relations between the identifications in the MCS and SD models with the quantum wires and the corresponding continuum theories. A direct comparison leads to the following relation between the gauge fields in the two models:

$$e_{1,j} = 2\Lambda_K(\alpha_2 - A_2), \quad e_{2,j} = -2\Lambda_K(\alpha_1 - A_1), \quad b_a = -\frac{1}{m}b_\alpha. \tag{3.113}$$

We can immediately see that these equations constitute a solution to the constraint (3.66) in the MCS theory. This provides an interesting perspective: we can think of the SD model as emerging from the MCS model written in terms of variables that automatically solve the constraint.

In the next sections we show that the two prescriptions reviewed in the previous section, relating quantum wires variables to gauge fields, can be naturally obtained from the quantum wires formalism when embedding the model (3.92) in a gauge invariant theory.

3.3.8 Self-Dual Model

In order to show how the SD model can be obtained as a low-energy limit of the theory (3.92) and then justify the prescriptions of section 3.3.7, we start with its corresponding action:

$$\begin{aligned} S &= \int dtdx \sum_y \left\{ -\frac{1}{\pi}\partial_x\theta_y \left(\partial_t\varphi_y - \sqrt{K}A_{0,y}\right) - \frac{\mathsf{v}}{2\pi}(\partial_x\varphi_y - \sqrt{K}A_{1,y})^2 - \frac{\mathsf{v}}{2\pi}\left(\partial_x\theta_y\right)^2 \right\} \\ &+ \int dtdx \sum_y g_{y,y+1} \cos\left(\Delta_y\varphi_y/\sqrt{K} - \epsilon_\perp A_{2,y} - m\sqrt{K}S\theta_y\right). \end{aligned} \tag{3.114}$$

The charge density couples to the A_0 component of the external field and is given by $\rho_y = \frac{\sqrt{K}}{\pi\epsilon_\perp}\partial_x\theta_y$.

The action (3.114) can be seen as the low-energy limit of a complex scalar field coupled to an external gauge field A_μ and a statistical gauge field α_μ in a specific gauge. The latter is responsible for the flux-attachment mechanism. Indeed, by choosing the gauge $\alpha_{1,y} = 0$, and making the identification $\alpha_{2,y} = -\frac{m\sqrt{K}}{\epsilon_\perp}S\theta_y$, we obtain the usual relation between magnetic flux and density implied by the flux-attachment:

$$b_y = \partial_x\alpha_{2,y} - \partial_y\alpha_{1,y} = -\frac{m\sqrt{K}}{\epsilon_\perp}\partial_x S\theta_y = -\pi m S\rho_y. \tag{3.115}$$

This identification can be implemented using a Lagrange multiplier α_0 in the action,

$$\begin{aligned} S &= \int dtdx \sum_y \left\{ -\frac{1}{\pi}\partial_x\theta_y \left(\partial_t\varphi_y - \sqrt{K}A_{0,y}\right) - \frac{\mathsf{v}}{2\pi}(\partial_x\varphi_y - \sqrt{K}A_{1,y})^2 - \frac{\mathsf{v}}{2\pi}\left(\partial_x\theta_y\right)^2 \right\} \\ &+ \int dtdx \sum_y g_{y,y+1} \cos\left(\Delta_y\varphi_y/\sqrt{K} - \epsilon_\perp A_{2,y} + \epsilon_\perp\alpha_{2,y}\right) \\ &+ \int dtdx \sum_y \frac{\epsilon_\perp}{2\pi m}\partial_x\alpha_{0,y}\left(\alpha_{2,y} + \frac{m\sqrt{K}}{\epsilon_\perp}S\theta_y\right). \end{aligned} \tag{3.116}$$

Gauge invariance can be made explicit after integrating by parts the last line,

$$\begin{aligned} S &= \int dtdx \sum_y \left\{ -\frac{1}{\pi}\partial_x\theta_y \left(\partial_t\varphi_y - \sqrt{K}A_{0,y} + \frac{\sqrt{K}}{2}S\alpha_{0,y}\right) - \frac{\mathsf{v}}{2\pi}(\partial_x\varphi_y - \sqrt{K}A_{1,y} + \sqrt{K}\alpha_{1,y})^2 \right\} \\ &+ \int dtdx \sum_y \left\{ -\frac{\mathsf{v}}{2\pi}\left(\partial_x\theta_y\right)^2 + g_{y,y+1}\cos\left(\Delta_y\varphi_y/\sqrt{K} - \epsilon_\perp A_{2,y} + \epsilon_\perp\alpha_{2,y}\right) \right\}. \\ &+ \int dtdx \sum_y \left\{ -\frac{\epsilon_\perp}{4\pi m}\epsilon^{\mu\nu\rho}\alpha_{\mu,y}\partial_\nu\alpha_{\rho,y} \right\}. \end{aligned} \tag{3.117}$$

Finally, the field θ can be integrated out, leading to

$$\begin{aligned} S &= \int dtdx \sum_y \left\{ \frac{1}{2\mathsf{v}\pi} \left(\partial_t \varphi_y - \sqrt{K} A_{0,y} + \frac{\sqrt{K}}{2} S\alpha_{0,y} \right)^2 - \frac{\mathsf{v}}{2\pi} (\partial_x \varphi_y - \sqrt{K} A_{1,y} + \sqrt{K}\alpha_{1,y})^2 \right\} \\ &+ \int dtdx \sum_y \left\{ g_{y,y+1} \cos\left(\Delta_y \varphi_y / \sqrt{K} - \epsilon_\perp A_{2,y} + \epsilon_\perp \alpha_{2,y} \right) - \frac{\epsilon_\perp}{4\pi m} \epsilon^{\mu\nu\rho} \alpha_{\mu,y} \partial_\nu \alpha_{\rho,y} \right\}. \end{aligned} \tag{3.118}$$

This is the low-energy limit of a Higgs phase of a complex scalar field coupled to a gauge field. To obtain the SD model we simply consider the unitary gauge $\varphi = 0$ and then take both the continuum and isotropic limits of this action. Proceeding as in the previous section, the continuum limit reads

$$S = \int d^3x \left[\frac{\Lambda_K}{2\pi\mathsf{v}} (A_0 - \alpha_0)^2 - \frac{\mathsf{v}\Lambda_K}{2\pi} (A_1 - \alpha_1)^2 - \frac{\Lambda_g}{2\pi} (A_2 - \alpha_2)^2 - \frac{1}{4\pi m} \epsilon^{\mu\nu\rho} \alpha_\mu \partial_\nu \alpha_\rho \right]. \tag{3.119}$$

After considering the isotropic situation, $\Lambda_K = \Lambda_g$ and $\mathsf{v} = 1$, and comparing this action with the right hand side of (3.52), we recover the relations in (3.112).

3.3.9 Maxwell-Chern-Simons: Particle-Vortex Duality

We have shown that the effective field theory for the Laughlin series can be naturally embedded in a gauge invariant theory, which coincides with the SD model upon a specific gauge choice. Next we will show that we can achieve the alternative MCS theory using the particle-vortex duality on the wires system in 1+1 dimensions.

It will now be convenient to consider the action (3.117) in the gauge $\alpha_2 = 0$. After integrating out the auxiliary field α_0, we are left with

$$\begin{aligned} S &= \int dtdx \sum_y \left\{ -\frac{1}{\pi} \partial_x \theta_y \left(\partial_t \varphi_y - \sqrt{K} A_{0,y} \right) - \frac{\mathsf{v}}{2\pi} \left(\partial_x \varphi_y - \sqrt{K} A_{1,y} - mK \partial_x \Delta^{-1} S\theta \right)^2 \right\} \\ &+ \int dtdx \sum_y \left\{ -\frac{\mathsf{v}}{2\pi} (\partial_x \theta_y)^2 + g_{y,y+1} \cos\left(\Delta_y \varphi_y / \sqrt{K} - \epsilon_\perp A_{2,y} \right) \right\} \\ &+ \int dtdx \sum_y \left\{ -\frac{\mathsf{u} - \mathsf{v}}{8\pi} \left[\Delta_y \left(\partial_x \varphi_y - \sqrt{K} A_{1,y} \right) \right]^2 \right\}. \end{aligned} \tag{3.120}$$

We have added an extra term with coupling $\mathsf{u} - \mathsf{v}$ for convenience. It does not change the qualitative features of the model but makes the quantum wires description more transparent. After some rearrangements, this action can be recast as

$$\begin{aligned} S &= \int dtdx \sum_y \left\{ -\frac{1}{\pi} \partial_x \theta_y \partial_t \varphi_y + \frac{\sqrt{K}}{\pi} \partial_x \theta_y A_{0,y} - \frac{\mathsf{v}}{8\pi} \left(S \left(\partial_x \varphi_y - \sqrt{K} A_{1,y} \right) \right)^2 \right\} \\ &+ \int dtdx \sum_y \left\{ -\frac{\mathsf{v} m^2 K^2}{2\pi} \left(\partial_x \Delta_y^{-1} S\theta \right)^2 + \frac{\mathsf{v} mK}{\pi} \left(\partial_x \varphi_y - \sqrt{K} A_{1,y} \right) \partial_x \Delta_y^{-1} S\theta - \frac{\mathsf{v}}{2\pi} (\partial_x \theta_y)^2 \right\} \\ &+ \int dtdx \sum_y \left\{ g_{y,y+1} \cos\left(\Delta_y \varphi_y / \sqrt{K} - \epsilon_\perp A_{2,y} \right) - \frac{\mathsf{u}}{8\pi} \left(\partial_x \Delta_y \varphi_y - \sqrt{K} A_{1,y} \right)^2 \right\}. \end{aligned} \tag{3.121}$$

Now we turn to the dual theory through the particle-vortex transformation, which is explicit in terms of quantum wires variables. According to [28, 29], the particle-vortex transformation has the form

$$\tilde{\varphi}_{y-1/2} = \sum_{y'} \mathrm{sign}(y'-y+1/2)\theta_{y'} = -2\Delta_y^{-1}\theta_y, \tag{3.122}$$

$$\tilde{\theta}_{y+1/2} = \frac{1}{2}\Delta_y \varphi_y. \tag{3.123}$$

The second equality in (3.122) follows form the identity $\sum_{y'}(\Delta_y)_{yy'}\,\mathrm{sign}(y'-y''+1/2) = 2\delta_{yy''}$, with $(\Delta_y)_{yy'} = \delta_{y+1,y'} - \delta_{y,y'}$ being the matrix elements of the Δ_y operator. The inverse transformations are given by

$$\varphi_y = 2\Delta_y^{-1}\tilde{\theta}_{y+1/2}, \tag{3.124}$$

$$\theta_y = -\frac{1}{2}\Delta_y\tilde{\varphi}_{y-1/2}. \tag{3.125}$$

Applying these transformations to the action (3.121), we obtain

$$\begin{aligned}
S &= \int dtdx \sum_y \left\{ -\frac{1}{\pi}\partial_x\tilde{\theta}_{y+1/2}\partial_t\tilde{\varphi}_{y+1/2} + \frac{\sqrt{K}}{2\pi}\partial_x\Delta_y^T\tilde{\varphi}_{y+1/2}A_{0,y} - \frac{\mathsf{v}m^2K^2}{8\pi}\left(\partial_x S^T\tilde{\varphi}_{y+1/2}\right)^2 \right\} \\
&+ \int dtdx \sum_y \left\{ -\frac{\mathsf{v}mK}{\pi}\left(\partial_x\Delta_y^{-1}\tilde{\theta}_{y+1/2} - \frac{1}{2}\sqrt{K}A_{1,y}\right)\left(\partial_x S^T\tilde{\varphi}_{y+1/2}\right) \right\} \\
&+ \int dtdx \sum_y \left\{ -\frac{\mathsf{v}K}{2\pi}\left(S\left(\partial_x\tilde{\theta}_{y+1/2} - \frac{1}{2}\sqrt{K}\Delta_y A_{1,y}\right)\right)^2 - \frac{\mathsf{u}}{2\pi}\left(\partial_x\tilde{\theta}_{y+1/2} - \frac{1}{2}\sqrt{K}\Delta_y A_{1,y}\right)^2 \right\} \\
&+ \int dtdx \sum_y \left\{ g_{y,y+1}\cos\left(2\tilde{\theta}_{y+1/2}/\sqrt{K} - \epsilon_\perp A_{2,y}\right) - \frac{\mathsf{v}}{8\pi}\left(\partial_x\Delta_y^T\tilde{\varphi}_{y+1/2}\right)^2 \right\},
\end{aligned} \tag{3.126}$$

which is nonlocal because of the presence of Δ_y^{-1}. However, this nonlocal action is equivalent to the following local model [60]:

$$\begin{aligned}
S &= \int dtdx \sum_y \left\{ -\frac{1}{\pi}\partial_x\tilde{\theta}_{y+1/2}\partial_t\tilde{\varphi}_{y+1/2} + \frac{\sqrt{K}}{2\pi}\partial_x\Delta_y^T\tilde{\varphi}_{y+1/2}A_{0,y} - \frac{\gamma}{2\pi}\left(\partial_x\tilde{\varphi}_{y+1/2} - \sqrt{K}a_{1,y+1/2}\right)^2 \right\} \\
&+ \int dtdx \sum_y \left\{ -\frac{\lambda}{8\pi}\left(\partial_x\Delta_y^T\tilde{\varphi}_{y+1/2}\right)^2 - \frac{\omega}{2\pi}\left(\partial_x\tilde{\theta}_{y+1/2} - \frac{\sqrt{K}}{2}\Delta_y A_{1,y}\right)^2 \right\} \\
&+ \int dtdx \sum_y \left\{ g_{y,y+1}\cos\left(2\tilde{\theta}_{y+1/2}/\sqrt{K} - \epsilon_\perp A_{2,y}\right) + \frac{m}{4\pi}\Delta_y a_{0,y}Sa_{1,y+1/2} \right\} \\
&+ \int dtdx \sum_y \left\{ +\frac{1}{\pi K^{3/2}}a_{0,y}\left(\partial_x\tilde{\theta}_{y+1/2} - \frac{\sqrt{K}}{2}\Delta_y A_{1,y}\right) \right\} \\
&+ \int dtdx \sum_y \left\{ \frac{1}{8\pi}\left[\frac{\alpha}{\gamma}\left(\Delta_y a_{0,y}\right)^2 + \beta\gamma\left(\Delta_y a_{1,y+1/2}\right)^2\right] \right\},
\end{aligned} \tag{3.127}$$

where the new parameters $\gamma, \lambda, \omega, \alpha, \beta$ are such that

$$\frac{\gamma}{K^2\left(\alpha K + m^2\right)} = \mathsf{v}, \quad \omega + \frac{\gamma}{\alpha K^3} = \mathsf{u}, \quad \text{and} \quad \lambda = \mathsf{v}\left(1 + k^2m^2\right), \tag{3.128}$$

leading to the expected match with (3.126) after integration over the emergent gauge fields. The above action describes scalar fields on the wires, minimally coupled to an emergent gauge field in the presence of Chern-Simons and Maxwell terms. We notice that this description is in the $a_2 = 0$ gauge and there is no x-component of the electric field. However, this component will emerge when we integrate over the matter fields.

In order to show that this local action reduces to Maxwell-Chern-Simons at low energies, we use the first relation in (3.128) to recast the local action (3.127) in terms of γ instead of v:

$$\begin{aligned}
S &= \int dtdx \sum_y \left\{ -\frac{1}{\pi}\partial_x\tilde{\theta}_{y+1/2}\partial_t\tilde{\varphi}_{y+1/2} + \frac{\sqrt{K}}{2\pi}\partial_x\Delta_y^T\tilde{\varphi}_{y+1/2}A_{0,y} - \frac{\gamma}{2\pi}\left(\partial_x\tilde{\varphi}_{y+1/2} - \sqrt{K}a_{1,y+1/2}\right)^2 \right\} \\
&+ \int dtdx \sum_y \left\{ -\frac{\gamma}{8\pi K^2}\frac{1-K^2m^2}{\alpha K + m^2}\left(\partial_x\Delta_y^T\tilde{\varphi}_{y+1/2}\right)^2 - \frac{\mathsf{u}\alpha K^3 - \gamma}{2\pi\alpha K^3}\left(\partial_x\tilde{\theta}_{y+1/2} - \frac{\sqrt{K}}{2}\Delta_y A_{1,y}\right)^2 \right\} \\
&+ \int dtdx \sum_y \left\{ g_{y,y+1}\cos\left(2\tilde{\theta}_{y+1/2}/\sqrt{K} - \epsilon_\perp A_{2,y}\right) + \frac{m}{4\pi}\Delta_y a_{0,y} S a_{1,y+1/2} \right\} \\
&+ \int dtdx \sum_y \left\{ \frac{1}{\pi K^{3/2}}a_{0,y}\left(\partial_x\tilde{\theta}_{y+1/2} - \frac{\sqrt{K}}{2}\Delta_y A_{1,y}\right) \right\} \\
&+ \int dtdx \sum_y \left\{ \frac{1}{8\pi}\left[\frac{\alpha}{\gamma}\left(\Delta_y a_{0,y}\right)^2 + \beta\gamma\left(\Delta_y a_{1,y+1/2}\right)^2\right] \right\}. \qquad (3.129)
\end{aligned}$$

Towards the continuum limit, we expand the cosine interaction up to quadratic terms and integrate out the θ. We disregard terms with more than two derivatives since they are irrelevant at low energies. In addition, we rescale the fields a_0 and a_1 to Ka_0 and $\frac{1}{K}a_1$, without affecting the Chern-Simons coefficient, and reintroduce the a_2 component to restore the gauge invariance of the model. We then have

$$\begin{aligned}
S &= \int dtdx \sum_y \left\{ -\frac{\gamma}{2\pi}\left(\partial_x\tilde{\varphi}_{y+1/2} - \frac{1}{\sqrt{K}}a_{1,y+1/2}\right)^2 + \frac{\alpha K^2\left(\epsilon_\perp\right)^2}{8\pi\gamma}\left(e_{2,y}\right)^2 + \frac{\beta\gamma\left(\epsilon_\perp\right)^2}{8\pi K^2}\left(b_{y+1/2}\right)^2 \right\} \\
&+ \int dtdx \sum_y \left\{ \frac{K}{8g\pi}\left(\partial_t\partial_x\tilde{\varphi}_{y+1/2} - \frac{1}{\sqrt{K}}\partial_x a_0\right)^2 + \frac{\epsilon_\perp}{2\pi}\left(\partial_t\partial_x\tilde{\varphi}_{y+1/2} - \frac{1}{\sqrt{K}}\partial_x a_{0,y}\right)\sqrt{K}A_{2,y} \right\} \\
&+ \int dtdx \sum_y \left\{ \frac{m\epsilon_\perp}{8\pi}\epsilon^{\mu\nu\rho}\left(Sa_\mu\right)\partial_\nu a_\rho + \frac{\epsilon_\perp}{2\pi}A_{1,y}\left(\frac{1}{\epsilon_\perp}\Delta_y a_{0,y-1} - \partial_t a_{2,y}\right) \right\} \\
&+ \int dtdx \sum_y \left\{ \frac{\sqrt{K}}{2\pi}\left(\Delta_y\tilde{\varphi}_{y-1/2} - \frac{1}{\sqrt{K}}a_{2,y-1/2}\right)\partial_x A_{0,y} \right\}, \qquad (3.130)
\end{aligned}$$

where $e_{2,y} = \partial_t a_2 - \partial_y a_0$, $b_{y+1/2} = \partial_x a_2 - \partial_y a_1$, and $\partial_y \equiv \frac{\Delta_y}{\epsilon_\perp}$. Integrating out the $\tilde{\varphi}$-field and retaining only two derivatives terms, we finally obtain

$$\begin{aligned}
S &= \int dtdx \sum_y \left\{ \frac{\alpha K^2\left(\epsilon_\perp\right)^2}{8\pi\gamma}\left(e_{2,y}\right)^2 + \frac{\beta\gamma\left(\epsilon_\perp\right)^2}{8\pi K^2}\left(b_{y+1/2}\right)^2 + \frac{1}{8g\pi^2}\left(e_{1,y}\right)^2 \right\} \qquad (3.131) \\
&+ \int dtdx \sum_y \left\{ +\frac{m\epsilon_\perp}{8\pi}\epsilon^{\mu\nu\rho}\left(Sa_\mu\right)\partial_\nu a_\rho + \frac{\epsilon_\perp}{2\pi}\epsilon^{\mu\nu\rho}A_{\mu,y}\partial_\nu a_\rho \right\}.
\end{aligned}$$

This is an anisotropic version of the MCS model on the wires system. For the continuum limit, we consider as before $\epsilon_\perp \to 0$, $K \to 0$, and $g \to \infty$, while keeping $K\epsilon_\perp^{-1} \equiv \Lambda_K$ and $\pi g \epsilon_\perp \equiv \Lambda_g$ fixed. To have finite Maxwell terms, we also consider that α and β go to infinity as $1/K$, i.e., given constants c and d, we take $\alpha = c/K$ and $\beta = -d/K$. With these choices, we obtain

$$\begin{aligned} S &= \int d^3x \left\{ \frac{1}{8\pi\tilde{\mathsf{v}}\Lambda_K} (e_2)^2 - \frac{cd\tilde{\mathsf{v}}}{8\pi\Lambda_K} b^2 + \frac{1}{8\pi\Lambda_g} (e_1)^2 \right\} \\ &+ \int d^3x \left\{ \frac{m}{4\pi} \epsilon^{\mu\nu\rho} a_\mu \partial_\nu a_\rho + \frac{1}{2\pi} \epsilon^{\mu\nu\rho} A_\mu \partial_\nu a_\rho \right\}, \end{aligned} \tag{3.132}$$

where the renormalized velocity is $\tilde{\mathsf{v}} \equiv \frac{\mathsf{v}(c+m^2)}{c}$. Now, in order to compare it with the MCS theory in 3.3.3, we consider again the isotropic limit of this action, which is attained by making $\Lambda_K = \Lambda_g = 6M$, $d = 1/c$ and $\tilde{\mathsf{v}} = 1$.

3.3.10 A More Direct Route to Maxwell-Chern-Simons Theory

As discussed in section 3.3.6, the same effective theory (3.132) was obtained in [31] using quantum wires, but relating the scalar field φ with components of the field strength of the emergent gauge fields. This can be seen as a shortcut of the above description, leading to the microscopic theory directly to the low-energy effective model. Here instead, we have attained the low-energy theory (3.132) using the particle-vortex transformation in the wires language and only after taking the low-energy limit. Therefore, it would be interesting to recast the results of [31] in a more convenient language, making explicit the connection with particle-vortex duality. To this end, we first obtain the relation between the canonical momenta and gauge fields from (3.101)-(3.103),

$$\Pi_{1,y} = \frac{1}{4\pi\Lambda_g} e_{1,y} + \frac{1}{2\pi} A_{2,y} + \frac{m}{4\pi} a_{2,y} \tag{3.133}$$

$$\Pi_{2,y} = \frac{1}{4\pi\mathsf{v}\Lambda_K} e_{2,y} - \frac{1}{2\pi} A_{1,y} - \frac{m}{4\pi} a_{1,y}, \tag{3.134}$$

and rewrite the relations (3.93) accordingly, obtaining

$$\Pi_{1,y} + \frac{m}{4\pi} a_{2,y} = \frac{1}{2\pi\sqrt{K}\epsilon_\perp} \Delta_y \varphi_y \tag{3.135}$$

$$\Pi_{2,y} - \frac{m}{4\pi} a_{1,y} = -\frac{1}{2\pi\sqrt{K}} \partial_x \varphi_y \tag{3.136}$$

$$\partial_x a_{2,y} - \frac{1}{\epsilon_\perp} \Delta_y a_{1,y} = \frac{2\sqrt{K}}{\epsilon_\perp} \partial_x \theta_y. \tag{3.137}$$

In the gauge $a_{1,y} = 0$ we immediately have $a_{2,y} = \frac{2\sqrt{K}}{\epsilon_\perp}\theta_y$, yielding the constraint

$$\partial_x \Pi_{1,y} + \frac{1}{\epsilon_\perp} \Delta_y \Pi_{2,y} + \frac{m}{4\pi} b = 0. \tag{3.138}$$

The relations above can be seen as a generalization of winding-momentum duality between Maxwell theory and the XY model in 2+1 dimensions, which is an equivalent way to view the particle-vortex duality. Alternatively, we can view (3.135)-(3.137) as a direct connection between the action (3.118), which is the SD model after choosing the unitary gauge, and the MCS model. This is made explicit after rewriting (3.135)-(3.137) in a covariant form,

$$\frac{1}{4\pi\Lambda_K} f_{\mu\nu} - \frac{m}{2\pi}\epsilon_{\mu\nu\rho}a^{\rho} - \frac{1}{2\pi}\epsilon_{\mu\nu\rho}A^{\rho} = -\frac{1}{2\pi\sqrt{\Lambda_K}}\epsilon_{\mu\nu\rho}\partial^{\rho}\varphi, \tag{3.139}$$

where we already considered the isotropic and continuum limits ($\Lambda_K = \Lambda_g$ and $\varphi(x,y,t) = \frac{1}{\epsilon_\perp}\varphi_y(x,t)$). To obtain the last relation (3.137) from (3.139), we use the equation of motion for θ in (3.120), given by

$$\partial_x\theta_y = -\frac{1}{\mathsf{v}}\left(\partial_t\varphi_y + \frac{\sqrt{K}}{2}S\alpha_{0,y} - \sqrt{K}A_{0,y}\right), \tag{3.140}$$

and make the identification $a_\mu = -m^{-1}\alpha_\mu$ between the gauge fields in the two models. Furthermore, we can express the inverse of the relation (3.139) as

$$\frac{1}{4\pi\sqrt{\Lambda_K}}\epsilon^{\mu\nu\rho}f_{\nu\rho} = -\frac{1}{\pi}\left(\partial^{\mu}\varphi + \sqrt{\Lambda_K}\alpha^{\mu} - \sqrt{\Lambda_K}A^{\mu}\right). \tag{3.141}$$

Notice we recover the equations in (3.113) in the gauge $\varphi = 0$. The relations (3.139) and (3.141) clearly display a winding-momentum structure, which is typical of particle-vortex duality: the equation of motion of the MCS model is obtained taking the divergence of (3.139), which from the form of the left hand side of this equation is identically satisfied in terms of the φ variable. Analogously, the equation of motion for φ is obtained by taking the divergence of (3.141), which is again trivially satisfied in terms of the gauge field a_μ from the Bianchi identity.

We conclude this subsection by pointing out that the relation between the prescriptions used in [71] and [31] are connected by particle-vortex duality. This can be verified either from the quantum wires approach using the particle-vortex transformation proposed in [29], which lead us from (3.120) to (3.132), or via the expressions relating momentum and winding number (3.135)-(3.137) or (3.139) and (3.141), which directly lead to the low-energy effective theory.

3.3.11 Vortex Creation Operators

In the previous section we have shown that the microscopic Hamiltonian for the Laughlin series of QH states can be macroscopically described either by the SD or MCS models, and that these descriptions are connected by the particle-vortex duality transformations (3.139)-(3.141). This duality was derived both from the microscopic wires in 1+1 dimensions and directly in terms of emergent gauge fields in 2+1 dimensions. Here we

furhter explore this view and investigate the vortex creation operators in terms of both wires and emergent gauge fields in the continuum.

Applying $\Delta_y\partial_x$ to particle vortex relations (3.122) and ∂_x to (3.123), we get

$$\frac{1}{2\pi}\partial_x\Delta_y\tilde{\varphi}_{y-1/2} = p_y \tag{3.142}$$

$$\tilde{p}_{y+1/2} = -\frac{1}{2\pi}\Delta_y\partial_x\varphi_y, \tag{3.143}$$

where $p_y \equiv -\frac{1}{\pi}\partial_x\theta_y$ and $\tilde{p}_{y+1/2} \equiv -\frac{1}{\pi}\partial_x\tilde{\theta}_{y+1/2}$ are the canonical momentum of φ_y and $\tilde{\varphi}_{y+1/2}$, respectively. We will show that $\Delta_y\partial_x\varphi_y$ measures the winding number of a specific vortex configuration of φ in 2+1 dimensions with the branch cut of the compact variable φ running along the y direction. Thus, (3.142) and (3.143) express the momentum-winding duality in the quantum wires variables.

To understand how the winding number can be described this way, we note that the operator

$$e^{i\tilde{\varphi}_{y+1/2}} = \ldots e^{-i\theta_{y-1}}e^{-i\theta_y}e^{i\theta_{y+1}}\ldots \tag{3.144}$$

creates a half-phase slip of $-\pi$ in all the wires with $y' \le y$ and a half-phase slip of $+\pi$ in all the wires with $y' > y$, both for $x' > x$. Since, φ is a compact variable, a nontrivial winding configuration around $x, y+1/2$ contains a branch cut starting at this point and extending to infinity along some line through which φ is discontinuous.

For the vortex configuration created by $e^{i\tilde{\varphi}}$, which we will denote by $\lambda_{y'}(x')$, the branch cut is a straight line along the dual wire $y+1/2$. The circulation of $\lambda_{y'}(x')$ along a small square centered at the point $x, y+1/2$ in the quantum wires system can be calculated by $\sum \eta^i\bar{\Delta}_i\lambda_y(x) = \sum \bar{\Delta}_x\lambda_y(x) + \bar{\Delta}_y\lambda_y(x)$, with η^i being an unitary vector tangent to the closed path and $\bar{\Delta}_i \equiv \Delta_i \mod 2\pi$. For smooth φ configurations, $\bar{\Delta}_i\varphi \equiv \Delta_i\varphi$. Considering the branch cut position for the vortex field λ, we have $\bar{\Delta}_x\lambda_y = \Delta_x\lambda_y$ and $\bar{\Delta}_{y'}\lambda_{y'} = \Delta_{y'}\lambda_{y'} - 2\pi\Theta(x'-x)\delta_{y,y'}$. Therefore, $\sum \eta^i\bar{\Delta}_i\lambda_y(x) = \epsilon_{ij}\Delta_i\bar{\Delta}_j\lambda_y(x) = \Delta_y\Delta_x\lambda_y(x)$. Considering the continuum limit of the relations (3.142) and (3.143) and taking into account our discussion of the mod 2π derivative, we can rewrite them in a more convenient form as

$$\frac{1}{2\pi}\epsilon_{ij}\partial_i\bar{\partial}_j\tilde{\varphi}(x,y) = p(x,y) \tag{3.145}$$

$$\tilde{p}(x,y) = -\frac{1}{2\pi}\epsilon_{ij}\partial_i\bar{\partial}_j\varphi(x,y). \tag{3.146}$$

Here $p(x,y) = -\frac{1}{\pi}\partial_x\theta(x,y)$, $\tilde{p} = -\frac{1}{\pi}\partial_x\tilde{\theta}(x,y)$, with $\tilde{\varphi}(x,y) = \lim_{\epsilon_\perp\to 0}\epsilon_\perp\tilde{\varphi}_{y+1/2}(x)$ and $\tilde{\theta}(x,y) = \lim_{\epsilon_\perp\to 0}\frac{1}{\epsilon_\perp^{3/2}}\tilde{\theta}_{y+1/2}(x)$.

Defining Π_i and a_i via

$$\tilde{p} = -\sqrt{\Lambda_K}\left(\nabla\cdot\Pi + \frac{m}{4\pi}\epsilon_{ij}\partial_i a_j\right), \tag{3.147}$$

$$a_i = -\sqrt{\Lambda_K}\bar{\partial}_i\tilde{\varphi}, \tag{3.148}$$

we finally obtain

$$-\frac{1}{2\pi}\epsilon_{ij}\partial_i a_j = \sqrt{\Lambda_K}p(x,y), \tag{3.149}$$

$$\Pi_i + \frac{m}{4\pi}\epsilon_{ij}a_j = \frac{1}{2\pi\sqrt{\Lambda_K}}\epsilon_{ij}\bar{\partial}_j\varphi(x,y), \tag{3.150}$$

which are the relations (3.135)-(3.137) for the winding-momentum duality.

From this discussion and the rescaling (3.91) we see that $e^{i\sqrt{K}\tilde{\varphi}_{y+1/2}(x)}$ creates a vortex of φ_y at the dual wire $y+1/2$ and $x'=x$, whereas $e^{\frac{1}{\sqrt{K}}\varphi_y(x)}$ creates a vortex of $\tilde{\varphi}_{y+1/2}$ at the wire y and $x'=x$. We have shown that when taking the continuum limit, the original quantum wires system (3.92) can be identified directly as the self dual model (3.119), and with the MCS model (3.132) using the particle-vortex duality (3.122)-(3.123). Therefore, we should be able to show that when written in terms of the emergent gauge fields α_μ and a_μ, the operators $e^{i\sqrt{K}\tilde{\varphi}_{y+1/2}(x)}$ and $e^{i\frac{1}{\sqrt{K}}\varphi_y(x)}$ create vortices in the SD and MCS models, respectively.

We start with $e^{i\sqrt{K}\tilde{\varphi}_{y+1/2}(x)}$. From (3.142),

$$\sqrt{K}\tilde{\varphi}_{y+1/2}(x) = \pi\sqrt{\Lambda_K}\int^x dx'\left(\int_{-\infty}^{y} dy' p(x',y') - \int_y^{\infty} dy' p(x',y')\right), \tag{3.151}$$

where we took the continuum limit on the right hand side. Since $p(x,y) = -\frac{1}{\pi}\partial_x\theta(x,y)$ and using (3.115), we get

$$\sqrt{K}\tilde{\varphi}_{y+1/2}(x) = \frac{1}{2m}\int dx'dy'\Theta(x-x')\left(\Theta(y-y') - \Theta(y'-y)\right)b_\alpha(x',y'). \tag{3.152}$$

Defining $\lambda(\vec{r}-\vec{r}') \equiv \pi\Theta(x-x')[\Theta(y-y') - \Theta(y'-y)]$, we can write the vortex creating operator in the SD model as

$$V_\alpha(\vec{r}) = \exp\left\{\frac{i}{2\pi m}\int d^2\vec{r}'\lambda(\vec{r}-\vec{r}')b_\alpha(\vec{r}')\right\}. \tag{3.153}$$

From the algebra (3.75) with $k=m$, we can show how the gauge field α_i transforms under the action of V_α:

$$V_\alpha(\vec{r})\alpha_i(\vec{r}')V_\alpha^\dagger(\vec{r}) = \alpha_i(\vec{r}') + \bar{\partial}_i\lambda(\vec{r}-\vec{r}'). \tag{3.154}$$

The function λ has a 2π discontinuity at $y'=y$ for $x'<x$ and discontinuities π or $-\pi$ at $x'=x$ depending if $y>y'$ or $y<y'$. Since the derivative $\bar{\partial}$ is mod 2π, the operator V_α generates singular gauge transformations over α_i, such that $\alpha_i' = V_\alpha\alpha_i V_\alpha^\dagger$ satisfies

$$\epsilon_{ij}\partial_i\alpha_j'(\vec{r}') = \epsilon_{ij}\partial_i\alpha_j(\vec{r}') + 2\pi\delta(\vec{r}-\vec{r}'), \tag{3.155}$$

which corresponds to a creation of a unit of flux at $\vec{r}=\vec{r}'$.

Similarly, we can investigate the vortex creating operator $V_a(\vec{r}) = e^{i\frac{1}{\sqrt{K}}\varphi(\vec{r})}$ in the MCS model. From (3.146) and (3.147), we obtain

$$V_a(\vec{r}) = \exp\left\{i\int d^2\vec{r}'\lambda(\vec{r}-\vec{r}')\left(\nabla\cdot\Pi(\vec{r}') + \frac{m}{4\pi}b_a(\vec{r}')\right)\right\}. \tag{3.156}$$

Then, using the canonical algebra between π_i and a_j, we obtain

$$a_i'(\vec{r}') = a_i(\vec{r}') - \bar{\partial}_i \lambda(\vec{r} - \vec{r}'), \tag{3.157}$$

which again represents a creation of a negative unit of flux at $\vec{r}' = \vec{r}$.

The above discussion provides an alternative way to understand the identification of the low-energy effective theory for the Laughlin series of QH effect either as the SD or MCS models. In the previous sections we have shown that the SD model can be identified directly in terms of a statistical gauge field, whereas MCS is the effective theory describing low-energy vortices of the original quantum wires model. And now we have presented the low-energy limit of the particle and vortex creating operators in the quantum wires model and shown that they indeed coincide with the corresponding operators in the effective theories in the low-energy limit.

4 Final Remarks

In this thesis, we explored a variety of theoretical frameworks that describe and classify topological phases of matter through the lens of generalized symmetries and anomalies. While many open questions remain, we manage to explore a non-trivial interplay between symmetric SRE systems, mixed anomalies, and gapped LRE systems using layer constructions.

A central contribution of this work is the proposal of the anomalous stacking construction. This framework allows us to generate higher-dimensional topological orders from stacks of lower-dimensional SPT phases by introducing suitable interactions between the layers, and the coupling guide principle was the enforcing of 't Hooft anomalies. The ASC acts as a bridge between protected boundary phenomena and bulk topological order.

We also introduced and studied the LGF code, a novel model that combines ingredients from the original Levin-Gu construction with exotic features arising from geometric constraints and mixed anomalies. The LGF code serves as a platform to analyze how symmetry, geometry, and topology interplay in systems with restricted mobility and subsystem symmetries. The model suggests signs of hosting fracton excitations, from its sub-extensive ground state degeneracy. This construction also reinforces the utility of the ASC framework as a tool to generate new quantum phases.

Another major result of this thesis is the quantum wire approach to topological orders, particularly in the context of quantum Hall systems. Using an array of interacting $D = 2$ systems, we were able to recover and reinterpret key features of the Laughlin states and explore connections to Chern-Simons theory and dualities. This approach not only provides a useful computational framework, but also offers direct connections between microscopic and macroscopic, effective degrees of freedom.

Looking ahead, there are several directions that emerge naturally from the results presented here. One avenue is to further constrain the ASC by identifying physical or mathematical principles that reduce its arbitrariness, possibly leading to a classification scheme for the resulting topological orders. It is also possible to investigate ASC framework without the imposition of periodic boundary conditions to understand the emergence of edge theories for the topological orders obtained from the ASC . Another possible direction is to investigate the LGF code in more depth, including its excitations, stability, and potential generalizations to other lattice geometries or symmetry classes.

Finally, the quantum wire construction provides a framework that could be naturally extended to the construction and analysis of non-Abelian fractional quantum Hall states. Additionally, the quantum wire perspective presents opportunities to connect fractional quantum Hall physics with recent theoretical developments in high-energy and condensed matter physics, particularly the web of dualities, generalized symmetries, and anomalies.

References

1 SCHWICHTENBERG, J. **Physics from symmetry**. [S.l.]: Springer, 2018. Cited on page 15.

2 NOETHER, E. Invariante variationsprobleme, nachrichten der königlichen gesellschaft der wissenschaften zu göttingen, mathematisch-physikalische klasse book 2: 235–57, english translation by ma tavel. **English Translation**, 1918. Cited on page 15.

3 SEIBERG, N. et al. A Duality Web in 2+1 Dimensions and Condensed Matter Physics. **Annals Phys.**, v. 374, p. 395–433, 2016. Cited 2 times on page 15 and 45.

4 KARCH, A.; TONG, D. Particle-Vortex Duality from 3d Bosonization. **Phys. Rev. X**, v. 6, n. 3, p. 031043, 2016. Cited 2 times on page 15 and 61.

5 BEEKMAN, A.; RADEMAKER, L.; WEZEL, J. V. An introduction to spontaneous symmetry breaking. **SciPost Physics Lecture Notes**, p. 011, 2019. Cited on page 15.

6 BILAL, A. Lectures on anomalies. **arXiv preprint arXiv:0802.0634**, 2008. Cited on page 15.

7 DELMASTRO, D. G. et al. Anomalies and symmetry fractionalization. **SciPost Physics**, v. 15, n. 3, p. 079, 2023. Cited on page 15.

8 CHEN, X. et al. Symmetry protected topological orders and the group cohomology of their symmetry group. **Physical Review B**, v. 87, n. 15, p. 155114, abr. 2013. ISSN 1098-0121, 1550-235X. Disponível em: <https://link.aps.org/doi/10.1103/PhysRevB.87.155114>. Cited 5 times on page 15, 16, 17, 22, and 45.

9 BI, Z.; LAKE, E.; SENTHIL, T. Landau ordering phase transitions beyond the landau paradigm. **Physical Review Research**, APS, v. 2, n. 2, p. 023031, 2020. Cited on page 16.

10 GIRVIN, S.; PRANGE, R. The quantum hall effect. 1987. Cited on page 16.

11 WEN, X.-G. Theory of the edge states in fractional quantum Hall effects. **Int. J. Mod. Phys. B**, v. 6, p. 1711–1762, 1992. Cited on page 16.

12 ZHANG, S. C.; HANSSON, T. H.; KIVELSON, S. An effective field theory model for the fractional quantum hall effect. **Phys. Rev. Lett.**, v. 62, p. 82–85, 1988. Cited on page 16.

13 ZEE, A. Quantum Hall fluids. **Lect. Notes Phys.**, v. 456, p. 99–153, 1995. Cited 3 times on page 16, 61, and 62.

14 SAVARY, L.; BALENTS, L. Quantum spin liquids: a review. **Reports on Progress in Physics**, IOP Publishing, v. 80, n. 1, p. 016502, 2016. Cited on page 16.

15 WEN, X. G. **Quantum field theory of many-body systems: From the origin of sound to an origin of light and electrons**. [S.l.: s.n.], 2004. Cited 2 times on page 16 and 34.

16 CHEN, X.; LIU, Z.-X.; WEN, X.-G. Two-dimensional symmetry-protected topological orders and their protected gapless edge excitations. **Phys. Rev. B**, v. 84, n. 23, p. 235141, 2011. Cited 4 times on page 16, 17, 22, and 45.

17 GAIOTTO, D. et al. Generalized Global Symmetries. **JHEP**, v. 02, p. 172, 2015. Cited 2 times on page 16 and 35.

18 MCGREEVY, J. Generalized Symmetries in Condensed Matter. **Ann. Rev. Condensed Matter Phys.**, v. 14, p. 57–82, 2023. Cited on page 16.

19 CORDOVA, C. et al. Snowmass White Paper: Generalized Symmetries in Quantum Field Theory and Beyond. In: **Snowmass 2021**. [S.l.: s.n.], 2022. Cited on page 16.

20 SCHAFER-NAMEKI, S. ICTP lectures on (non-)invertible generalized symmetries. **Phys. Rept.**, v. 1063, p. 1–55, 2024. Cited on page 16.

21 BHARDWAJ, L. et al. **Lectures on Generalized Symmetries**. arXiv, 2023. ArXiv:2307.07547 [hep-th]. Disponível em: <http://arxiv.org/abs/2307.07547>. Cited on page 16.

22 GOMES, P. R. S. An Introduction to Higher-Form Symmetries. **SciPost Physics Lecture Notes**, p. 74, set. 2023. ISSN 2590-1990. ArXiv:2303.01817 [hep-th]. Disponível em: <http://arxiv.org/abs/2303.01817>. Cited 3 times on page 16, 19, and 35.

23 SHIRLEY, W.; SLAGLE, K.; CHEN, X. Foliated fracton order from gauging subsystem symmetries. **SciPost Phys.**, v. 6, n. 4, p. 041, 2019. Cited 2 times on page 16 and 45.

24 HSIN, P.-S. et al. Subsystem symmetry fractionalization and foliated field theory. arXiv, mar. 2024. Cited on page 16.

25 BHARDWAJ, L. et al. **Categorical Landau Paradigm for Gapped Phases**. arXiv, 2023. ArXiv:2310.03786 [cond-mat]. Disponível em: <http://arxiv.org/abs/2310.03786>. Cited on page 17.

26 BHARDWAJ, L.; TACHIKAWA, Y. On finite symmetries and their gauging in two dimensions. **Journal of High Energy Physics**, v. 2018, n. 3, p. 189, mar. 2018. ISSN 1029-8479. Disponível em: <https://link.springer.com/10.1007/JHEP03(2018)189>. Cited 2 times on page 17 and 35.

27 KITAEV, A. Y. Fault tolerant quantum computation by anyons. **Annals Phys.**, v. 303, p. 2–30, 2003. Cited 3 times on page 17, 36, and 48.

28 MROSS, D. F.; ALICEA, J.; MOTRUNICH, O. I. Explicit derivation of duality between a free Dirac cone and quantum electrodynamics in (2+1) dimensions. **Phys. Rev. Lett.**, v. 117, n. 1, p. 016802, 2016. Cited 2 times on page 17 and 73.

29 MROSS, D. F.; ALICEA, J.; MOTRUNICH, O. I. Symmetry and duality in bosonization of two-dimensional Dirac fermions. **Phys. Rev. X**, v. 7, n. 4, p. 041016, 2017. Cited 4 times on page 17, 61, 73, and 76.

30 FUJI, Y.; FURUSAKI, A. Quantum Hall hierarchy from coupled wires. **Phys. Rev. B**, v. 99, n. 3, p. 035130, 2019. Cited on page 17.

31 FONTANA, W. B.; GOMES, P. R. S.; HERNASKI, C. A. From Quantum Wires to the Chern-Simons Description of the Fractional Quantum Hall Effect. **Phys. Rev. B**, v. 99, n. 20, p. 201113, 2019. Cited 4 times on page 17, 68, 75, and 76.

32 CHEN, X.; GU, Z. C.; WEN, X. G. Local unitary transformation, long-range quantum entanglement, wave function renormalization, and topological order. **Phys. Rev. B**, v. 82, p. 155138, 2010. Cited on page 19.

33 LEVIN, M.; GU, Z.-C. Braiding statistics approach to symmetry-protected topological phases. **Physical Review B**, v. 86, n. 11, p. 115109, set. 2012. ISSN 1098-0121, 1550-235X. Disponível em: <https://link.aps.org/doi/10.1103/PhysRevB.86.115109>. Cited 4 times on page 22, 30, 41, and 51.

34 SUZUKI, M. The dimer problem and the generalized x-model. **Physics Letters A**, v. 34, n. 6, p. 338–339, 1971. ISSN 0375-9601. Disponível em: <https://www.sciencedirect.com/science/article/pii/0375960171909017>. Cited on page 23.

35 SON, W. et al. Quantum phase transition between cluster and antiferromagnetic states. **Europhysics Letters**, IOP Publishing, v. 95, n. 5, p. 50001, 2011. Cited on page 23.

36 SEIFNASHRI, S.; SHAO, S.-H. Cluster State as a Noninvertible Symmetry-Protected Topological Phase. **Phys. Rev. Lett.**, v. 133, n. 11, p. 116601, 2024. Cited 2 times on page 25 and 27.

37 SEIFNASHRI, S.; SHAO, S.-H. **Cluster state as a non-invertible symmetry protected topological phase**. arXiv, 2024. ArXiv:2404.01369 [cond-mat]. Disponível em: <http://arxiv.org/abs/2404.01369>. Cited on page 26.

38 HASTINGS, M. B.; KOMA, T. Spectral gap and exponential decay of correlations. **Commun. Math. Phys.**, v. 265, p. 781–804, 2006. Cited on page 29.

39 WILLIAMSON, D. J.; DUA, A.; CHENG, M. Spurious topological entanglement entropy from subsystem symmetries. **Phys. Rev. Lett.**, v. 122, n. 14, p. 140506, 2019. Cited on page 33.

40 WEN, X.-G. Topological Order: From Long-Range Entangled Quantum Matter to a Unified Origin of Light and Electrons. **ISRN Condensed Matter Physics**, v. 2013, p. 1–20, mar. 2013. ISSN 2090-7400. Disponível em: <https://www.hindawi.com/journals/isrn/2013/198710/>. Cited 2 times on page 33 and 34.

41 WEN, X.-G. An introduction of topological orders. **URL http://web.mit.edu/physics/people/faculty/docs/wen_intro_topological_orders.pdf**, v. 34, p. 54, 2016. Cited on page 34.

42 WEN, X.-G. Colloquium: Zoo of quantum-topological phases of matter. **Reviews of Modern Physics**, APS, v. 89, n. 4, p. 041004, 2017. Cited on page 34.

43 HSIN, P.-S.; KOBAYASHI, R.; PREM, A. Higher-Form Anomalies Imply Intrinsic Long-Range Entanglement. 4 2025. Cited on page 40.

44 PRETKO, M.; CHEN, X.; YOU, Y. Fracton Phases of Matter. **Int. J. Mod. Phys. A**, v. 35, n. 06, p. 2030003, 2020. Cited 2 times on page 40 and 42.

45 NANDKISHORE, R. M.; HERMELE, M. Fractons. **Ann. Rev. Condensed Matter Phys.**, v. 10, p. 295–313, 2019. Cited 2 times on page 40 and 42.

46 AASEN, D. et al. Topological Defect Networks for Fractons of all Types. **Phys. Rev. Res.**, v. 2, p. 043165, 2020. Cited on page 41.

47 VIJAY, S.; HAAH, J.; FU, L. Fracton Topological Order, Generalized Lattice Gauge Theory and Duality. **Phys. Rev. B**, v. 94, n. 23, p. 235157, 2016. Cited on page 42.

48 SEIBERG, N.; SHAO, S.-H. Exotic Symmetries, Duality, and Fractons in 2+1-Dimensional Quantum Field Theory. **SciPost Phys.**, v. 10, n. 2, p. 027, 2021. Cited on page 42.

49 SEIBERG, N.; SHAO, S.-H. Exotic $U(1)$ Symmetries, Duality, and Fractons in 3+1-Dimensional Quantum Field Theory. **SciPost Phys.**, v. 9, n. 4, p. 046, 2020. Cited on page 42.

50 SEIBERG, N.; SHAO, S.-H. Exotic $\mathbb{Z}_N$ symmetries, duality, and fractons in 3+1-dimensional quantum field theory. **SciPost Phys.**, v. 10, n. 1, p. 003, 2021. Cited on page 42.

51 XU, C.; MOORE, J. E. Strong-weak coupling self-duality in the two-dimensional quantum phase transition of p+ip superconducting arrays. **Physical review letters**, APS, v. 93, n. 4, p. 047003, 2004. Cited on page 42.

52 VIJAY, S.; HAAH, J.; FU, L. A New Kind of Topological Quantum Order: A Dimensional Hierarchy of Quasiparticles Built from Stationary Excitations. **Phys. Rev. B**, v. 92, n. 23, p. 235136, 2015. Cited on page 43.

53 WEN, X. G.; ZEE, A. Shift and spin vector: New topological quantum numbers for the Hall fluids. **Phys. Rev. Lett.**, v. 69, p. 953–956, 1992. [Erratum: Phys.Rev.Lett. 69, 3000 (1992)]. Cited on page 45.

54 WEN, X. G.; ZEE, A. Compressibility and Superfluidity in the Fractional Statistics Liquid. **Phys. Rev. B**, v. 41, p. 240–253, 1990. Cited on page 45.

55 SLAGLE, K. Foliated Quantum Field Theory of Fracton Order. **Phys. Rev. Lett.**, v. 126, n. 10, p. 101603, 2021. Cited on page 45.

56 CHATTERJEE, A.; WEN, X.-G. Symmetry as a shadow of topological order and a derivation of topological holographic principle. **Phys. Rev. B**, v. 107, n. 15, p. 155136, 2023. Cited on page 46.

57 VERRESEN, R. et al. Higgs condensates are symmetry-protected topological phases: I. discrete symmetries. arXiv, nov. 2022. Cited on page 50.

58 HAMMA, A.; ZANARDI, P.; WEN, X. G. String and membrane condensation on 3-D lattices. **Phys. Rev. B**, v. 72, p. 035307, 2005. Cited on page 50.

59 BRAVYI, S.; LEEMHUIS, B.; TERHAL, B. M. Topological order in an exactly solvable 3d spin model. **Annals of Physics**, Elsevier, v. 326, n. 4, p. 839–866, 2011. Cited on page 54.

60 TOLEDO, J. et al. Quantum wires, Chern-Simons theory, and dualities in the quantum Hall system. **Phys. Rev. B**, v. 106, n. 7, p. 075122, 2022. Cited 2 times on page 61 and 73.

61 SEIBERG, N. et al. A Duality Web in 2+1 Dimensions and Condensed Matter Physics. **Annals Phys.**, v. 374, p. 395–433, 2016. Cited on page 61.

62 MURUGAN, J.; NASTASE, H. Particle-vortex duality in topological insulators and superconductors. **JHEP**, v. 05, p. 159, 2017. Cited on page 61.

63 FUJI, Y.; FURUSAKI, A. Quantum Hall hierarchy from coupled wires. **Phys. Rev. B**, v. 99, n. 3, p. 035130, 2019. Cited on page 61.

64 Lee, D.-H.; Fisher, M. P. A. Anyon Superconductivity and Charge-Vortex Duality. **International Journal of Modern Physics B**, v. 5, n. 16-17, p. 2675–2699, jan. 1991. Cited 2 times on page 61 and 62.

65 BURGESS, C. P.; DOLAN, B. P. Particle vortex duality and the modular group: Applications to the quantum Hall effect and other 2-D systems. **Phys. Rev. B**, v. 63, p. 155309, 2001. Cited on page 61.

66 TONG, D. Lectures on the Quantum Hall Effect. In: . [S.l.: s.n.], 2016. Cited on page 61.

67 DESER, S.; JACKIW, R. 'Selfduality' of Topologically Massive Gauge Theories. **Phys. Lett. B**, v. 139, p. 371–373, 1984. Cited on page 62.

68 KANE, C. L.; MUKHOPADHYAY, R.; LUBENSKY, T. C. Fractional quantum hall effect in an array of quantum wires. **Phys. Rev. Lett.**, American Physical Society, v. 88, p. 036401, Jan 2002. Disponível em: <https://link.aps.org/doi/10.1103/PhysRevLett.88.036401>. Cited on page 66.

69 TEO, J. C. Y.; KANE, C. L. From Luttinger liquid to non-Abelian quantum Hall states. **Phys. Rev. B**, v. 89, n. 8, p. 085101, 2014. Cited on page 66.

70 SANTOS, R. A. et al. Fractional Topological Insulators: from sliding Luttinger Liquids to Chern-Simons theory. **Phys. Rev. B**, v. 91, n. 20, p. 205141, 2015. Cited on page 66.

71 IMAMURA, Y.; TOTSUKA, K.; HANSSON, T. H. From coupled-wire construction of quantum Hall states to wave functions and hydrodynamics. **Phys. Rev. B**, v. 100, n. 12, p. 125148, 2019. Cited 3 times on page 68, 69, and 76.